Large Mode Area Photonic Crystal Fibers

Nielsen, Martin Dybendal

Publication date:
2004

Document Version
Publisher's PDF, also known as Version of record

Large Mode Area Photonic Crystal Fibers

Martin Dybendal Nielsen

Crystal Fibre A/S
Blokken 84
3460 Birkerød, Denmark

COM, Technical University of Denmark
Ørsteds plads 345
2800 Kgs. Lyngby, Denmark

Abstract

The photonic crystal fiber (PCF) is a novel single-material optical waveguide realized by an arrangement of air-holes running along the full length of the fiber. Since the proposal of the PCF in 1996, the technology has developed into being a well-established area of research and commercialization. The work presented in this thesis deals with the optical properties of large-mode area PCFs for which the mode-field diameter, typically, is an order of magnitude larger than the free-space optical wavelength. Special emphasis is put on the description of relevant mechanisms of attenuation in these fibers. This includes design guidelines for optimizing the robustness of single-mode fibers and expressions for predicting the mode-field diameter and dispersion properties for a given choice of structural parameters. Micro-deformation induced attenuation is addressed and shown to play a critical role for the limitation of the available bandwidth. Screening of such deformations is explained from a theoretical point of view and experimentally verified. Furthermore, macro-bending induced attenuation is addressed and an analytical expression predicting the spectral dependency is proposed. The expression can be evaluated based on the structural parameters and predicted data agree within ~100 nm with experimental observations. Attenuation related to the fabrication process is described including central issues such as hydroxyl contamination, defect centers in the glass, along with contamination and roughness of surfaces in the preform. As a result of fabrication optimization, a single-mode fiber with an effective area of 130 μm^2 and attenuation of 0.48 dB/km at the 1550 nm wavelength is reported. Based on the general considerations of the introducing chapters, 5 different examples of large-mode area PCFs are presented. The first is a large-mode area fiber optimized for visible light applications. The second is a fiber optimized for the telecommunication band realizing a nonlinear effective area 5 times larger than state of the art conventional fibers. Two examples of

alternative designs are demonstrated addressing the core and the cladding region, respectively. The last of the five examples is the first polarization-maintaining large-mode area PCF to be reported. The fiber design combines the benefits of the PCF with utilization of stress applying parts for the realization of material birefringence in the core region of the fiber. The result is a large-mode area fiber which is both endlessly single-mode and endlessly birefringent.

Keywords: Photonic Crystal Fiber, Attenuation, Large-mode area

Large Mode Area Photonic Crystal fibers

Martin Dybendal Nielsen

Crystal Fibre A/S
Blokken 84
3460 Birkerød, Denmark

COM, Technical University of Denmark
Ørsteds plads 345
2800 Kgs. Lyngby, Denmark

Resume (Danish)

Den fotoniske krystalfiber er en ny type optisk bølgeleder skabt i ét materiale via en fordeling af luft huller, der løber langs hele fiberens længderetning. Siden den fotoniske krystalfiber blev foreslået i 1996, har teknologien udviklet sig til at være et veletableret forsknings- og erhvervsrettet område. Arbejdet præsenteret i denne afhandling omhandler de optiske egenskaber for storkerne fotoniske krystalfibre, for hvilke pletstørrelsen typisk er en størrelsesorden større end fritrumsbølgelængden. Beskrivelse af mekanismer, der er af betydning for den optiske dæmpning i disse fibre, er tillagt speciel vægt. Dette inkluderer retningslinier for optimalt design af robuste monomode fibre og udtryk til bestemmelse af pletstørrelse og dispersionsegenskaber for et givent valg af strukturelle parametre. Dæmpning introduceret af små deformationer er beskrevet og det påvises at disse spiller en afgørende rolle i begrænsningen af den anvendelige båndbredde. Afskærmning af sådanne deformationer er beskrevet teoretisk og eftervist eksperimentelt. Ydermere er dæmpning, der skyldes bøjning af fiberen, beskrevet, og et analytisk udtryk til bestemmelse af bølgelængdeafhængigheden af en sådan type dæmpning præsenteres. Udtrykket kan evalueres ud fra de strukturelle parametre, og beregnede værdier stemmer overens med eksperimentelle observationer indenfor ~100 nm. Dæmpning relateret til fremstillingsprocessen er beskrevet, deriblandt emner som hydroxyl kontaminering, defektcentre i glasset samt forurening og ruhed af overflader i præformen. Som et resultat af fabrikationsoptimering præsenteres en monomode fiber med et effektivt areal på 130 μm^2 og en dæmpning på 0.48 dB/km ved en bølgelængde på 1550 nm. Baseret på de generelle betragtninger i den første del af afhandlingen gives 5 eksempler på storkerne fotoniske

krystalfibre. Den første er en storkernefiber optimeret til synligt lys. Den anden er en fiber optimeret til telekommunikationsbåndet med et effektivt areal 5 gange højere end de bedste konventionelle fibre. To eksempler på alternative designs, der retter sig mod henholdsvis kernen og kappen bliver demonstreret. Det sidste af de 5 eksempler er den først rapporterede polarisationsbevarende storkerne fotoniske krystalfiber. Fiberdesignet kombinerer fordelene ved den fotoniske krystalfiber med anvendelsen af stressinducerende elementer til frembringelse af dobbeltbrydning i kernen af fiberen. Resultatet er en storkernefiber, der er både monomode og dobbeltbrydende uafhængigt af bølgelændgden.

Keywords: Fotonisk krystal fiber, dæmpning, Storkerne fiber.

Author's notes

The subject of this thesis, the photonic crystal fiber, has alternative names in different parts of the world. In the United States and Australia the term "Microstructured Optical Fiber" (MOF) is frequently used while some groups in Britain use "Holey Fiber" (HF). However, in recent years the term photonic crystal fiber, used throughout most of Europe including Denmark, has earned it placed as the most frequently used term and is also used throughout this thesis.

This thesis is based on a number of appended applications. However, not all publications of this work have been chosen for the thesis. The publications appended have been picked on the basis that they are part of a unified whole and that they are journal papers. Conference contributions have been discounted due to their typical abstract form.

Appended papers are labeled with capital letters such as Paper A, Paper B … etc. and referred to in the text by these labels. The remaining publications of this work which are not appended to this thesis are listed in the section "*List of not appended publications*" and numbered 1, 2, 3 etc. A reference in the text placed in square brackets refers to the list of references found on the last pages of the thesis.

In this thesis the choice has been made to minimize the use of abbreviations and acronyms. As principle rule, these are used when the acronym would be used as a word in spoken language as for instance PCF and PMD over "photonic crystal fiber" and "polarization mode dispersion", respectively. Acronyms that are not used in spoken language, like MFD for mode-field diameter, are not used in the body text.

Finally, I would like to thank my colleagues at Crystal Fibre A/S. Especially, Niels Asger Mortensen and Jacob Riis Folkenberg, who have both been a great inspiration, and Christian Jacobsen and Harald R. Simonsen for sharing their expertise on production related issues.

Project data

The project has been carried out in collaboration between Crystal Fibre A/S and the COM center at the Technical University of Denmark. The project has received financial support from Erhvervsfremmestyrelsen.

Project info:

Project title (Danish):	"Dæmpning i fotoniske krystalfibre"
Project title (English):	"Attenuation in photonic crystal fibers"
Period of project:	01.04.2001 – 31.03.2004
Field of subject:	Optics

Ph.D. candidate:

Title:	M.Sc.
Name:	Martin Dybendal Nielsen
Telephone number (company):	(+45) 43 48 28 19
E-mail:	mdn@crystal-fibre.com

Company:

Name:	Crystal Fibre A/S
Address:	Blokken 84
Zip code:	3460 Denmark
City:	Birkerød
Telephone number:	(+45) 43 48 28 00
Fax number:	(+45) 43 48 28 01
Web site:	www.crystal-fibre.com

Company supervisor:

Title:	Cand.Scient., Ph.D.
Name:	Harald R. Simonsen
Phone number:	(+45) 43 48 28 12
E-mail:	hrs@crystal-fibre.com

University:

Name:	Technical University of Denmark
Institute:	COM
Address:	Technical University of Denmark, Ørsteds plads 345
Zip code	2800 Denmark
City:	Kgs. Lyngby
Telephone number:	(+45) 45 25 63 52
Web site	www.com.dtu.dk

The university supervisor:

Title:	Professor, Dr.Techn.
Name:	Anders Bjarklev
Telephone number:	(+45) 45 25 38 09
E-mail:	ab@com.dtu.dk

List of appended publications

Appended publications listed in order of appearance.

Paper A. **M.D. Nielsen,** C. Jacobsen, N.A. Mortensen, J.R. Folkenberg, and H.R. Simonsen: "*Low-loss photonic crystal fibers for data transmission and their dispersion properties*", Accepted for Opt. Express, (2004).

Paper B. N.A. Mortensen, J.R. Folkenberg, **M.D. Nielsen**, and K.P. Hansen "*Modal cut-off and the V-parameter in photonic crystal fibers*", Opt. Lett. **28**, 1879, (2003).

Paper C. **M.D. Nielsen** and N.A. Mortensen "*Photonic Crystal Fiber design based on the V-parameter*", Opt. Express **11**, 2762, (2003).

Paper D. N.A. Mortensen, **M.D. Nielsen**, J.R. Folkenberg, K.P. Hansen, J. Lægsgaard, "*Small-core photonic crystal fibers with weakly disordered air-hole claddings*", J. Opt. A: Pure. Appl. Opt. **6**, 221, (2004).

Paper E. **M.D. Nielsen,** N.A. Mortensen, J.R. Folkenberg, and A. Bjarklev "*Mode Field Radius of Photonic Crystal Fibers Expressed by the V-parameter*", Opt. Lett. **28**, 2309, (2003).

Paper F. **M.D. Nielsen**, G. Vienne, J.R. Folkenberg, and A. Bjarklev *"Investigation of micro deformation induced attenuation spectra in a photonic crystal fiber"*, Opt. Lett. **28**, 236 (2003).

Paper G. **M.D. Nielsen**, N.A. Mortensen, and J.R. Folkenberg, *"Reduced micro-deformation attenuation in large-mode area photonic crystal fibers for visible applications"*, Opt. Lett. **28**, 1645 (2003).

Paper H. **M.D. Nielsen,** N.A. Mortensen, M. Albertsen, J.R. Folkenberg, A. Bjarklev, and C. Dominica, "*Predicting macrobending-loss for large-mode area photonic crystal fibers*" submitted for Opt. Express (2004).

Paper I. **M.D. Nielsen**, J.R. Folkenberg, N.A. Mortensen, and A. Bjarklev: "*Bandwidth comparison of photonic crystal fibers and conventional single-mode fibers*" Opt. Express **12**, 430, (2004).

Paper J. **M.D. Nielsen**, J.R. Folkenberg and N.A. Mortensen "*Photonic Crystal Fiber with an effective area of 600 μm^2 and low bending loss*" Electron. Lett. **39**, 1802, (2003).

Paper K. N.A. Mortensen, **M.D. Nielsen**, J.R. Folkenberg, A. Petersson, and H.R. Simonsen, *"Improved large-mode area endlessly single-mode photonic crystal fibers"*, Opt. Lett. **28**, 393 (2003).

Paper L. N.A. Mortensen, **M.D. Nielsen**, J.R. Folkenberg, C. Jacobsen, and H.R. Simonsen, "*Photonic Crystal Fiber with a Hybrid honeycomb cladding*", Opt. Express **12**, 468, (2004).

Paper M. J.R. Folkenberg, **M.D. Nielsen**, N.A. Mortensen, C. Jacobsen, and H.R. Simonsen, "*Polarization Maintaining Large-mode area Photonic Crystal Fiber*", Opt. Express **12**, 956, (2004).

List of not appended publications

This section contains a list of publications written as part of this work but not appended to this thesis.

Journal publications:

1. B. Zsigri, C. Peucheret, **M.D. Nielsen**, and P. Jeppesen, *"Transmission over 5.6 km large effective area and low-loss (1.7 dB/km) photonic crystal fibre"* Electron. Lett. **39**, 796, (2003).

2. C. Peucheret, B. Zsigri, P.A. Andersen, K.S. Berg, A. Tersigni, P. Jeppesen, K.P. Hansen, and **M.D. Nielsen,** "*40 Gbit/s transmission over photonic crystal fibre using mid-span spectral inversion in a highly nonlinear photonic crystal fibre*", Electron. Lett. **39**, 919, (2003).

3. T.P. Hansen, J. Broeng, C. Jakobsen, G. Vienne, H.R. Simonsen, **M.D. Nielsen**, P.M.W. Skovgaard, J.R. Folkenberg, and A. Bjarklev, "*Air-guiding photonic Bandgap fibers: Spectal properties, macrobending loss and practical handling*", J. Lightwave Technol. **22**, 11, (2003).

4. N.A. Mortensen and **M.D. Nielsen**, "*Modeling of realistic cladding structures for photonic band-gap fibers*", Opt. Lett. **29**, 349, (2004).

Conference contributions:

5. K.P. Hansen, **M.D. Nielsen**, T.P. Hansen, T. Sorensen, J. Broeng, S.B. Libori, H.R. Simonsen, J.R. Jensen, and A. Bjarklev, *"Novel design properties of photonic crystal fibers"* DOPS-NYT **16**, 16 (2001).

6. **M.D. Nielsen**, G. Vienne, J.R. Jensen and A. Bjarklev: "*Modeling Birefringence in isolated elliptical core photonic crystal fibers*" 14th annual meeting of the Laser and Electro-Optics Society LEOS 2001, (San Diego, CA, USA, 2001).

7. S.E.B. Libori, A. Bjarklev, J. Broeng, **M.D. Nielsen**, K.P. Hansen: "*Recent Development on Photonic Crystal Fibres*" Conference Digest 6th optical fibre measurement conference OFMC´01, pp 83-88, (Cambridge, UK, 2001).

8. **M.D. Nielsen**, A. Petersson, C. Jacobsen, H.R. Simonsen, G. Vienne, and A. Bjarklev, *"All-silica photonic crystal fiber with large mode area"* 28th

European Conference on Optical Communication ECOC´ 02 (Copenhagen, Denmark, 2002).

9. A. Bjarklev, K.P. Hansen, T.P. Hansen, K. Hougaard, E. Knudsen, S.E.B. Libori, J. Lægsgaard, **M.D. Nielsen**, J.Riishede, and T.T. Larsen, *"Photonic crystal fibres - the state-of-the-art"* 28th European Conference on Optical Communication ECOC´ 02, invited paper (Copenhagen, Denmark, 2002).

10. **M.D. Nielsen**, N.A. Mortensen, J.R. Folkenberg, A. Petersson, and A. Bjarklev, *"Improved All-Silica Endlessly Single-Mode Photonic Crystal Fiber"*, Optical Fiber Communications Conference OFC´03 (Atlanta, Georgia, USA, March 2003).

11. T.P. Hansen, J. Broeng, C. Jakobsen, G. Vienne, H.R. Simonsen, **M.D. Nielsen**, P.M.W. Skovgaard, J.R. Folkenberg, and A. Bjarklev, *"Air-guidance over 345 m of large-core photonic bandgap fiber"* Optical Fiber Communication Conference OFC'03, Post Deadline paper (Atlanta, Georgia, March 2003).

12. C. Peucheret, B. Zsigri, P.A. Andersen, K.S. Berg, A. Tersigni, P. Jeppesen, K.P. Hansen, and **M.D. Nielsen**, *"Transmission over photonic crystal fiber at 40 Gbit/s using mid-span spectral inversion in a highly nonlinear photonic crystal fiber",* Conference on Lasers and Electro Optics CLEO´03, Post deadline paper (Baltimore, MD, June 2003).

13. **M.D. Nielsen**, N.A. Mortensen, J.R. Folkenberg, K.P. Hansen, and A. Bjarklev, *"Optical Properties of Photonic Crystal Fibers Expressed by the V-parameter"*, 29th European Conference on Optical Communication ECOC´03 (Rimini, Italy, September 2003).

14. J. Lægsgaard, K.P. Hansen, **M.D. Nielsen**, T.P. Hansen, J. Riishede, K. Hougaard, T. Sørensen, T.T. Larsen, N.A. Mortensen, J. Broeng, J.B. Jensen and A. Bjarklev, "*Photonic Crystal Fibers*", Invited paper, 10th international microwave and optoelectronics conference IMOC'03 (Foz do Igacu, Brazil, September 2003).

15. J. Lægsgaard, S.E.B. Libori, K. Hougaard, J. Riishede, T.T. Larsen, T. Sørensen, T.P. Hansen, K.P. Hansen, **M.D. Nielsen**, J.B. Jensen, and A. Bjarklev, "*Dispersion Properties of Photonic Crystal Fibers - Issues and opportunities*", 2003 MRS Fall Meeting, invited paper (Boston, USA, December 2003).

16. J. Broeng, G. Vienne, A. Petersson, P.M.W. Skovgaard, J.R. Folkenberg, **M.D. Nielsen**, C. Jakobsen, H.R. Simonsen, and N.A. Mortensen, "*Air-clad photonic crystal fibers for high power single-mode lasers*", Proceedings of the SPIE **5335**, 192 (2004)

17. P.A. Andersen, B. Zsigri, C. Peucheret, P. Jeppesen, K.P. Hansen, and **M.D. Nielsen**, "*Photonic Crystal Fibers used in a Multi-Wavelength Source and as Transmission Fiber in a WDM System*" Accepted for Conference on lasers and electro optics 2004 - CLEO (2004)

18. J. Broeng, P.M.W. Skovgaard, A. Petersson, J.R. Folkenberg, C. Jacobsen, H.R. Simonsen, **M.D. Nielsen**, T.P. Hansen, and K.P. Hansen, "*Recent progress on photonic crystal fibers for high-power laser applications*", 17 th Annual meeting of Lasers and Electro-Optics Society LEOS, Invited paper (2004)

19. B. Zsigri, C. Peucheret, **M.D. Nielsen**, and P. Jeppesen, "*Transmission over 57.6 km of photonic crystal fiber*", submitted for EOCC (2004)

Book Chapter:

20. **M.D. Nielsen**: "*All-silica large-mode area Photonic crystal fibers*", Optical and fiber communications reports (2004), Ed. Anders Bjarklev, Springer Verlag, New York – *to appear*.

Patents:

21. **M.D. Nielsen**, P.M.W. Skovgaard, J. Broeng, E. Knudsen, J.B. Bevensee, "*Optical waveguide, method of its production, and its use*", WO3100488 (2004)

22. **M.D. Nielsen**, T. Søndergaard, A. Bjarklev, J. Broeng, S.E.B. Libori "*Dispersion manipulating fiber*", WO0212931 (2002)

23. J.R. Folkenberg, M**.D. Nielsen**, and N.A. Mortensen "*Title to be announced*" Patent application (2003)

List of symbols and acronyms

Symbols:

a	:	*Core radius of a conventional step-index fiber*
c	:	*Speed of light*
d	:	*Diameter of air hole*
D	:	*Cladding diameter*
D_{coat}	:	*Coating diameter*
D_w	:	*Waveguide dispersion*
$E(x,y,z)$	:	*Electric field in Cartesian coordinates*
E_c	:	*Elastic modulus of the coating material*
E_f	:	*Elastic modulus of the fiber material*
L_B	:	*Beat length between two modes (same as coupling length)*
n	:	*Mode index*
n_{cl}	:	*Refractive index of a homogeneous cladding of an arbitrary waveguide*
n_{co}	:	*Highest refractive index in the core of an arbitrary waveguide*
n_{FSM}	:	*Effective refractive index of the fundamental space-filling mode*
$Q(\Omega)$	:	*Deformation power spectrum at the fiber surface*
R	:	*Bend radius*
R_C	:	*Critical bend radius*
$T(\Omega)$	:	*Parameter accounting for the thickness of the coating layer*
v_g	:	*Group velocity*
v_p	:	*Phase velocity*
V_{PCF}	:	*V-parameter for the PCF*
V_{SIF}	:	*V-parameter for a conventional step-index fiber*
w_{PCF}	:	*Equivalent mode-field radius of a photonic crystal fiber*
w_{SIF}	:	*Mode-field radius of a conventional step-index fiber*
z_c	:	*Coupling length between two modes (same as beat length)*
Δn	:	*Difference in mode index between two modes*
$\Delta\beta$	:	*Difference in propagation constant between two modes*
Λ	:	*Hole to hole center spacing*
Ω	:	*Spatial deformation frequency*
β	:	*Propagation constant*
β_{FSM}	:	*Propagation constant of the fundamental space-filling mode*
$\beta_{max,cl}$	:	*Maximal allowed propagation constant in the cladding region*

$\beta_{max,co}$	:	*Maximal allowed propagation constant in the core region*
δ	:	*Thickness of coating layer*
κ	:	*Parameter accounting for the elasticity of the coating material*
λ	:	*Free-space optical wavelength*
$\theta(\Omega)$	:	*Displacement power spectrum at the fiber axis*
ω	:	*Angular frequency of the electrical field*

Acronyms:

CVD	:	*Chemical vapor deposition*
FSM	:	*Fundamental space-filling mode*
GVD	:	*Group velocity dispersion*
LMA	:	*Large mode area*
MCVD	:	*Modified chemical vapor deposition*
MFD	:	*Mode field diameter*
PCF	:	*Photonic crystal fiber*
PMD	:	*Polarization mode dispersion*
PSCF	:	*Pure silica core fiber*
VAD	:	*Vapor-phase axial deposition*

Table of contents

Abstract i

Resume (Danish) iii

Author's notes v

Project data vii

List of appended publications ix

List of not appended publications xi

List of symbols and acronyms 15

1 Introduction 1

2 Basic properties 5

2.1 PCFs with triangular-lattice cladding structures 5
2.2 Guiding mechanism 6
2.3 Wavelength dependency of the effective refractive indices 9
2.4 Introduction of the V-parameter 12
2.5 Single-mode criterion 13
2.6 Mode-field diameter 16

3 Waveguide related attenuation 19

3.1 Generalized low-loss criterion 19
3.2 Micro-deformation induced attenuation 20
3.3 Periodic micro deformations 22
3.4 Random micro deformations 23
3.5 Macro-bending induced attenuation 25
3.6 Design space of large-mode area PCFs 27

4 Fabrication related attenuation 29

4.1 Reported attenuation levels 29
4.2 Fabrication Techniques 30
4.3 Contamination and surface roughness 32
4.4 OH contamination in silica glass 33
4.5 Defect centers in silica glass 35
4.6 Results of optimized fabrication process 37

5 Examples of large-mode area PCFs 39

5.1 Single-mode PCF for visible light applications 39
5.2 Large-mode area PCF for telecom wavelengths 40

5.3 Triangular core large-mode area PCF 42
5.4 Large-mode area PCF with fluorine doped cladding 44
5.5 Polarization maintaining large-mode area PCF 45
6 Conclusion and Outlook 49

References 53

1 Introduction

With the inventions of the optical fiber and the laser in the second half of the 20th century, the basic elements for one of the most significant and important technological achievements of modern society were realized. The high-bandwidth optical communication systems which span the globe today have drastically affected people's everyday life as well as paved the way for the development of many areas such as trade, the financial sector as well as the political and cultural debate. Most of the technological improvements accomplished on the communication systems, from the first optical communication links to the high-bandwidth systems of present time, have been driven by the continuing development of ultra-fast electronics for transmitters and receivers along with the multiplexing of several wavelength channels on a single fiber. Also the deployment of specialty fiber, such as Erbium-doped fibers for optical amplification and dispersion compensating fibers for coping with pulse spreading, has been essential steps forward. However, the one thing which has not changed much is the transmission fiber itself. The changes made to the fiber must be considered as minor and, besides slight changes in the design of the index profile allowing for the shifting of the zero-dispersion wavelength, it has been a matter of perfecting production rather than fundamentally changing the fiber itself.

With the proposal of the photonic crystal fiber in 1996 [1], the first steps towards the greatest revolution within the field of fiber optics were taken. Within a relatively short period of time it became obvious that photonic crystal fibers could be realized with novel properties compared to those known from conventional solid fibers. Among others, these include fibers that guide light only in the fundamental mode regardless of wavelength referred to as endlessly single-mode fibers [2], and the possibility for guiding of light in an air core based on the photonic bandgap effect [3]. These properties could, in theory, help to overcome limitations of conventional transmission fibers such as the single-mode bandwidth and nonlinear performance. For the first time, a serious alternative for the realization of an optical fiber was laid out and the challenge was picked up by numerous groups from Europe, the United States and Asia, representing both the well-established companies from conventional fiber technology as well as small start-up companies spun out of universities.

Unfortunately, the new millennium was followed by the burst of the bobble causing an economical depression in the telecom sector and over night the driver for the development of photonic crystal fibers seemed to have disappeared.

However, the novel properties of the photonic crystal fiber have turned out to stand the test of economical hardship and found applications in many other technological areas than telecommunication. The lowering of the nonlinear threshold by tight mode confinement, useful for generation of broad super continuums [4], and the degree at which the refractive index profile can be controlled have evolved into some of the well established trademarks of photonic crystal fiber technology. Also, the endlessly single-mode fibers and the air core fibers originally intended for telecommunication have found other applications. Currently, high-power fiber lasers aiming for kW-operation [5] and wideband light sources [6] are both part of the growing research area of photonic crystal fibers with potential for commercialization.

The broad aim of the work presented in this thesis is to investigate the attenuation properties of photonic crystal fibers. Clearly, the attenuation is a central parameter for most waveguides although the requirements depend on the specific application. In the low-power limit, low attenuation is important in order to have an acceptable signal-to-noise ratio and in the extreme high-power limit, attenuation is critical due to the thermal load. This thesis deals with the large-mode area photonic crystal fiber since this is the strongest candidate for a low-loss photonic crystal fiber for data transmission. The potential of the air-core fiber is still an open question and the development in this area has only recently started to pick up speed [7,8]. At the beginning of this work in 2001, the large-mode area photonic crystal fiber had already been experimentally demonstrated [9]. However, besides the significant endlessly single-mode property, almost nothing had been reported on the detailed optical properties such as single-mode conditions, mode-field diameter and group velocity dispersion. The work described in this thesis addresses these issues along with investigation of the attenuation characteristics such as waveguide related attenuation, intrinsic attenuation and fabrication induced attenuation.

The character of the work has been both theoretical, experimental, and production oriented. The theoretical work has been based on numerical simulations carried out to investigate the fundamental optical properties of the

fibers. For the numerical work, a freely available software package, named MIT Photonic Bands (MPB), based on the plane-wave expansion method [10], has been applied. The experimental work has been aimed at characterization of fabricated fibers including the development of measurement techniques. The fabrication aspect has primarily been to reduce the attenuation arising from the fabrication process. This has included a thorough investigation of each step in the fabrication process and in this thesis the most critical aspects are pointed out.

The thesis consists of 13 papers and an introducing text. Each paper has been carried out as a part of this work and covers a specific topic. The purpose of the introducing text is to provide the necessary background for the appended papers and to put them into a clear context.
In chapter 2, the generalized fiber structure considered throughout most of this work is introduced. The chapter contains the results from the study of the basic properties including central issues such as single-mode criteria, parameter dependency of the mode-field diameter, dispersion properties and mode profiles. An overall goal of this work has been to provide expressions which are easy to evaluate, and to present the reader with proper design guidelines for optimized operation.

In chapter 3, description of the relevant attenuation contributions related to waveguide imperfections are given. This includes both periodic and non-periodic micro deformations as well as macro-bending induced attenuation. In addition to the description of these issues, design guidelines for minimizing their influence are discussed.

In chapter 4, the most basic aspects of fiber fabrication are covered. The fabrication procedure is described with emphasis on the issues critical to the attenuation level of the final fiber. This includes descriptions of OH-contamination, drawing induced defects, general contamination, and what can be done to deal with these aspects.

In chapter 5, widely different large-mode area fibers developed as part of this work are presented. This includes fibers for visible light applications, fibers optimized for the telecommunication band, alternative design directions, and, finally, a polarization-maintaining large-mode area photonic crystal fiber.

2 Basic properties

Photonic crystal fibers (PCFs) have been realized in a large variety. In this chapter, the basic properties of the central fiber type in this work – the triangular cladding PCF – are introduced. This includes general issues such as the guiding mechanism but also results of this work including single-mode properties, mode-field diameter relations and dispersion dependency.

2.1 PCFs with triangular-lattice cladding structures

The majority of the fibers considered throughout this work are single-material fibers made of pure silica. They all have a solid core region surrounded by a microstructured cladding region consisting of a triangular arrangement of air holes running along the full length of the fiber. The cladding structure is characterized by the air-hole diameter, d, the hole-to-hole center spacing referred to as the pitch, Λ, and the number of air holes, typically expressed by the number of periods around the core. The core region is realized by omitting one or more of the central air holes in the otherwise periodic structure thereby creating a high-index defect. Most of the fibers presented have core regions corresponding to a single omitted air hole.

All fibers in this work have a single-layer coating in order to protect the fiber against mechanical damage and to screen the waveguide from external perturbations. Furthermore, the coating has the property of stripping off unwanted light in the cladding and is therefore chosen to have a higher refractive index than that of silica. In Figure 2.1, a schematic drawing of such a PCF is shown with a cladding diameter, D, and a coating layer with diameter, D_{coat}.

Dependent on the relative air-hole diameter, d/Λ, and the free-space optical wavelength, λ, relative to Λ, referred to as to normalized wavelength, λ/Λ, this simple structure comprises a broad range of fiber types. In the case where $\lambda \sim \Lambda$, the resulting small structures along with the tight confinement offered by relatively large air holes, such as $d/\Lambda > 0.5$, can lead to small effective areas of the guided mode and thereby to a high nonlinear coefficient. These fibers are therefore referred to as highly nonlinear PCFs and have the possibility to be realized with unique dispersion properties. These include flat

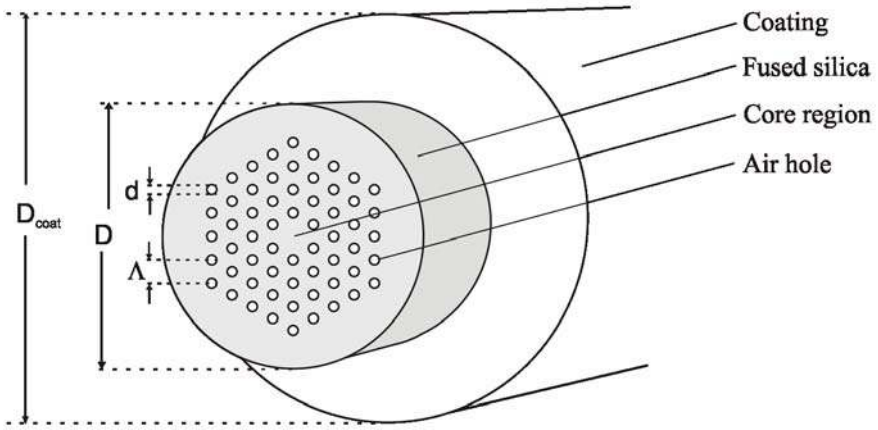

Figure 2.1 ***A schematic drawing of a PCF with a cladding structure consisting of a triangular arrangement of air holes.***

near-zero dispersion over broad wavelength ranges [11,12] and the possibility for realizing a zero-dispersion wavelength below the zero-material dispersion wavelength of silica [4,13].

The fiber designs considered in this work all have a $\lambda << \Lambda$ and, typically, d/Λ is between 0.4 and 0.5. This leads to large effective areas of the guided mode and these fibers are therefore referred to as large-mode area (LMA) fibers.

2.2 Guiding mechanism

One of the initial drivers for the interest in PCFs was the demonstration of the photonic bandgap (PGB) effect [3] allowing for the guiding of light in an air core surrounded by a periodic cladding structure. The periodic cladding structure can be designed to exhibit bandgaps such that light within the range of these bands launched in the core region is confined here. As indicated in Figure 2.1, the PCFs considered in this work also have a periodic cladding structure but in contrast to the photonic bandgap fibers the guiding mechanism does not rely on the strict periodicity of the air holes. The guiding mechanism of these fibers is based on the difference in effective refractive index between the core and the cladding region in much the same way as known from conventional solid-fibers. For this reason, this type of PCF is often said to rely on modified total-internal

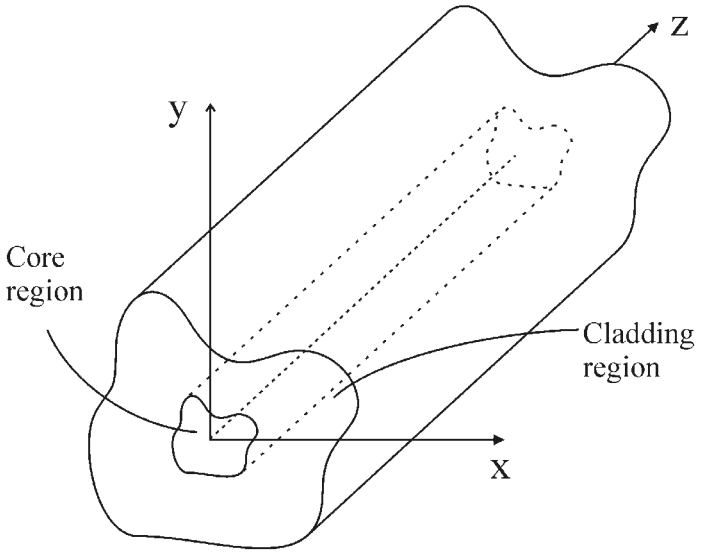

Figure 2.2 ***Generalized drawing of a waveguide invariant in the z-direction comprised of an arbitrarily shaped core region surrounded by a cladding region.***

reflection (M-TIR). However, as the word "modified" indicates, total-internal reflection is not a satisfactory description since no strict boundary between the core and the cladding can be defined and because the assumptions of geometrical optics are not valid for single-mode fibers where diffraction plays a central role. This is also the case for standard single-mode fibers and geometrical optics should, strictly speaking, only be used for description of multi-mode fibers.

Consider instead an arbitrary waveguide as shown in Figure 2.2 with a core region surrounded by a cladding region which, in principle, extends to infinity. The highest refractive index of the core is n_{co}, the cladding has the refractive index, n_{cl}, and the waveguide is invariant in the z-direction.

Because of the longitudinal invariance, an electric field, $E(x,y,z)$, propagating in the positive z-direction with a propagation constant, β, and frequency, ω, can be written as [14]:

$$E(x,y,z) = E(x,y)\exp(i\beta z - i\omega t) \tag{2-1}$$

The wave described by Eq. (2-1) propagates with a velocity, $v_p = \omega/\beta$, referred to as the phase velocity while the velocity at which energy (a wave packet) propagates along the waveguide is referred to as the group velocity, $v_g = d\omega/d\beta$. Inserting Eq. (2-1) in Maxwell's equations leads to an eigenvalue equation in β, and for a given refractive index profile, allowed β-values can be found as function of λ or ω.

If a solution to the wave equation for propagation in a non-absorbing material has a real propagation constant, the propagation is lossless and the mode is referred to as a bound mode. The phase velocity of a mode propagating in the core region cannot exceed the maximum speed of light in the cladding, c/n_{cl}, without loosing power. The minimum speed of light in the core is given by c/n_{co} and the requirement for a bound mode can therefore be formulated as $c/n_{cl} > v_p > c/n_{co}$ which can be written as $n_{cl} < c\beta/\omega < n_{co}$, where $c\beta/\omega$ is referred to as the effective index of the propagating mode or the mode index.

Because of the broad interest in the bandgap guidance it is interesting to note that conventional fibers and index-guiding PCFs also can be understood using a bandgap argument. The minimum phase velocity of the core region is, for a given frequency, ω, equivalent to a maximum propagation constant, $\beta_{max,co} = \omega n_{co}/c$. For larger propagation constants, the core region exhibits a semi-infinite bandgap. In the same way, there is a maximum propagation constant allowed in the cladding region, $\beta_{max,cl} = \omega n_{cl}/c < \beta_{max,co}$. There will therefore be a range of propagation constants $\beta_{max,cl} < \beta < \beta_{max,co}$, at a given ω, allowed in the core region but forbidden in the cladding in just the same way as for the photonic bandgap fiber.

These arguments of the guiding mechanism only assume that the cladding region at a fixed wavelength can be viewed as a homogeneous infinite cladding material referred to as the effective index approximation. The cladding mode with the largest propagation constant for a given frequency is referred to as the fundamental space-filling mode (FSM) and the corresponding effective index is denoted n_{FSM}. Thus, a mode with an effective index, n, can be guided in the core region provided that $n_{co} > n > n_{FSM}$.

In most cases, the effect of the finite cladding structure of a real fiber is only a small perturbation. However, for a single-material fiber, where the refractive index of the core region is the same as beyond the microstructured cladding region, there will be a certain leakage of power from the core through the cladding being absorbed in the coating material. All guided modes will

therefore have complex propagation constants and exhibit some degree of intrinsic attenuation also referred to as leakage loss or confinement loss [15]. The effect is comparable to a tunneling process where the cladding functions as a boundary for the light propagating in the core and the decay rate is dependent on the width and depth of the boundary. Therefore, confinement loss generally decreases as d/Λ is increased, corresponding to a higher barrier, and as Λ/λ and the number of air holes are increased, corresponding to a wider barrier. For a large-mode area PCF, where $\Lambda >> \lambda$, confinement loss is, typically, not a problem for designs with more than 3-4 periods of air holes and the confinement loss can in this case be orders of magnitude lower than the intrinsic material absorption.

This is in contrast to nonlinear fibers for which confinement loss can be quite problematic and require many periods of air holes for acceptable attenuation levels [16]. For completeness it should be mentioned that confinement loss is not a unique phenomenon for PCFs. Most optical fibers have a high-index coating in order to strip of possible cladding modes and the refractive index of the coating is typically higher than that of the core causing leakage loss [17] and in a pure silica core fiber with an outer cladding of fluorine doped silica, leakage loss can also be observed [18,19].

2.3 Wavelength dependency of the effective refractive indices

According to the description of the guiding mechanism, the properties of the PCF at a fixed wavelength are not very different to those of the conventional single-mode fiber. However, the effective index of the microstructured cladding region is strongly dependent on the normalized wavelength, λ/Λ. At small λ/Λ, the field resolves the microstructure and avoids the air regions leading to a mode index close to that of the background material both for the fundamental mode and the fundamental space-filling mode. In the other extreme, $\Lambda < \lambda$, the field can no longer resolve the structure and the effective index approaches an average of the refractive index of the background material and air weighted with the air filling fraction.

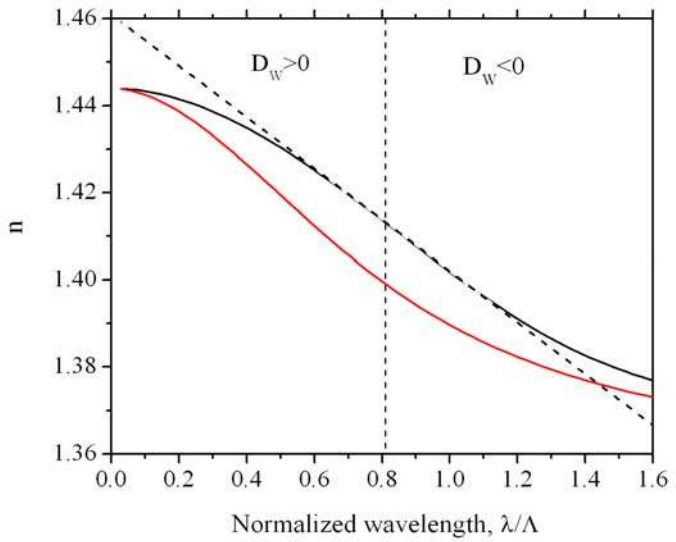

Figure 2.3 ***Mode index of the fundamental mode and the fundamental space-filling mode for d/Λ = 0.44 indicated by the solid black and red line, respectively. The point of zero waveguide dispersion is indicated by the dashed lines also showing the regions of positive and negative DW.***

For both short and long wavelengths, the effective index of core and cladding will therefore asymptotically approach constant values and the mode spacing will approach zero. In Figure 2.3, the numerically calculated effective index for the fundamental mode and the fundamental space-filling mode of a triangular cladding PCF with $d/\Lambda = 0.44$ is shown. This strongly dispersive nature of the indices is in contrast to that of conventional solid fibers where both core and cladding consists of a homogenous material with an approximately constant refractive index.

In an optical waveguide, the group velocity will depend on the wavelength. This effect is referred to as the group-velocity dispersion (GVD). The group-velocity dispersion is defined as the differential change in the time of flight pr. unit length as function of wavelength. With good approximation the group-velocity dispersion can be calculated as the sum of the material dispersion and the waveguide dispersion, D_w, calculated for a fixed refractive index, provided that $\Lambda >> \lambda$ [20]. The waveguide dispersion is given by Eq. (2-2) where n is the mode index calculated for a constant refractive index.

$$D_w \equiv \frac{d}{d\lambda}\left(\frac{1}{v_g}\right) = \frac{d}{d\lambda}\left(\frac{d\beta}{d\omega}\right) = -\frac{\lambda}{c}\frac{d^2 n}{d\lambda^2} \tag{2-2}$$

The waveguide dispersion is thus related to the 2. derivative of the mode index with respect to wavelength and thereby to the curvature of the index curves shown in Figure 2.3. For the fundamental mode, the point of zero curvature is indicated by the dashed lines. At shorter λ/Λ, the curvature is negative and $D_w > 0$, while $D_w < 0$ for larger values of λ/Λ where the curvature is positive. Since $\lambda << \Lambda$ in the large-mode area limit, D_w will in these fibers always be positive and decreasing as λ/Λ approaches zero.

In the case of large-mode area fibers for data transmission, the group-velocity dispersion at 1550 nm plays a central role and was therefore studied as a part of this work. A significant result of this study is that there is a unique relation between the group-velocity dispersion and the mode-field diameter regardless of d/Λ. This is illustrated in Figure 2.4 where both calculated and measured group-velocity dispersion data are shown. Since the effective area and the dispersion are among the most important parameters for a transmission fiber, the relation between the two is very useful. Further details on this work are given in Paper A.

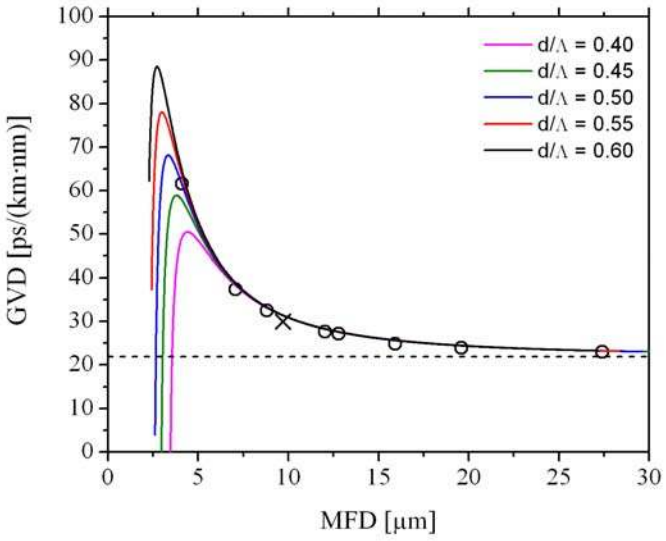

Figure 2.4 ***Calculated (solid lines) and measured (circles) group-velocity dispersion as function of mode-field diameter for a broad range of d/Λ values. The cross indicates measured data from an independent publication*** *[21]* ***(figure from*** *Paper A****).***

2.4 Introduction of the V-parameter

Due to the fact, that analytical descriptions of the PCF must be considered quite difficult it has not proven to be possible to arrive at analytical expressions for relevant fiber parameters such as the single-mode criteria, the mode-field diameter or dispersion characteristics. Even for a simple step-index fiber, analytical descriptions are limited and empirical relations have traditionally been employed [22-24]. This has also been the approach of this work and inspired by the expressions for conventional solid fibers, a V-parameter for the PCF has defined by the following expression:

$$V_{PCF} = \Lambda\sqrt{\beta^2 - \beta_{FSM}^2} \tag{2-3}$$

Here, β and β_{FSM} are the propagation constants of the fundamental mode and the fundamental space-filling mode, respectively. This parameter is in fact more closely related to the W-parameter of conventional fibers also referred to as the cladding parameter for bound modes [14]. From an intuitive point of view, this parameter is the product of the defect size and the spacing between the guided mode and the delocalized FSM. Thus, the larger V_{PCF}, the more modes are likely to be guided.

In Figure 2.5, V_{PCF} as defined in Eq. (2-3) is plotted as function of Λ/λ for d/Λ ranging from 0.30 to 0.70 in steps of 0.05. For small values of Λ/λ corresponding to the nonlinear limit, V_{PCF}, is strongly wavelength dependent whereas it approaches a constant level dependent on d/Λ in the large-mode area limit. Since V_{PCF} is intuitively related to the number of guided modes, the curves in the Figure 2.5 indicate that the PCF only supports a finite number of modes regardless of the optical wavelength and the number of modes decreases with d/Λ. This observation illustrates the endlessly single-mode property which refers to the case where the upper limit on the number of modes equals one and only the fundamental mode is guided regardless of the optical wavelength. Further details on Eq. (2-3) are given in Paper B.

Provided that Eq. (2-3) can describe optical properties of the PCF, the practical applicability of the expression is limited since β and β_{FSM} can only be evaluated numerically. Therefore, as a part of this work, a set of empirical relations expressing V_{PCF} as function of d/Λ and λ/Λ have been derived.

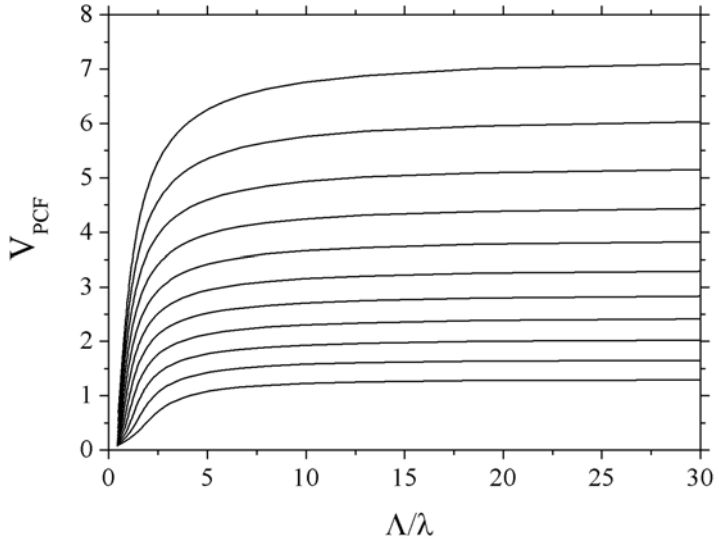

Figure 2.5 ***Calculated VPCF according to Eq.*** *(2-3)* ***as function of*** *Λ/λ* ***(solid lines) for*** *d/Λ* ***ranging from 0.30 (lower curve) to 0.70 (top curve) in steps of 0.05. (Figure from*** *Paper E)*.

The basis for these empirical relations are numerical calculations of β and β_{FSM} as function of λ/Λ for a broad range of d/Λ values. The emperical relations approximate V_{PCF} with a deviation < 3% compared to the numerical results for $\lambda/\Lambda < 2$ and $V_{PCF} > 0.5$. The relations and details of this work are given in Paper C.

2.5 Single-mode criterion

For many applications it is required that a fiber only supports the fundamental mode in order to have diffraction limited beam with good beam quality and to avoid effects such as inter-modal dispersion. However, prediction of the wavelength at which no higher-order modes are guided, referred to as the higher-order mode cutoff, is no simple task because this parameter is very sensitive to structural variations and external perturbations. Even for an ideal fiber, numerical calculations of cutoff are not straight forward since the results are sensitive to the exact modeling of the cladding region. When employing the plane-wave expansion method as done throughout this work, the criterion that the higher-order mode must have an effective index higher than the fundamental

space-filling mode is problematic because the predicted wavelength tends to dependent on the size of the chosen super cell. In other words, it is difficult to obtain convergence for such calculations for numerical methods based on periodic boundary conditions. And alternative criterion is to compare the effective area of the higher-order mode with that of the fundamental mode giving a measure for when the higher-order is guided [25] but also in this case the results are dependent on numerical parameters.

Based on a numerical method referred to as the multipole method [26,27] an alternative definition of cutoff has been suggested [28]. The multipole method takes advantage of the localized nature of the guided modes and expands these in Bessel functions. Due to the relaxed requirements on periodicity, the structure can in principle comprise the entire fiber cross section including the coating layer and the result is in general a complex propagation constant allowing for the determination of confinement loss. When calculating the confinement loss it turns out that there is a sharp transition in the attenuation dependent on the structural parameters which can be interpreted as a higher-order mode cutoff. Based on this criterion, an empirical relation for the boundary between single-mode and multi-mode fibers has been proposed [28]. This boundary have been compared with measurements in the nonlinear limit and good agreement was reported [29].

In this work, the aim has been to describe the single-mode boundary based on the previously introduced V_{PCF}. Based on simple arguments, V_{PCF} can be interpreted as a transverse wave vector, k_T, multiplied with Λ. Furthermore, heuristic arguments for when k_T of the second-order mode can be supported by the core defect lead to the conclusion that V_{PCF} should equal π at the higher-order mode cutoff. In Figure 2.6, the single-mode boundary predicted by the multipole method is shown (solid line) in a λ/Λ vs. d/Λ diagram. The red circles indicate $V_{PCF} = \pi$ calculated from Eq. (2-3). The agreement between the results given by the two cutoff criteria is very good indicating a consistent definition. For $\lambda/\Lambda < 0.1$, fiber will according to Figure 2.6 tend to be either single mode or multi mode regardless of λ/Λ but dependent of d/Λ. This is consistent with Figure 2.5 showing approximately constant values of V_{PCF} in the large-mode area limit only dependent on d/Λ. This behavior also explains the difficulty with calculating a cutoff wavelength since there with good approximation are no such wavelength for a given d/Λ. The fiber is either single mode or multi mode at all wavelengths. More details on these considerations are given in Paper B.

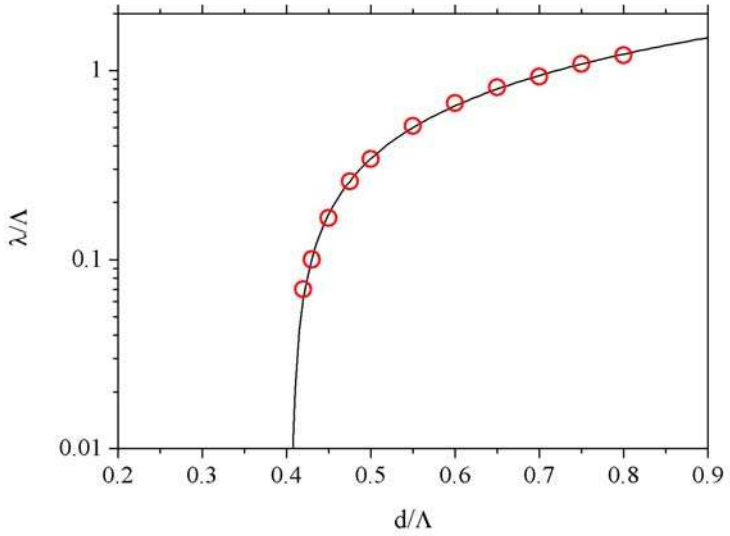

Figure 2.6 ***Single mode boundary plotted in a λ/Λ vs. d/Λ diagram. The solid line corresponds to the boundary predicted by the multi-pole method [28] while the circles indicate calculated values from Eq. (2-3) of VPCF=π.***

When a fiber is to be characterized experimentally as either single-mode or multi-mode, the near field is often inspected while varying the launching conditions of light into the fiber. Figure 2.7 shows an image of the fundamental mode (left) and the first higher-order mode (right) recorded with an infrared camera. The fundamental mode has en overall Gaussian profile with a symmetry in the low intensity tails resembling the hexagonal symmetry of the core region. The higher-order mode has a characteristic double-peak structure with minima in the center. Whereas the intensity distribution of the fundamental mode agrees well with numerically predictions for ideal structures, the higher-order mode does not. As a part of this work, this discrepancy was investigated. For the ideal structure, the higher-order mode has the same symmetry as the fundamental mode. However, small perturbations in the symmetry of the ideal structure cause a splitting of this mode into two nearly degenerate double-peak modes agreeing well with the experimental observations. The details of higher-order mode intensity distributions of ideal, as well as non-ideal, structures are given in Paper D.

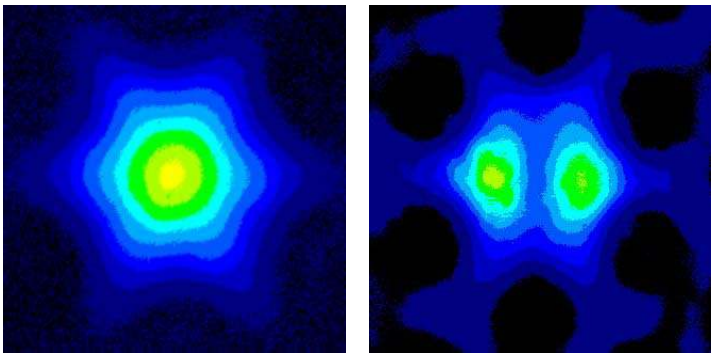

Figure 2.7 ***Near field images of the fundamental mode (left) and a higher-order mode (right) obtained at 1550 nm.***

2.6 Mode-field diameter

The successful description of the single-mode boundary based on the *V*-parameter makes it natural to investigate whether V_{PCF} has a wider validity for the description of the optical properties. A central parameter for most optical fibers in relation to optical nonlinearity, coupling and splicing issues, is the extension of the guided mode often described through the effective area, A_{eff}, or the mode-field diameter. In this work, the mode-field diameter is defined as the $1/e^2$ width of the equivalent Gaussian distribution with the same effective area. For conventional graded-index fibers, the V-parameter is closely related to the mode-field diameter through an empirical relation [24]. In this work it was shown, that the mode-field radius relative to the pitch, w_{PCF}/Λ, is a function of V_{PCF} and independent of the value of d/Λ.

As a result, an empirical function fitted to numerical data with a deviation < 1% for $V_{PCF} > 0.5$ was provided. In Figure 2.8, the w_{PCF}/Λ is plotted as function of V_{PCF} (solid line). In the same plot the corresponding relation for a step-index fiber is shown (dashed line) represented by the mode-field radius normalized with the core radius, w_{PCF}/a as function of the V-parameter for a step-index fiber, V_{SIF}. For both the PCF and the step-index fiber, the position of the higher-order mode cutoff is indicated.

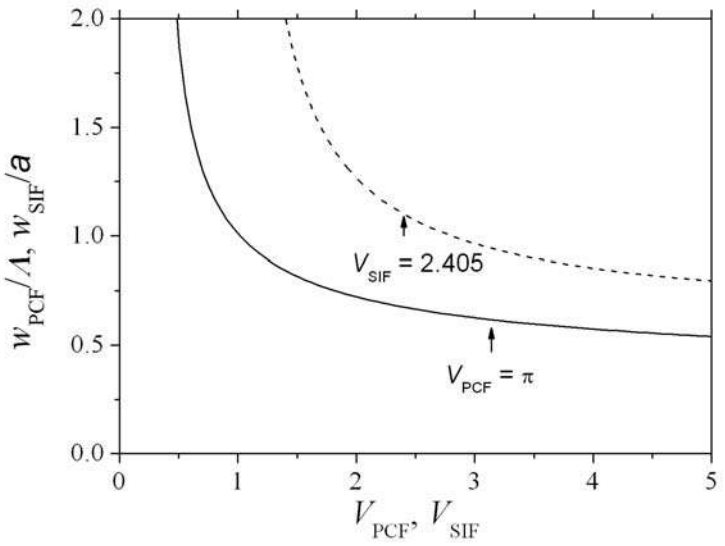

Figure 2.8 ***Normalized mode-field radius, wPCF/Λ, as function of VPCF for the PCF (solid line) and wSIF/a, as function of VSIF for the conventional step-index fiber (dashed line). The arrows indicate the higher-order mode cutoff (Figure from*** *Paper E)*.

The cutoff for step-index fiber is located at a point where w_{PCF}/a starts to increase fast with decreasing V_{SIF}. Since V_{SIF} is proportional to λ^{-1}, an increase in wavelength, relative to the cutoff wavelength, will cause a rapid dispersion of the mode into the cladding region. For the PCF the picture is different. Not only is V_{PCF} almost independent of wavelength in the large-mode area limit, but w_{PCF}/Λ does not depend strongly on V_{PCF} either. As a result, the mode-field diameter of the PCF can be made almost wavelength independent. This is a key point for understanding the enhanced bandwidth properties of PCF over conventional fibers. Further details on this issue are given in Paper E.

In this context it should be emphasized that, generally, the numerical aperture decreases as the mode-field diameter of a single-mode fiber is increased. Since these are uniquely related [30] the expression provided here also indirectly allows for prediction of the numerical aperture. The numerical aperture is important for coupling issues and, generally, for configurations where the fiber is part of an optical system.

3 Waveguide related attenuation

The leaky nature of the PCF guided modes is an example of waveguide related attenuation. However, confinement loss is present even in a perfect waveguide kept absolutely straight and free of any kind of external perturbation. This chapter concerns the attenuating effects of non-ideal waveguides and external perturbations.

3.1 Generalized low-loss criterion

Attenuation caused by non-ideal waveguides and external perturbation can in general be described as scattering loss or mode-coupling loss. Scattering loss becomes dominant when the length scale of non-uniformities, L_n, is longer than the optical wavelength in the material. Coupling loss will occur if L_n is less than the coupling length from the fundamental mode to a radiation mode, z_c. A generalized loss criterion can therefore be formulated as [31]

$$\lambda / n < L_n < z_c \tag{3-1}$$

If L_n is outside this range, attenuation due to non-uniformities can be expected to be small. Scattering loss due to index- and density variations in the glass is referred to as Rayleigh scattering and considered as intrinsic material attenuation. In conventional fibers, additional scattering occurs in the interface between the core and the cladding material. Similarly, scattering can be caused by imperfections in the fused interfaces of the PCF preform (see section 4.2) and at the air-glass interfaces.

Coupling loss is related to mode coupling from the guided mode to a continuum of radiating cladding modes. The coupling length between two such modes, z_c, is also referred to as the beat length, L_B, and given by $L_B = 2\pi/\Delta\beta = \lambda/\Delta n$. Here $\Delta\beta$ and Δn are the difference between the propagation constants and effective refractive indices of the two modes, respectively.

3.2 Micro-deformation induced attenuation

Micro deformations of conventional fibers has been an area of much research [32-36]. The main reason for this interest is that when an optical fiber is put into a cable, the cable will inevitably apply forces in the transverse direction of the fiber thereby inducing micro deformations. This is due to differences in the thermal expansion coefficients of the fiber and the cable material along with roughness of the material interfaces. In the same way, micro deformations can arise from the interface between the cladding and the coating material.
Both from an intuitive point of view and from Eq. (3-1) it is clear that waveguides with a small Δn are more sensitive to non-uniformities since L_B is long. For the large-mode area fibers considered throughout this work L_B of ~1 mm can readily occur causing micro deformation induced attenuation to be an important issue. Based on coupled mode theory, the power loss from the fundamental mode can be expressed as [37]

$$\alpha = \frac{1}{2}\sum_{p=1}^{\infty} C_{1p}^2 \Phi\left(\Delta\beta_{1p}\right) \tag{3-2}$$

In this expression, C_{1p} is the coupling coefficient form the fundamental mode to the p'th cladding mode and $\Phi(\Delta\beta_{1p})$ is the deformation spectrum. From an optical point of view, attenuation is caused by displacements at the fiber axis, referred to as the displacement power spectrum, $\theta(\Omega)$, while the deformations, from a practical point of view, are given by the power spectrum of deformations at the outer surface of the fiber described by $Q(\Omega)$. From elasticity theory, the relation between power spectra $\theta(\Omega)$ and $Q(\Omega)$ can be expressed as [38]

$$\theta(\Omega) = \left[\frac{4\kappa^2 T(\Omega)}{4\kappa^2 T(\Omega) + \Omega^4}\right] Q(\Omega) \tag{3-3}$$

The thickness of the coating material is taken into account through $T(\Omega) = (1+\delta\Omega)e^{-\delta\Omega}$, where δ is the thickness of the coating layer. The elasticity is accounted for through $\kappa = (2/D)(E_c/\pi E_f)^{1/4}$, where D is the fiber diameter and E_c and E_f are the elastic modulus of the coating and fiber material, respectively.

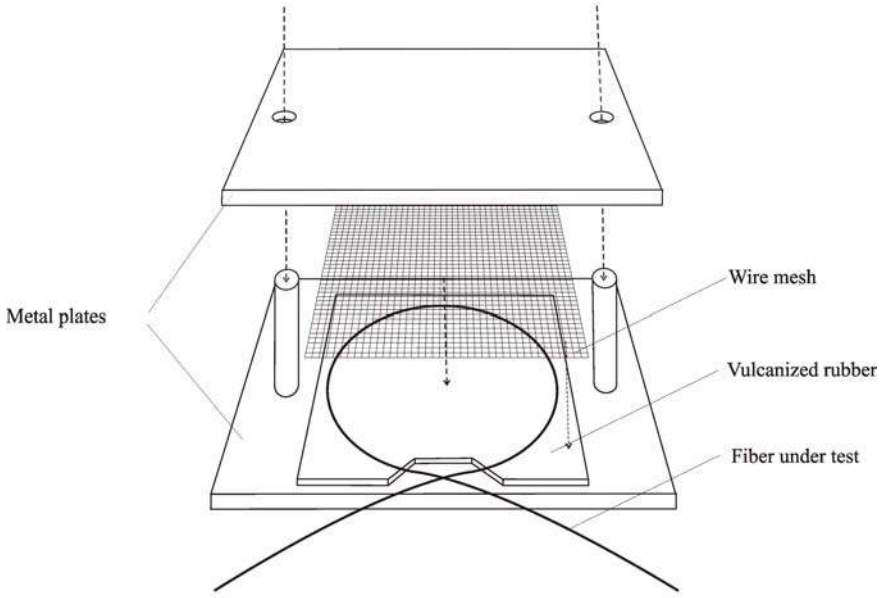

Figure 3.1 ***Deformation device for sensitivity tests and mode-spacing measurements of optical fibers.***

Despite that Eq. (3-3) is based on simplified assumptions, and does not take the microstructure of the fiber into account, it contains the overall correct physics of the mechanical problem.In order to have low loss it should be attempted to have $\theta(\Omega)\rightarrow 0$. This can be obtained for $\kappa \approx 0$, $T \approx 0$ and $\Omega\rightarrow\infty$. Small values of κ are realized by choosing large values of D, corresponding to a thick fiber, and small values of E_c, corresponding to a soft coating material which can effectively absorb deformations. Small values of $T(\Omega)$ can be realized by choosing δ to be large, corresponding to a thick coating layer. In conclusion, the larger the physical dimensions and the softer the coating relative to the glass the better screening of the fiber axis is obtained. Even better screening properties can be obtained with advanced coating schemes typically applying a dual-layer coating consisting of a soft inner coating and a harder outer coating layer.

The approach of this work with respect to investigation of micro deformation has been mostly experimental and based on the general physics of Eq. (3-3). In Figure 3.1, a schematic drawing of a deformation device used in this work to characterize the sensitivity of fibers is shown. The device is constructed in accordance with given standards [39] and consists of two parallel metal plates, a plate of vulcanized rubber, and a rectangular wire mesh with a well-defined period. The fiber under test is placed between the rubber plate and the wire

mesh which are again placed between the metal plates. When a force is applied on the top plate, the fiber is subjected to deformations by the mesh.

3.3 Periodic micro deformations

When placing the fiber parallel to one of the axis of the mesh, a deformation with the period of the mesh is induced. The effect is similar to that of a long period grating resulting in narrow attenuation peaks being observed when L_B is equal to an integer times the grating period. This method can therefore be applied to perform a measurement of the mode spacing between the guided mode and the radiation mode from the spectral position of the peaks and Eq. (3-1). A detailed description of this work is given in Paper F.

In Figure 3.2, a practical example of attenuation induced by a periodic deformation is shown. The figure shows measured spectral attenuation of a large-mode area PCF with a mode-field diameter of 13 μm. The dashed line corresponds to the situation where the fiber is placed in a single layer on a spool while the solid line corresponds to the fiber being placed in two layers. When the second layer is placed on top of the initial layer, deformation of the fiber with a fixed period is introduced. This period depends on the exact spooling conditions and fiber diameter.

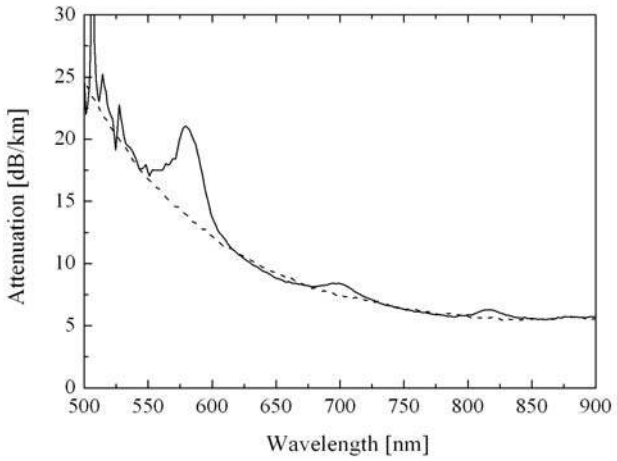

Figure 3.2 ***Measured spectral attenuation of a large-mode area PCF with a mode-field diameter of 13 μm. For the dashed curve, the fiber is placed on a spool in a single layer, while the solid line represents the fiber placed in two layers.***

The result, in this case, is an attenuation peak of ~8 dB/km at 580 nm along with two smaller features at 700 nm and 820 nm. It should be emphasized that this is an extreme example. The mode spacing successfully controlled at 600 nm is in this case around $3 \cdot 10^{-4}$ corresponding to a beat length of 2 mm.

3.4 Random micro deformations

A more commonly occurring type of deformation is a non-periodic or random deformation distribution which is likely to resemble that of the cabling process [40]. For testing the response to this type of deformation, the fiber is placed in the deformation device arranged in a circle relative to the mesh as indicated in Figure 3.1. In Figure 3.3, the measured attenuation induced by a ~ 10 N deformation force is shown. The graph to the left shows measurements for a mesh with a period of 1.34 µm, corresponding to $\Omega = 0.8$ µm^{-1}, while the period for the graph to the right is 0.325 µm, corresponding to $\Omega = 3.1$ µm^{-1}. Furthermore, black and red curves correspond to a cladding diameter of 173 µm and 125 µm, respectively. As predicted by Eq. (3-3), the screening improves when Ω increases and also the influence of the increased fiber diameter is clearly observed.

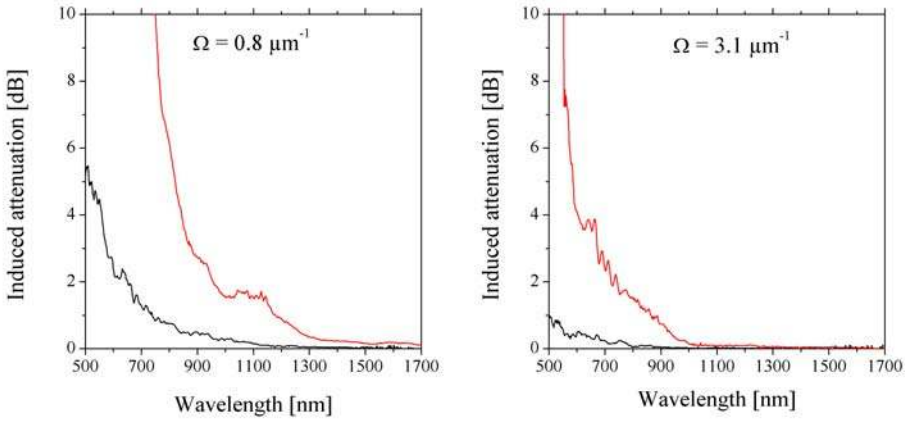

Figure 3.3 ***Spectral attenuation induced by non-periodic micro deformations in two similar PCFs only differing by their cladding diameters of 125 µm and 173 µm, respectively (red and black curves). The two graphs correspond to two different deformation periods of the applied wire mesh.***

Like a cabled fiber, the coating layer itself can apply forces in the transverse direction of the fiber thereby inducing attenuation. Since the coating used throughout this work is a single-layer coating it is also relatively hard and can therefore have decisive influence on the useable bandwidth of the fiber. The only alternative to improving the coating properties is to increase the fiber diameter. In Figure 3.4, the measured spectral attenuation of a large-mode area PCF with a mode-field diameter of 16 μm is shown. The graph to the left corresponds to a cladding diameter of 125 μm while the graph to the right corresponds to a 230 μm cladding. All other parameters are identical. The dashed lines in the two graphs indicate a spool radius of 8 cm while the solid lines correspond to a radius of 16 cm. For the 125 μm cladding diameter, the attenuation curves for the two different bend radii are almost identical and actually, the largest bend radius corresponds to the highest loss indicating that macro bending cannot account for the attenuation. Instead, the attenuation is caused by micro-deformation loss and the attenuation variation observed is due to spooling conditions such as tension and more layers of fiber on the spool for the small radius. For the increased diameter of 230 μm, the bandwidth is seen to increase and a splitting of the attenuation curves corresponding to different spool radii is observed. This indicates that the micro deformations have been screened and that the bandwidth now is limited by macro-bend loss. The influence of the fiber diameter on the operational bandwidth is addressed in detail in Paper G.

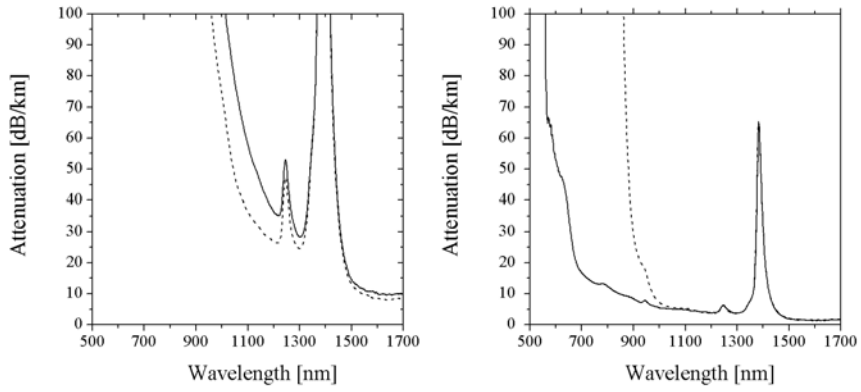

Figure 3.4 ***Influence of the fiber diameter on the screening of micro-deformation induced attenuation. The graph to the left shows data for a fiber with a 125 μm cladding diameter while the graph to the right corresponds to a 230 μm cladding diameter. The solid and dashed lines indicate bend radius of 16 cm and 8 cm, respectively.***

3.5 Macro-bending induced attenuation

When a waveguide is bend, light is lost to radiation modes [14]. In an ideal and completely straight waveguide, modes propagate with a constant phase front (see section 2.2) and the planes of constant phase are perpendicular to the fiber axis. Bending of the waveguide will cause the planes not to be parallel and therefore the phase velocity will increase across the waveguide from the inner radius to the outer radius of the bend. Since light can only propagate without loosing power to radiation modes if $v_p < c/n_{cl}$, there will be a certain critical bend radius, R_c, where the guided mode starts to loose power at a certain rate. This description is illustrated in Figure 3.5 and accounts for the steep loss edge observed experimentally.

A significant difference compared to conventional single-mode fibers, is that bend loss for large-mode area PCFs is observed at short and not at long wavelengths - Just as in the case of micro-deformation induced attenuation. The attenuation observed for some PCFs at long wavelengths is in reality caused by a combination of confinement loss and bend loss. The bend loss at short wavelengths is easily understood by considering the decreasing mode spacing with decreasing wavelength.

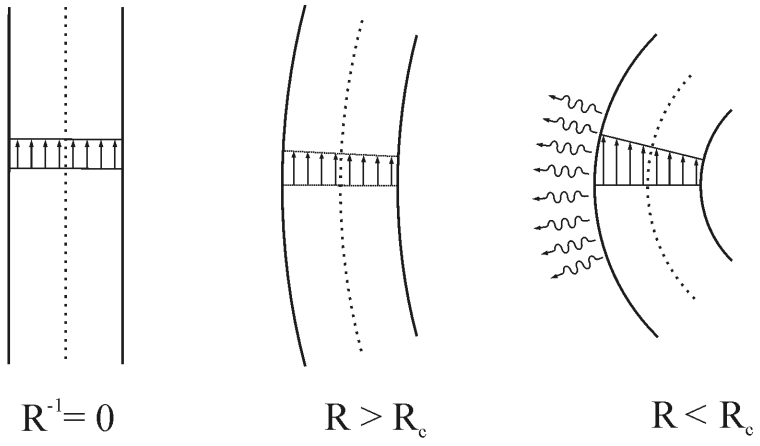

Figure 3.5 ***Schematic drawing of a straight waveguide, a situation where the waveguide is bent at a radius R>Rc, and at R<Rc.***

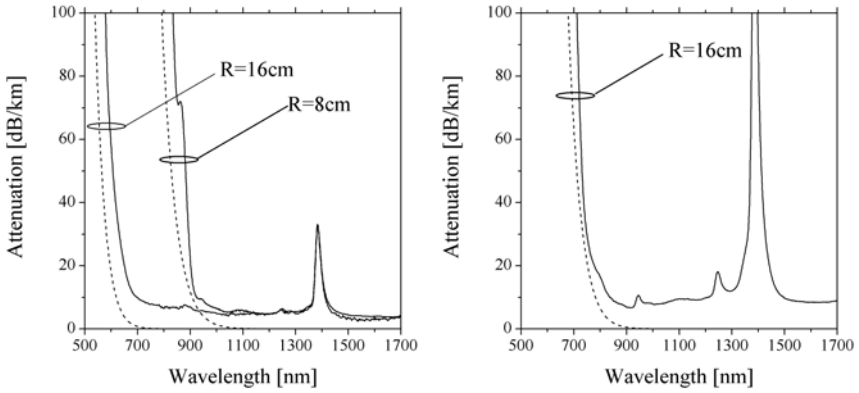

Figure 3.6 ***Bend-loss curves for a fiber with a mode-field diameter of 16 µm (left) and 20 µm (right), respectively. Measurements are indicated by solid lines while predicted bend loss are indicated by dashed lines. A bend radius of 16 cm is indicated by black curves while R=8 cm corresponds to red curves.***

As a part of this work, macro-bend loss was investigated. Macro-bend loss in PCFs has previously been addressed in literature using coupling length criteria [2,41], tilted index profiles [42], or simply by directly using expressions available for conventional fibers [43,44] derived on the basis of antenna theory [45,46]. The approach of this work has been to follow the lines of antenna theory, but instead of simply adopting the equations for an equivalent conventional fiber these were derived specifically for the PCF and based on the V_{PCF} introduced previously. The result of this derivation is an analytical expression dependent on V_{PCF}, the effective area, the pitch and the bend radius. Bend loss for optical fibers is in general relatively difficult to predict. However, using the empirical relations provided previously, this simple model is capable of predicting the spectral position of the macro-bend loss edge within ~50 nm of measured values. This is illustrated in Figure 3.6 for two different fibers (left and right graph, respectively). Solid lines indicate measured data while dashed lines indicate the predicted curves. The analytical expression and more details on its derivation are given in Paper H.

3.6 Design space of large-mode area PCFs

In principle, any combination of d/Λ and λ/Λ is contained in the general triangular cladding PCF. However, in reality the available parameter space for single-mode large-mode area designs is limited by several factors already described. The conclusions are combined in Figure 3.7. The single-mode boundary shown in Figure 2.6 requires that $V_{PCF}<\pi$, excluding the blue hatched area. From a mode-field diameter point of view, a lower limit for V_{PCF} should also be defined in order to have the mode properly confined to the core. An appropriate measure is to require $w_{PCF}/\Lambda < 1.0$ equivalent to $V_{PCF} > 1.0$ (see Figure 2.8). This requirement excludes the red hatched area. From the remaining design space it is necessary to distinguish between nonlinear fibers and large-mode area fibers. Setting the limit at $A_{eff}/\lambda^2 = 10$, corresponds to an effective area of 24 μm^2 at 1550 nm and 11 μm^2 at 1064 nm. As described elsewhere in this chapter it must also be ensured that L_B is kept at a reasonable low level in order to limit the effects of mode-coupling loss. A limit of caution set at $\Delta n=10^{-3}$, corresponding to at beat length of 1 mm at a wavelength of 1 μm, seems appropriate.

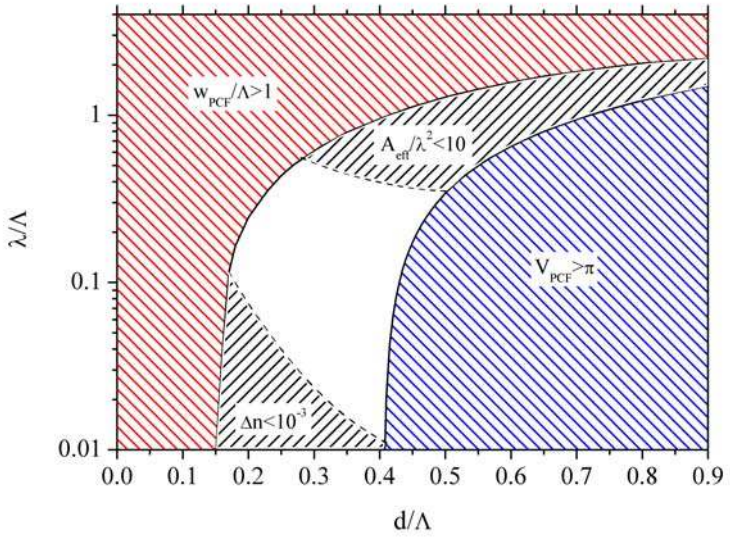

Figure 3.7 ***Phase diagram of the PCF parameter space. The blue region shows the region of multi-mode fibers, the red region shows the region where the mode has penetrated deeply into the cladding, the upper black region indicates nonlinear fibers, and, finally, the lower black region indicates the region of increased coupling loss.***

However, it should be emphasized that the tolerable mode spacing depends on the wavelength because the beat length is proportional to the wavelength. Finally, it should also be mentioned that fibers operated in the theoretical higher-order mode regime are possible up to $d/\Lambda \sim 0.5$. This is because the higher-order modes still have extremely high attenuation close to cutoff and the fiber therefore is effectively single-mode. The benefit of crossing the boundary is increased robustness and typical d/Λ values for large-mode area PCFs are therefore 0.48-0.50.

4 Fabrication related attenuation

Despite the challenges offered by confinement loss, micro deformations and macro-bend loss, PCFs only limited by intrinsic material effects and fabrication related imperfections have been fabricated. In this chapter, the main aspects of the fabrication process are outlined with specific focus on the attenuation related issues relevant for large-mode area fibers.

4.1 Reported attenuation levels

Many of the early reports on fabricated PCFs concerned nonlinear fibers which, generally, had attenuation levels in the order of 0.1 dB/m [47,48]. Attenuation values in this range are often associated with design related issues such as confinement loss and insufficient control of the fiber structure. In year 2001, attenuation at 1550 nm of 3.2 dB/km was reported [49] and already in year 2002 the 1 dB/km limit at 1550 nm was reached [50]. Since then, the attenuation has gradually been improved [51,52] to a current record level of 0.28 dB/km at 1550 nm [21]. The most recent advances have been obtained using high-purity, low-OH content synthetic silica prepared by the vapor-phase axial deposition (VAD) method [21,52]. Previously reported results have been based on commercially available silica tubes intended as over-cladding or substrate tubes in conventional fiber fabrication (see section 4.2). The development in the reported attenuation values is shown in Figure 4.1.

The lowest attenuation value reported for a conventional single-mode fiber is 0.1484 dB/km [53] obtained in a pure-silica core fiber (PSCF) with a fluorine-doped cladding region. Comparing this type of fiber to the large-mode area PCF, the most interesting difference regarding attenuation is that the guided mode in the conventional fiber overlaps with the core-cladding boundary, while the guided mode of the PCF propagates in pure silica only. Since there, inevitably, will be an attenuation contribution from scattering in the core-cladding boundary caused by the difference in thermal expansion coefficients, it may be argued [54] that the PCF holds the potential for achieving even lower loss than reported in Ref. [53].

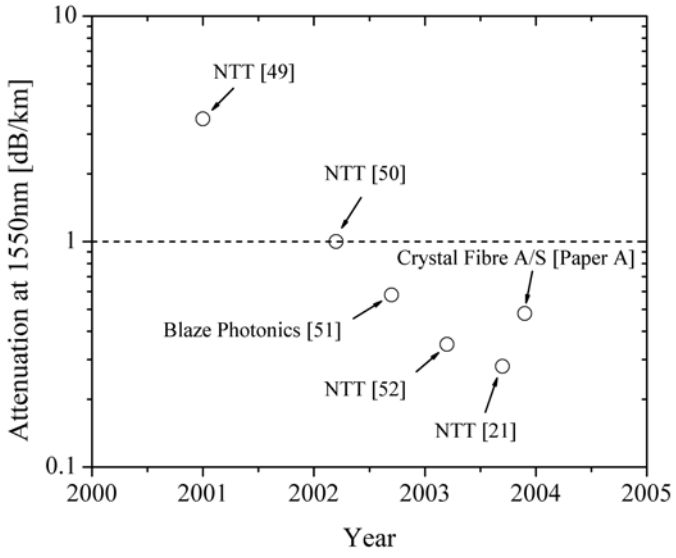

Figure 4.1 ***The development in the reported attenuation values at 1550 nm. The labels indicate the company or group to report the value.***

4.2 Fabrication Techniques

The fabrication of the PCF is based on the manufacturing process of conventional solid fibers. In both cases a preform, with a diameter in the 1-10 cm range is drawn to fiber dimensions on a fiber-drawing tower. This is done by heating the preform beyond the softening point of the glass using a furnace, while carefully controlling the viscosity through the furnace temperature and other drawing parameters.

For conventional fiber fabrication the preform is, typically, made by a chemical vapor deposition (CVD) technique of which modified chemical vapor deposition (MCVD) is the most widespread process. The principle of MCVD is to deposit a soot layer on the inside of a silica substrate tube and then to sinter the soot into glass during the collapse of the tube into a solid rod [55]. The soot deposition is created by oxidization or hydrolysis of a metal halide vapor, such as $SiCl_4$, which, in the case of oxidization, forms SiO_2 and Cl_2 by reaction with O_2. In order to add refractive index altering dopants to the core, $GeCl_4$ is

typically added forming GeO_2. One of the advantages of MCVD is that the purity of the glass depends on the purity of the metal halides, which can be refined by repeated distillation. Also, the process is flexible since many dopants, such as Erbium and other rare earths, can easily be added. A disadvantage of the process is that it is not possible to alter the index profile after the preform has been sintered. Since MCVD is also difficult to control, it is also difficult to obtain a large yield. Also, the number of soot layers that can be deposited is limited, restricting for the resolution of the created index profiles. Finally, the diameter and length of the MCVD prepared preform is limited and the process takes many hours. These issues cause MVCD to be a relatively expensive process.

For the fabrication of PCF preforms, the so-called stack and draw fabrication method is exclusively used although two alternatives have been proposed. One comprises the drilling of holes in a pure-silica rod [56] while the other propose to use a sol-gel process to cast the preform [57]. There are many disadvantages of both these methods.

The drilling of many holes in a rod is challenging and the depth of the hole relative to its diameter is limited. The preform will therefore be limited to have only a few large holes and also to be thick and short. For comparison, a PCF preform made by the stack and draw method is, typically, in the order of 1 m in length and has in the order of 100 voids each with a diameter of ~1 mm or less.

The sol-gel process is appealing for PCF fabrication because it, in principle, allows for any geometrical cross section without constraints set by a given period in the structure or even shape of the air holes. However, sol-gel technology has still not matured sufficiently even for solid-fiber fabrication [58]. Typical problems associated with the process are high attenuation, bubbles in the glass, and the realization of sufficiently large glass bodies.

In the stack and draw fabrication method, the preform is constructed by stacking a number of capillary tubes around a central rod and fitting the stack into a support tube. The capillary tubes are drawn from a larger tube on a drawing tower. The method allows for a great flexibility in the design of the fiber cross section and doped materials are easily introduced by adding rods or tubes drawn from commercially available preforms.

4.3 Contamination and surface roughness

In contrast to CVD prepared preforms, where the core region is build from synthetic glass and collapsed without being exposed to the environment, the process of stacking a preform from capillary tubes and rods is more sensitive to contamination. This makes the surfaces quality of the applied tubes and rods important and when aiming for low attenuation it is therefore necessary to address the surface roughness and contamination of the elements [50]. This point is illustrated in Figure 4.2, showing a schematic drawing of a core region comprised of a center rod surrounded by 6 capillary tubes.
When the stack is reduced to fiber dimensions, the position of the surfaces in the core region will be as indicated by the dashed hexagons. The dashed circle indicates the mode-field diameter at $V_{PCF}=\pi$ (equal to 1.24Λ, see section 2.6). This illustrates that there is a significant overlap between the fundamental mode and the fused surfaces of the original elements. In this work, fabrication tests were performed to experimentally illustrate the influence of surface contamination. A typical type of contamination is expected to be organic compounds introduced during the fabrication process. To measure the possible effect of such contamination, elements for a preform were contaminated by applying a covering organic layer. In Figure 4.3, the measured spectral attenuation of a fiber drawn from this preform is indicated by the red curve.

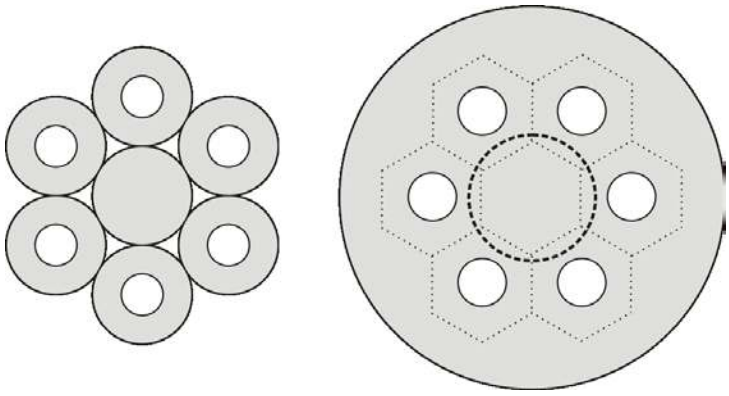

Figure 4.2 ***Schematic drawing of the surfaces position of the capillary tubes and rods in the fused fiber. The dashed circle indicates a mode-field diameter of 1.24Λ.***

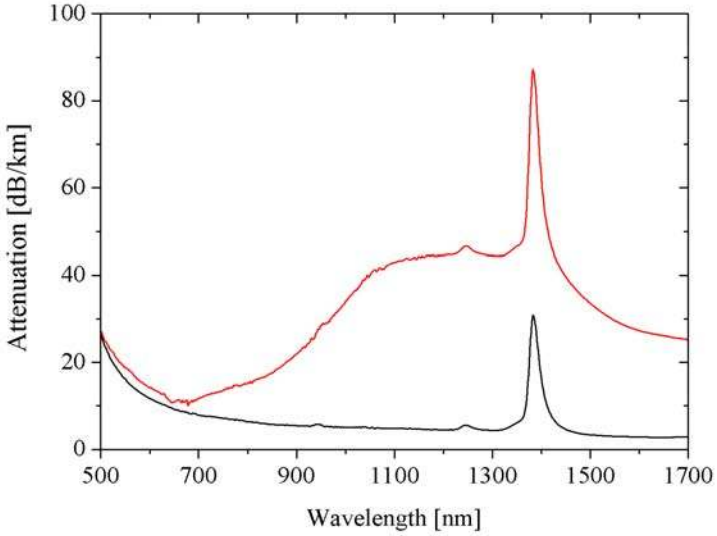

Figure 4.3 ***Measured spectral attenuation from 500 nm to 1700 nm for two fibers with identical structural dimension drawn from two different preforms. The red curve corresponds to a preform where the surfaces of the elements have been contaminated with an organic compound while the black curve is drawn from a reference preform.***

For comparison, the attenuation of a fiber drawn from a reference preform is shown in the same plot by the black curve. The effect of the contamination is seen to be a strong attenuation for wavelengths above 700 nm. The induced absorption will depend on the chemical composition of the contamination such as the presence of metals [55] and the spectral characteristics shown in Figure 4.3 can therefore not be considered as general. However, the conclusion remains that the quality of the surfaces in the preform is essential for the achievement of low-loss fibers.

4.4 OH contamination in silica glass

The effects of hydroxyl (OH) contamination are well known from conventional fiber technology. The OH groups, often originating from H_2O, bind to the SiO_2 glass matrix forming SiOH groups. In extreme concentrations, glass properties such as crystallization rate, viscosity and fatigue resistance can be influenced [59]. For typical concentrations in the order of a few ppm the primary effect is a

strong absorption at the 2.73 μm wavelength. This wavelength is generally not of concern for silica based fibers because the wavelength is outside the transparency window. The inferred absorption of silica is in the order of 10 dB/m at the 2.73 μm wavelength [60].

The reason for the problems caused by OH contamination is due to overtones of the fundamental absorption resonance located at shorter wavelengths. The most significant are positioned at the 1383 nm, 1246 nm, and 943 nm wavelength [61]. Especially the strongest peak at 1383 nm, having a value of ~50 dB/(km·ppm) [61], is of concern because the tails of the peak can influence the attenuation at 1550 nm. The contribution to the attenuation at 1550 nm in a pure silica core fiber is around 0.5-1% of the peak value at 1383 nm [62]. This contribution increases with increasing Germanium content [63] making the problem even more relevant for conventional fibers. In order for the OH induced attenuation at 1550 nm to be insignificant (such as lower than 0.01 dB/km) the concentration should be reduced to less than ~20 ppb. Furthermore, if the potential of the wide bandwidth of the PCF is to be utilized, attenuation at 1383 nm is also critical imposing even stronger demands on purity.

The OH contamination in a given fiber is related to the raw materials and the preform fabrication process. The typical OH content of the bulk glass used in this work is 0.5 ppm. One of the advantages of both MCVD and VAD prepared preforms is that they can be realized with very low levels of OH [64]. In addition, the distance from the preform surface to the core region is typically much longer than the diffusion length of OH, and it is therefore possible to eliminate OH induced attenuation. However, PCFs fabricated by the stack and draw method are generally more susceptible to OH contamination and for low-loss applications great care must be taken in order to eliminate this potential problem. Even if the raw materials have a low OH content, the surfaces in the core of the preform ensures a potential overlap between the field and OH contaminated regions for instance from H_2O in the ambient atmosphere. It can therefore be necessary to construct the preform in a dry environment in order to prevent water from forming on the surface of the elements [21].

4.5 Defect centers in silica glass

Defect centers in silica glass is an entire research area on its own and also in the specific context of silica based optical fibers much work has been done [65-68]. The motivation for this effort is that defect centers can cause strong attenuation and, in some cases, can be the limiting factor for the application of the fiber. Most defect centers observed in pure-silica fibers are located in the ultra-violet region of the optical spectrum but can have tails deep into the visible part. In the case of Germanium-doped silica, the absorption peaks are even stronger and the tails therefore extend to even longer wavelengths [69]. Fibers for applications in the ultra-violet part of the spectrum are therefore often pure-silica core fibers with a Fluorine-doped cladding [70-72].

The most important examples of defect centers are the E′ center (≡ Si·), the non-bridging-oxygen hole center (≡ Si−O·), and the peroxy radical (≡ Si−O−O·) [73]. In this notation "≡ " represents bonds with 3 other oxygen atoms in the network while "·" represents an unpaired electron. Such an unpaired electron is sometimes referred to as an unpassivated bond or a dangling bond. The E′ center is related to strong absorption at the 206 nm wavelength (5.8 eV) but has no additional absorption bands in the visible part of the spectrum. The peroxy radical has been related to attenuation at 158 nm (7.6 eV) while the non-bridging-oxygen hole center accounts for attenuation at both 260 nm (4.8 eV) and 630 nm (2.0 eV) [74]. For this work absorption at 630 nm has been the defect center of primary concern.

Defect centers can be created as a result of electromagnetic or electron irradiation [75-77]. However, an alternative formation mechanism in the case of optical fibers has been shown to be the fiber drawing process itself. Especially, the details of the drawing induced attenuation at 630 nm have attracted much attention since the relation was first reported [78]. It has been shown that the formation of 630 nm absorption increases with increasing reduction ratio [78] and drawing tension [79]. This suggests that the defect arise as a result of the breaking of Si−O due the shear stress. Similar results have been reported for the peroxy radical [80] and the E′ center [81].

Although the most attractive solution is to avoid the 630 nm absorption by avoiding the tension regimes responsible for the problem, this might not always be possible. An alternative solution is to eliminate the 630 nm absorption after the fiber drawing process by loading the fiber with hydrogen or

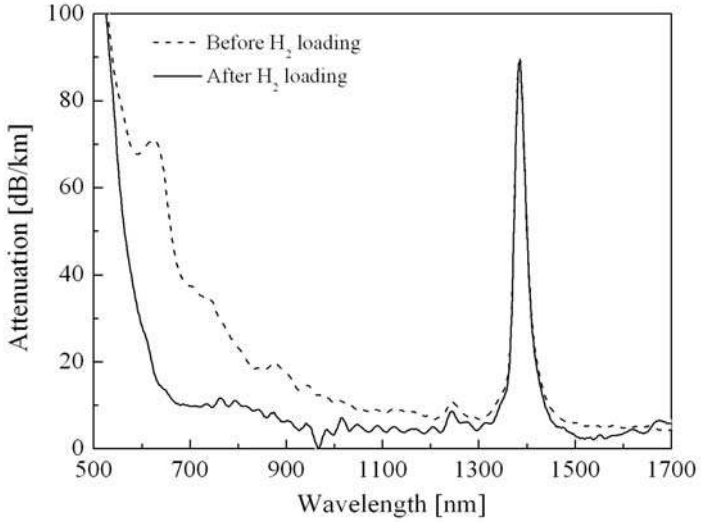

Figure 4.4 ***Attenuation spectrum of a PCF before (dashed line) and after (solid line) hydrogen loading.***

deuterium [82]. Hydrogen easily diffuses into the glass matrix where it dissociates and passivates the free electrons creating SiOH groups. In Figure 4.4, the measured spectral attenuation of a 50 m fiber sample before and after hydrogen loading is shown. A clear reduction of the attenuation level at short wavelengths is observed. The noisy character of the spectrum after loading is caused by the short length of the fiber and the low attenuation obtained. In order to verify if the effect was permanent, the measurement was repeated after storing the fiber for a period of 2 years under normal ambient conditions. Within the measurement uncertainty the attenuation characteristics were confirmed.

Even though hydrogen loading has been shown to be possible, it is not attractive from a practical point of view. The aim should therefore be to avoid the occurrence of defects centers. Annealing of the preform prior to fiber drawing can help to eliminate defects formed in the first steps of the fabrication process [76] and during fiber draw, and also the atmosphere in the furnace plays a role [83]. In this work, pulling bands have been eliminated by annealing, hydrogen loading and, most importantly, by carefully controlling the drawing parameters in order to avoid high tension regimes.

4.6 Results of optimized fabrication process

The previous sections highlight the central issues identified as critical for the PCF fabrication process. As a result of this work and by addressing each of these issues, a fiber with an effective area of 130 μm^2 and attenuation as low as 0.48 dB/km at 1550 nm was fabricated. This is the lowest attenuation reported for a PCF not fabricated from VAD prepared silica and, at the same time, the largest effective area reported for a low-loss (< 1dB/km) PCF. The fiber was drawn at a length of 2.5 km and inspected along the length with an optical time-domain reflectometer (OTDR). From this measurement, no trace of scatter points or other inhomogenities along the length was observed. In Figure 4.5, the measured spectral attenuation from 1000 nm to 1600 nm for this fiber is shown. The largest contributions to the attenuation at 1550 nm are due to the tails of the OH-induced absorption and the intrinsic Rayleigh scattering in the glass material.

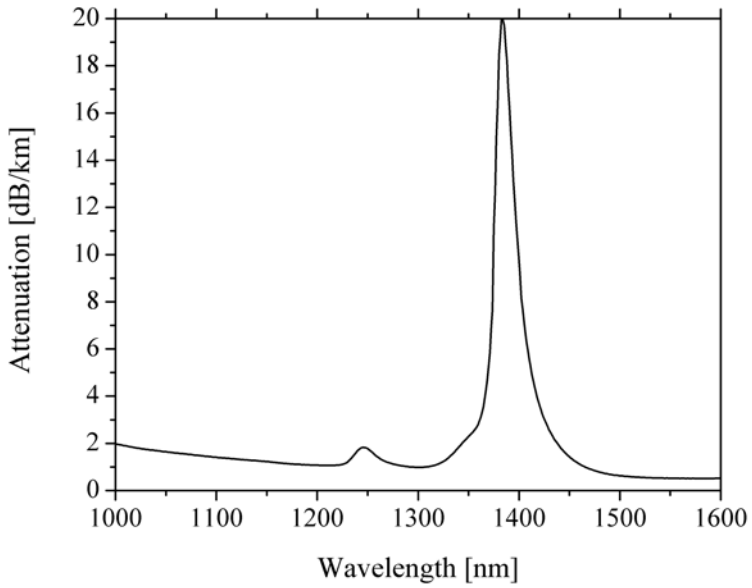

Figure 4.5 ***Measured spectral attenuation from 1000 nm to 1600 nm of a fabricated low-loss PCF. (Figure from*** *Paper A)*

The peak value of ~20 dB/km at the 1383 nm wavelength corresponds to an OH concentration ~0.4 ppm which is in good agreement with the typical OH concentration for the applied raw glass materials. This indicates that no excess OH contamination has been introduced during the fabrication process, at least not compared to the concentration in the raw glass. A further reduction of the attenuation therefore requires the use of better raw materials such as low-OH content VAD prepared silica. More details on this low loss fiber can be found in Paper A.

The findings of this work have not revealed any fundamental attenuation limitations other than those known from conventional fiber technology. In fact, the single-material nature of the PCF seems promising for eventually obtaining lower loss than state-of-the art conventional fibers.

5 Examples of large-mode area PCFs

In this chapter, examples of large-mode area PCFs developed as a part of this work are presented. These examples cover fibers optimized for visible as well as infrared wavelengths. The diversity of PCF technology is illustrated by presenting alternative designs of both the core and the cladding region. Finally, a polarization maintaining large-mode area fiber is presented.

5.1 Single-mode PCF for visible light applications

In the case of conventional single-mode fibers, the single-mode optical bandwidth is limited by the presence of higher-order modes at short wavelengths and lack of guidance associated with bend-loss at long wavelengths. Especially, when the higher-order mode cutoff is scaled to visible wavelengths, the bandwidth limitations become apparent.
In this work, the bandwidth performance of both conventional and PCF single-mode fibers for visible light applications have been investigated. In Figure 5.1, the spectral attenuation of a conventional fiber (red curve) and a large-mode area PCF (black curve) are shown obtained under comparable conditions.

The PCF matches the 4.0 μm mode-field diameter of the conventional fiber at visible wavelengths. As a consequence of the dispersive properties of the mode indices, the PCF was found to support a significantly larger bandwidth than the conventional fiber. Where the conventional fiber is seen to have a single-mode bandwidth of ~400 nm, no bandwidth limitations are observed for the PCF in the spectral region of measurement ranging from 400 nm to 1700 nm.

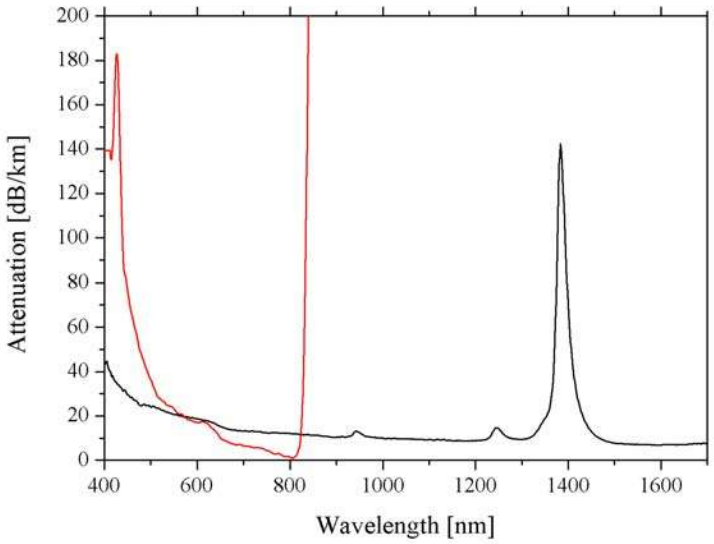

Figure 5.1 ***Measured spectral attenuation from 400 nm to 1700 nm of a conventional fiber (red curve) and a PCF (black curve) both with a mode-field diameter of 4.0 µm at visible wavelengths (figure from*** *Paper I*)***.***

While the wide bandwidth of the PCF is desirable for some applications, the conventional fiber also covers the entire visible region and in applications where only visible wavelengths are of interest, the advantages of the PCF are of little use. It was therefore investigated how the potential of the PCF could be utilized to increase the mode-field diameter while still matching the bandwidth of the conventional fiber. A single-mode PCF with an effective area almost 3 times larger than that of the conventional fiber was demonstrated. Besides demonstrating an important difference between conventional fibers and PCFs, such fibers might find use in display systems or in other applications where high-power single-mode light at visible wavelengths needs to be delivered. The details of this work are given in Paper I.

5.2 Large-mode area PCF for telecom wavelengths

An interesting potential of PCFs is their application as transmission fibers in optical communication systems. The performance of a transmission fiber is determined by the attenuation, group velocity dispersion (GVD), polarization

mode dispersion (PMD), effective area, and single-mode bandwidth. As argued

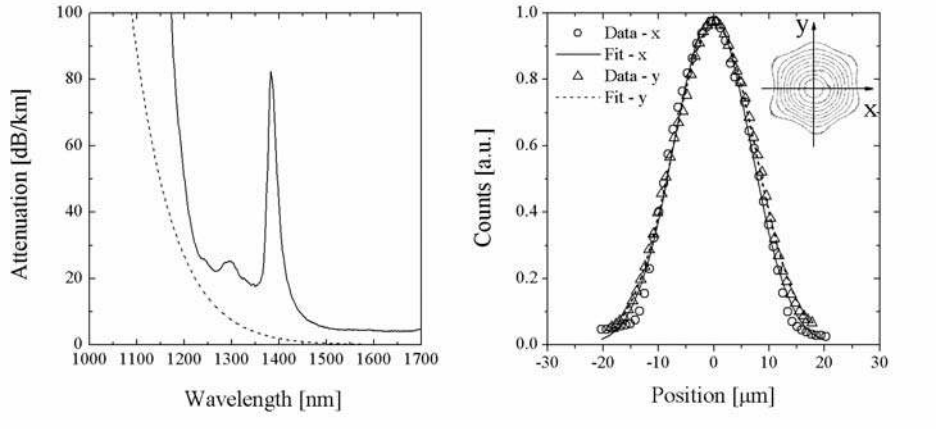

Figure 5.2 ***Spectral attenuation (left) and near field-profile of the fundamental mode along two orthogonal directions (right) for the 600 µm2 PCF (figures from*** *Paper J)*

and demonstrated (see sections **Error! Reference source not found.** and 4.6) the large-mode area PCF has the potential to achieve attenuation levels comparable to those of conventional transmission fibers and possibly even lower. Early investigations of PMD in large-mode area PCFs have indicated that the performance is as good as that of conventional fibers [84]. For large effective areas the group velocity dispersion is only slightly higher than the material dispersion of bulk silica (section 2.3) and these values of more than 22 ps/(nm·km) are relatively high compared to values typical for conventional transmission fibers. However, for high-bit rate systems, it can be beneficial to have a high dispersion value at every point along the transmission line in order to suppress nonlinear interaction between the individual channels in a multi-wavelength system [85]. The possibility for realizing endlessly single-mode fibers is a property unique to PCF technology and interesting for wide-bandwidth systems. Several transmission experiments have already been reported such as transmission over small-core polarization-maintaining fiber [86], wavelength-multiplexed transmission in the 1550 nm band at a bit rate of 10 Gbit/s [52] and simultaneous transmission at wavelengths from 800 nm to 1550 nm with an overall bit rate of 190 Gbit/s demonstrating the potential for as much as 10 Tbit/s.

As a part of this work fibers for data transmission have been developed and tested for both single- and multi-wavelength transmission at 10 Gbit/s [87,88] as well as for the first 40 Gbit/s transmission experiment to be reported [89,90]. Finally, transmission fiber developed as part of this work has been used in the first loop experiments with a total transmission distance of 57.6 km without dispersion compensation [91].
Most of the fiber used for transmission test was fabricated with a typical mode-field diameter of 8-9 μm comparable to that of conventional transmission fibers. However, in order to take advantage of the PCF potential it was attempted to increase the mode-field diameter in the telecommunication band. As a result a single-mode PCF with an effective area of 600 μm^2 at 1550 nm was fabricated. The fiber was designed to optimize the mode-field diameter under the criteria of single-mode operation and no influence of macro-bend induced attenuation at 1550 nm for a bend radius of 16 cm. Screening of micro deformations was ensured by choosing a cladding diameter of 230 μm. In Figure 5.2 (left), the measured spectral attenuation (solid line) and the predicted macro-bending induced attenuation (dashed line) are shown. Figure 5.2 (right) shows the measured intensity profiles along two orthogonal directions in the near field along with fitted Gaussian functions. The mode-field diameter extracted from these data is ~27.7 μm and in good agreement with the predicted effective area of 600 μm^2. Such a fiber is expected to be able to increase the transmission distance in communication systems limited by nonlinear interaction. More details of this fiber are given in Paper J.

5.3 Triangular core large-mode area PCF

The structures considered in the preceding chapters have all had a triangular cladding structure and a core region corresponding to a single missing air hole. An alterative approach is to remove additional air holes and thereby to create a larger core relative to the pitch of the cladding structure.
Removing two neighboring air holes will lead to a splitting of the two degenerate polarization states of the fundamental mode causing the fiber to be birefringent. This design has previously been utilized for obtaining a polarization maintaining PCF [92]. More generally a mode with a preferred

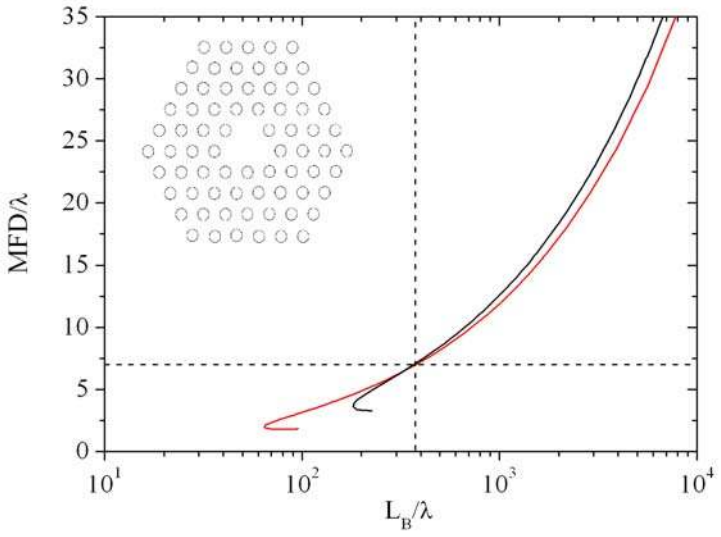

Figure 5.3 ***Normalized mode-field diameter as function of the normalized coupling length. The red curve represents a single-rod PCF with d/Λ = 0.45 while the black curve represents the triangular core PCF (schematically drawn in the insert) with d/Λ=0.25 (Figure from*** *Paper K)***.**

direction will in a structure with m-fold rotational symmetry and $m > 2$ be one of a pair [93].

In this work, large-mode area PCFs obtained by removing three air holes, as schematically shown in the insert of Figure 5.3, have been investigated. This deign is referred to as the trirod design. Simply increasing the size of the core region in a waveguide operated close to cutoff will cause the waveguide to be multi mode unless the index difference between core and cladding is decreased correspondingly. Therefore, the value of

d/Λ at which endlessly single-mode operation can be obtained is smaller than that of the single-rod design and the endlessly single-mode limit for the triangular core PCF is determined to be around $d/\Lambda \sim 0.25$. The trirod design has the benefit of being more robust in the limit of large mode fields. This is illustrated in Figure 5.3 showing the mode-field diameter relative to the free-space wavelength as function of the normalized beat length, L_B/λ. The red curve represents the relation for a single-rod core with $d/\Lambda = 0.45$ while the black curve represents the trirod design for $d/\Lambda = 0.25$. For a mode-field diameter larger than 7λ, the beat length is smaller for the trirod design than for the single-rod design. The advantage of the trirod design is used in active

double-clad fibers for high-power applications [5,94]. These results are discussed in detail in Paper K.

5.4 Large-mode area PCF with fluorine doped cladding

The trirod design (section 5.3) is an example of an alternative way of realizing a large-mode area fiber by altering the core region. In this work, the possibility of alternative cladding designs has also been investigated. Besides the triangular cladding structure, the most frequently used air-hole arrangement is the honeycomb structure, shown in Figure 5.4. The honeycomb structure has primarily been studied for bandgap fibers by introducing a central defect with a lower refractive index than silica (Figure 5.4 left). The most simple way of creating a low-index defect is by adding an air hole in the center of the structure [95] or alternatively, by using fluorine doping of the core [96]. Instead of altering the core region of the honeycomb structure, bandgap guidance has been predicted by increasing the refractive index of the pure silica regions in the cladding by Ge-doping [97].

In this work, an index-guiding PCF based on a honeycomb arrangement of air holes has been considered as an alternative way of designing the cladding of a large-mode area PCF. This was done by lowering the refractive index of the solid silica regions in the cladding using fluorine-doped elements (Figure 5.4 – right). At sufficiently short wavelengths, the field avoids both the air holes and the fluorine-doped regions. The result is a cladding mode resembling that of the triangular-cladding structure. At increasing wavelength the field rapidly averages over the fluorine doped regions and the behavior resembles that of a honeycomb structure with a slightly lowered background index. The obtained mode-field diameters and beat lengths were found to be similar to those of the triangular cladding PCF. The details of this work are given in Paper L.

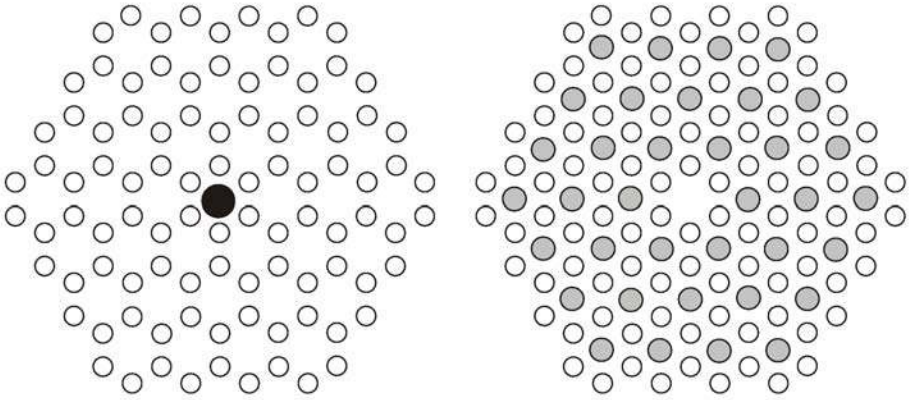

Figure 5.4 ***PCF structures based on a honeycomb arrangement of air holes (white circles). For the structure to the left the dark region in the center indicates a low-index area such as an air hole or a fluorine-doped region. For the structure to the right the gray areas indicate doped elements in the solid cladding regions.***

5.5 Polarization maintaining large-mode area PCF

In most single-mode fibers, two degenerate modes with orthogonal polarization are actually present. Since the modes are degenerate, they propagate with the same group velocity and for un-polarized light the result is effectively a single mode. When launching polarized light in such a fiber, the polarization state is generally not preserved due to random mode coupling between the two polarization states. In real fibers, external perturbations and imperfections in the symmetry of the fiber cause splitting between the two polarization states resulting in a slow and a fast polarization axis. Furthermore, the splitting between these states fluctuates in a stochastic way along the length of the fiber, giving rise to negative effects such as polarization-mode dispersion (PMD).

A solution to the polarization problems can be to make a fiber that only supports one of the two polarization states, referred to as a polarizing fiber, or to maximize the splitting between the two polarization states in order to reduce the random coupling. If the coupling is eliminated the fiber will preserve a given polarization state and such fibers are therefore referred to as polarization maintaining (PM) fibers.

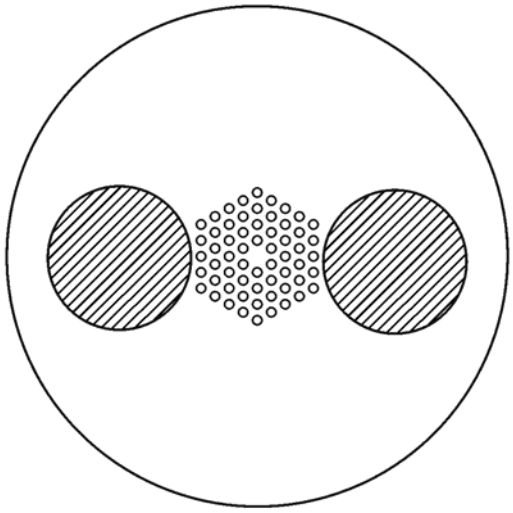

Figure 5.5 ***Schematic drawing of the fiber cross section of a polarization maintaining large-mode area PCF. The hatched areas indicate stress-applying parts.***

For polarizing fibers, birefringence is introduced together with preferential loss for one of the polarization states resulting in the guidance of a true single mode. Polarizing fibers can be realized in conventional fiber technology but are extremely difficult to fabricate due to the limited index contrasts and the inherent rotational symmetry. Therefore, polarizing conventional fibers are currently not commercially available.The microstructure of the PCF provides excellent possibility for tailoring of the index profile of the cladding region. This flexibility has given new life to polarizing fibers which have been fabricated with specifications superior those known from conventional technology [98,99]. Also polarization maintaining PCFs have been fabricated in a large variety of designs [92,100-102] typically offering high birefringence in the order of $\Delta n \sim 10^{-3}$. Common for these fibers is that they take advantage of the large index contrast between air and glass while shaping the core region to have a 2-fold symmetry. Birefringence obtained in this way is referred to as form birefringence. The limitation of form birefringence is that the splitting of the two polarization states decreases rapidly for increasing structural dimensions. Therefore, form birefringence cannot be used for large-mode area fibers. In conventional polarization-maintaining fibers, birefringence is typically based on material birefringence induced by stress.

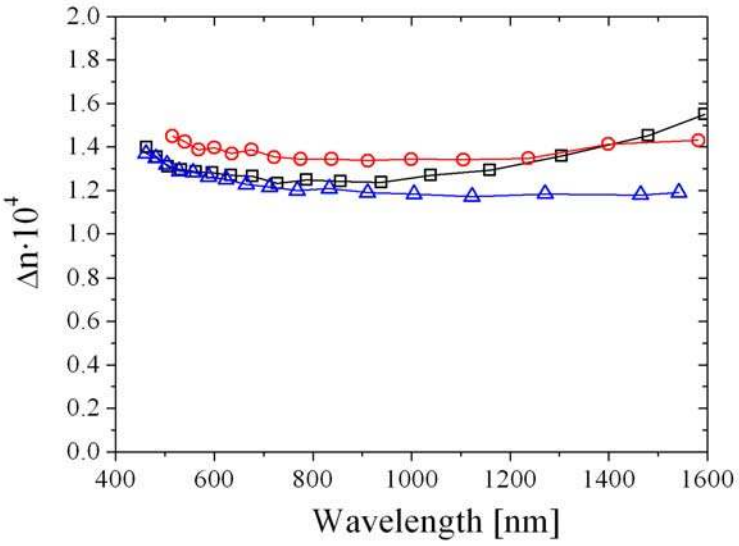

Figure 5.6 ***Measured birefringence from 400 nm to 1600 nm of 3 different fibers drawn from the same preform with varying structural dimensions. Black, red, and blue datasets correspond to a Λ of 3.20 µm, 4.40 µm, and 5.94 µm, respectively (figure from*** *Paper M)*.

The stress field is realized by introducing so-called stress-applying parts in the cladding region which are solid regions of highly doped glass, typically with a combination of B_2O_3 and GeO_2, causing a shift in the thermal expansion coefficient compared to silica. The most widespread design of such fibers is the PANDA fiber [103,104].

In this work, the advantages of the large-mode area PCF and the polarization maintaining properties of the PANDA fiber have been combined. The result of this work was the first report of a polarization-maintaining endlessly single-mode PCF. A schematic drawing of thefiber is shown in Figure 5.5 comprising a triangular arrangement of air holes placed in between two stress-applying parts. For a polarization maintaining fiber, the most important parameters are the birefringence and the polarization holding parameter, also referred to as the H-parameter.

The H-parameter is a measure of how well coupling between the two polarization states is suppressed. In Figure 5.6, measured birefringence in the 400 nm to 1600 nm wavelength range is shown for 3 different scalings of the same fiber. The fibers are drawn from the same preform and simply scaled by

adjusting the outer diameter of the fiber. As seen, the birefringence is almost independent on both the scaling and the wavelength. The fiber is thus both endlessly single-mode and endlessly birefringent. One application is to incorporate this functionality into double-clad laser fibers which would allow for the control of the polarization of the output. More details on this fiber are given in Paper M.

The examples of this chapter, along with the description of the optical properties in the previous text, show that PCF technology indeed offers new possibilities for the further development of fiber optics.

6 Conclusion and Outlook

In the work presented in this thesis, the large-mode area photonic crystal fiber has been addressed in detail with specific focus on the description of the basic optical properties and attenuation related issues. An important element in this description is the suggestion of a V-parameter for the PCF from which the single-mode regime as well as the normalized mode-field diameter can be predicted. Furthermore, the group velocity dispersion was shown to be uniquely related to the mode-field diameter. Along with a set of empirical relations for analytical evaluation of the V-parameter, the work presented provides a detailed description of the central optical properties. It is believed that these descriptions will provide better understanding of the properties and potentials of PCFs.

The small mode spacing inherent to the large-mode areas, inevitably leads to an increased susceptibility towards attenuation caused by external perturbations such as micro deformations and macro bending. In this work it has been illustrated how these effects can limit the available bandwidth. For the screening of micro deformations the strong effect of increasing the fiber diameter has been investigated, and for the macro-bend loss an expression based on antenna theory has been presented and experimentally verified. The expression is based on the V-parameter and can predict the position of the macro-bending induced loss edge with an accuracy of ~100 nm. Based on the description of the optical properties and the attenuation related effects, a design space suitable for large-mode area PCFs has been pointed out. It is believed that these guidelines will help to realize optimized fiber designs.

In this work, production related attenuation has also been investigated. It has been demonstrated that the surface quality of the elements in the preform is critical for realizing low-loss fibers. Also issues such as hydroxyl contamination and defect centers in the glass introduced during the fiber drawing process have been addressed. As a result of this work a single-mode PCF with an effective area as large as 130 μm^2 was obtained with an attenuation level of 0.48 dB/km at 1550 nm. This is by far the largest effective area reported for a low loss (< 1 dB/km) PCF and at the same time the lowest attenuation level obtained without the use of high-quality VAD glass. An obvious next step is to use better raw materials. This is expected to give an immediate

improvement in the order of 0.2 dB/km and without question, the resulting attenuation regime will pose new unforeseen challenges.

The knowledge established as a result of this work has, furthermore, allowed for the realization of a large variety of large-mode area PCFs. This includes a single-mode PCF optimized for visible light with an effective area 3 times that of conventional fibers and a single-mode PCF for telecommunication wavelengths with a 5 times larger effective area than state of the art conventional fibers. Also, alternative designs have been explored for both the core and the cladding regions comprising a trirod design and a hybrid design based on down doped regions in the cladding. Finally, the first polarization-maintaining large-mode area PCF to be reported has been fabricated. This fiber has the unique property of being both endlessly single-mode and endlessly birefringent.

Along with the advances in production techniques the demonstration of the 600 μm^2 effective area fiber makes PCFs for data transmission an interesting area for further work. It is believed that the work presented here provides the first firm indications that PCFs can offer advantages over conventional transmission fibers. However, it still needs to be demonstrated that attenuation as low as < 0.20 dB/km can be obtained for these small mode spacings. Also, polarization-mode dispersion is a subject that needs a more detailed investigation.

The first demonstration of a polarization-maintaining large-mode area fiber has opened up for much interesting research. This work could aim at further increasing the mode-field diameter, the birefringence, and the H-parameter. Also, in the limit of large mode areas the birefringence might resemble the mode spacing from the fundamental mode to the cladding and one might speculate that polarizing large-mode area fibers could be realized. Finally, it is not yet clear how large an effect the screening of the air holes has on the birefringence. Besides the fabrication of polarization-maintaining passive fibers, the implementation of polarization-maintaining operation could have interesting potentials in the context of air-clad fibers for high-power lasers.

The advantages over conventional fibers based on index altering dopants can in general be summarized as follows. The air-hole arrangement allows for superior control of the index profile. Not only is it well known that it is difficult to control index variations less than $\sim 10^{-3}$ when preparing doped preforms, also the

diffusion of the dopants during the fiber drawing process is another problem eliminated in PCF technology. Here the corresponding index variations are those of pure silica which, in high quality materials, can be as low as 10^{-5}. While this control is a technological advantage giving improved performance at a fixed wavelength, another advantage is based on the variations of the mode indices as function of wavelength. This is what ensures the superior bandwidth performance of the PCF over conventional fibers. Finally, the preform fabrication procedure makes it relatively simple to incorporate doped elements, stress applying parts, air-clads, and make highly asymmetrical cores, air-guide fibers etc.

It is the combination of all these advantages that has created the biggest revolution in fiber optics since the field was first invented.

References

1. J. C. Knight, T. A. Birks, P. S. J. Russell, and D. M. Atkin, "All-silica single-mode optical fiber with photonic crystal cladding," Opt. Lett. **21**, 1547 (1996).

2. T. A. Birks, J. C. Knight, and P. S. J. Russell, "Endlessly single-mode photonic crystal fiber," Opt. Lett. **22**, 961 (1997).

3. R. F. Cregan, B. J. Mangan, J. C. Knight, T. A. Birks, P. S. J. Russell, P. J. Roberts, and D. C. Allan, "Single-Mode Photonic Band Gap Guidance of Light in Air," SCIENCE **285**, 1537 (1999).

4. J. K. Ranka, R. S. Windeler, and A. J. Stentz, "Visible continuum generation in air-silica microstructure optical fibers with anomalous dispersion at 800 nm," Opt. Lett. **25**, 25 (2000).

5. J. Limpert, T. Schreiber, S. Nolte, H. Zellmer, T. Tunnermann, R. Iliew, F. Lederer, J. Broeng, G. Vienne, A. Petersson, and C. Jacobsen, "High-power air-clad large-mode-area photonic crystal fiber laser," Opt. Express **11**, 818 (2003).

6. S. C. Buchter, M. Kaivola, H. Ludvigsen, and K. P. Hansen, "Miniature supercontinuum laser sources," in Proceedings of Conference on Lasers and Electro Optics, CLEO, (San Francisco, CA, 2004).

7. N. Venkataraman, M. T. Gallagher, C. M. Smith, D. Müller, J. A. West, K. W. Koch, and J.C. Fajardo, "Low Loss (13 dB/km) Air Core Photonic Crystal Band-Gap Fiber," in Proceedings of 28th European conference on optical communication, PD1.1 (Copenhagen, Denmark, 2002).

8. B. J. Mangan, L. Farr, A. Langford, P. J. Roberts, D. P. Williams, F. Couny, M. Lawman, M. Mason, S. Coupland, R. Flea, H. Sabert, T. A. Birks, J. C. Knight, and P. S. Russell, "Low loss (1.7 dB/km) hollow core photonic bandgap fiber," in Proceedings of Optical Fiber Communication Conference & Exhibition, OFC, PDP24 (Los Angeles, California, USA, 2004).

9. J. C. Knight, T. A. Birks, R.F Cregan, P. S. Russell, and J.-P. de Sandro, "Large Mode area photonic crystal fibre," Electron. Lett. **34**, 1347 (1998).

10. S. G. Johnson and J. D. Joannopoulos, "Block-iterative frequency-domain methods for Maxwell's equations in a planewave basis," Opt. Express **8**, 173 (2001).

11. W. H. Reeves, D. V. Skryabin, F. Biancalana, J. C. Knight, P. S. Russell, F. G. Omenetto, A. Efimov, and A. J. Taylor, "Transformation and control of ultra-short pulses in dispersion engineered photonic crystal fibers," Nature **424**, 511 (2003).

12. K. P. Hansen, "Dispersion flettened hybrid-core nonlinear photonic crystal fibre," Opt. Express **11**, 1503 (2003).

13. J. C. Knight, J. Arriaga, T. A. Birks, A. Ortogosa-Blanch, W. J. Wadsworth, and P. S. Russell, "Anomalous dispersion in photonic crystal fiber," IEEE Photonic Tech. L. **12**, 807 (2000).

14. A. W. Snyder and J. D. Love, *Optical Waveguide Theory*, (Kluwer Academic Publishers, 1983).

15. T. P. White, R.C. McPhedran, C. M. de Sterke, L.C. Botten, and M. J. Steel, "Confinement losses in microstructured optical fibers," Opt. Lett. **26**, 1660 (2001).

16. W. H. Reeves, J. C. Knight, and P. S. Russell, "Demonstration of ultra-flattened dispersion in photonic crystal fibers," Opt. Express **10**, 609 (2002).

17. H. Renner, "Leaky-mode loss in coated depresed-cladding fibers," IEEE Photon. Technol. Lett. **3**, 31 (1991).

18. L. G. Cohen, D. Marcuse, and W. L. Mammel, "Radiating Leaky-mode losses in single-mode lightguides with depressed-index claddings," Journal of Quantum Electronics **QE-18**, 1467 (1982).

19. J. B. MacChesney, D. W. Johnson, P. J. Lemarie, L. G. Cohen, and E. M. Rabinovich, "Depressed index substrate tubes to eliminate leaky-mode losses in single-mode fibers," J. Lightwave Technol. **LT-3**, 942 (1985).

20. J. Lægsgaard, A. Bjarklev, and S. E. B. Libori, "Chromatic dispersion in photonic crystal fibers: fast and accurate scheme for calculation," J. Opt. Soc. Am. B **20**, 443 (2003).

21. K. Tajima, J. Zhou, K. Kurokawa, and K. Nakajima, "Low water peak photonic crystal fibers," in Proceedings of 29th European Conference on Optical Communication, ECOC'03, Post deadline paper (Rimini, Italy, 2003), pp. 42.

22. W. A. Gambling, D. N. Payne, and H. Matsumyra, "Cut-off frequency in radially inhomogeneous single-mode fibre," Electron. Lett. **13**, 139 (1977).

23. D. Gloge, "Weakly guiding fibers," Appl. Optics **10**, 2252 (1971).

24. D. Marcuse, "Gaussian approximation of the fundamental modes of graded-index fibers," J. Opt. Soc. Am. **68**, 103 (1978).

25. N. A. Mortensen, "Effective Area of photonic crystal fibers," Opt. Express **10**, 341 (2002).

26. T. P. White, B. T. Kuhlmey, R.C.McPhedran, D.Maystre, G.Renversez, C. Martijn de Sterke, and L.C.Botten, "Multipole method for microstructured optical fibers. I. Formulation," J. Opt. Soc. Am. B **19**, 2322 (2002).

27. B. T. Kuhlmey, T. P. White, G. Renversez, D. Maystre, L.C. Botten, C. M. de Sterke, and R.C. McPhedran, "Multipole method for microstructured optical fibers. II. Implementation and results," J. Opt. Soc. Am. B **19**, 2331 (2002).

28. B. T. Kuhlmey, R.C. McPhedran and C. M. de Sterke, "Modal cutoff in microstructured optical fibers," Opt. Lett. **27**, 1684 (2002).

29. J. R. Folkenberg, N. A. Mortensen, K. P. Hansen, T. P. Hansen, H. R. Simonsen, and C. Jacobsen, "Experimental investigation of cut-off phenomena in non-linear photonic crystal fibers," Opt. Lett. **28**, 1882 (2003).

30. N. A. Mortensen, J. R. Folkenberg, P. M. W. Skovgaard, and J. Broeng, "Numerical Aperature of Single-Mode Photonic Crystal fibers," IEEE Photon. Technol. Lett. **14**, 1094 (2002).

31. J. D. Love, "Application of a low-loss criterion to optical waveguides and devices," IEE Proceedings J. **136**, 225 (1989).

32. D. Gloge, "Optical-fiber packaging and its influence on fiber straightness and loss," AT&T Tech. J. **54**, 245 (1974).

33. D. Marcuse, "Microbending losses of single-mode, step-index and multimode, parabolic-index fibers," AT&T Tech. J. 937 (1976).

34. W. A. Gambling, H. Matsumoto, and C. M. Ragdale, "Curvature and microbending losses in single-mode optical fibers," Optical and quantum electronics **11**, 43 (1978).

35. D. Marcuse, "Microdeformation losses of single-mode fibers," Appl. Optics **23**, 1082 (1984).

36. A. Bjarklev, "Microdeformation losses of single-mode fibers with step-index profiles," J. Lightwave Technol. **LT-4**, 341 (1986).

37. V. Arya, K. A. Murphy, A. Wang, and R. O. Claus, "Microbend Losses in Single-mode Optical Fibers: Theoretical and Experimental Investigation," J. Lightwave Technol. **13**, 1998 (1995).

38. A. Bjarklev and S. B. Andersen, "Microbending Characterization pf optical fibers from artificially induced deformation," Electron. Lett. **25**, 417 (1989).

39. IEC Tech. Rep. TR 62221, 1.0. *(International Electrotechnical Commision, Geneva, Switzerland, 2001)*.

40. K. Furuya and Y. Suematsu, "Random bend losses in single-mode optical fibre cables: power spectrum estimation from spectral losses," Electron. Lett. **14**, 653 (1978).

41. N. A. Mortensen and J. R. Folkenberg, "Low-loss criterion and effective area considerations for photonic crystal fibers," J. Opt. A: Pure Appl. Opt. **5**, 163 (2003).

42. J. C. Bagget, T. M. Monro, K. Furusawa, V. Finazzi, and D. J. Richardson, "Understanding bending losses in holey optical fibers," Opt. Commun. **227**, 317 (2003).

43. T. Sørensen, J. Broeng, A. Bjarklev, E. Knudsen, and S. E. B. Libori, "Macro-bending Loss Properties of Photonic Crystal Fibre," Electron. Lett. **37**, (2001).

44. T. Sørensen, J. Broeng, A. Bjarklev, T. P. Hansen, E. Knudsen, S. E. B. Libori, H. R. Simonsen, and J. R. Jensen, "Spectral macro-bending loss considerations for photonic crystal fibers," IEE Proc. -Optoelectronics **149**, 206 (2002).

45. J. Sakai and T. Kimura, "Bending loss of propagation modes in arbitrary-index profile optical fibers," Appl. Optics **17**, 1499 (1978).

46. J. Sakai, "Simplified bending loss formula for single-mode optical fibers," Appl. Optics **18**, 951 (1979).

47. W. J. Wadsworth, J. C. Knight, A. Ortogosa-Blanch, J. Arriaga, E. Silvestre, and P. S. Russell, "Soliton effects in photonic crystal fibers at 850 nm," Electron. Lett. **36**, (2000).

48. P.J.Bennett, T. M. Monro, and D. J. Richardson, "Toward practical holy fiber technology: fabrication, splicing, modeling, and characterization," Opt. Lett. **24**, 1203 (1999).

49. H. Kubota, K. Suzuki, S. Kawanishi, M. Nakazawa, M. Tanaka, and M. Fujita, "Low-loss, 2 km-long photonic crystal fiber with zero GVD in the near IR suitable for pico second pulse propagation at the 800 nm band," in Proceedings of Conference on Lasers and Electro Optics, CLEO 2001, CPD3 (Baltimore, Maryland, USA, 2001).

50. K. Tajima, K. Nakajima, K. Kurokawa, N. Yoshizawa, and M. Ohashi, "Low-loss photonic crystal fibers," in Proceedings of Optical Fiber Communication Conference & Exhibition, OFC, ThS3 (Anaheim, 2002), pp. 523.

51. L. Farr, J. C. Knight, B. J. Mangan, and P. J. Roberts, "Low loss photonic crystal fibre," in Proceedings of 28th European conference on optical communication, PD1.3 (Copenhagen, 2002).

52. K. Tajima, J. Zhou, K. Nakajima, and K. Sato, "Ultra low loss and long length photonic crystal fiber," in Proceedings of Optical Fiber Communication Conference & Exhibition, OFC, Post Deadline (Anaheim, CA, 2003).

53. K. Nagayama, M. Kakui, M. Matsui, T. Saitoh, and Y. Chigusa, "Ultra-low-loss (0.1484 dB/km) pure silica core fibre and extension of transmission distance," Electron. Lett. **38**, 1168 (2002).

54. K. Tsujikawa, K. Tajima, and J. Zhou, "Reduction in optical loss of conventional and photonic crystal fibers," in Proceedings of Optical Fiber Communication Conference & Exhibition, OFC, WI5 (Los Angeles, California, USA, 2004).

55. M. Yamane and Y. Asahara, *Glasses for Photonics*, (Cambridge University Press, 2000).

56. T. Hasegawwa and M. Onishi, Optical Fibre with Longitudinal holes and Manufacturing method thereof. 02003258.7. 2003. 2-21-2002. (patent application)

57. R.T. Bise, R. S. Windeler, K.S. Kranz, C. Kerbage, B. J. Eggleton, and D. J. Trevor, "Tunable photonic band gap fiber," in Proceedings of Optical Fiber Communication Conference & Exhibition, OFC, ThK3 (Anaheim, CA, 2002), pp. 466.

58. S. Shibata, "Sol-gel-derived silica preforms for optical fibers," J. Non-Cryst. Solids **178**, 272 (1994).

59. R. H. Doremus, "Diffusion of water in silica glass," J. Mater Res. **10**, 2379 (1995).

60. T. Izawa, N. Shibata, and A. Takeda, "Optical attenuation in pure and doped fused silica in the ir wavelength region," Appl. Phys. Lett. **31**, 33 (1977).

61. O. Humbach, H. Fabian, U. Grzesik, U. Haken, and W. Heitmann, "Analysis of OH absorption bands in synthetic silica," J. Non-Cryst. Solids **203**, 19 (1996).

62. M. Bredol, D. Leers, L. Bosselaar, and M. Huntjens, "Improved Model for OH Absorption in Optical Fibers," J. Lightwave Technol. **8**, 1536 (1990).

63. J. Stone and G.E. Walrafen, "Overtone vibrations of OH groups in fused silica optical fibers," J. Chem. Phys. **76**, 1712 (1982).

64. T. Moriyama, O. Fukuda, K. Sanada, K. Inada, T. Edahiro, and K. Chida, "Ultimately low OH content V.A.D. optical fibers," Electron. Lett. **16**, 698 (1980).

65. G. N. Greaves, "Intrinsic and Modified defect states in silica," J. Non-Cryst. Solids **32**, 295 (1979).

66. M. Stapelbroek, D. L. Griscom, E. J. Friebele, and G.H. Sigel, "Oxygen-associated trapped-hole centers in high-purity fused silicas," J. Non-Cryst. Solids **32**, 313 (1979).

67. D. L. Griscom, "Defect Structures of glasses," J. Non-Cryst. Solids **73**, 51 (1985).

68. G. N. Greaves, "Colour Centers in Vitreous Silica," Philos. Mag, B **37**, 447 (1978).

69. V. B. Neustruev, "Colour centers in germanosilicate glass and optical fibers," J. Phys.: Condensed Mat. **6**, 6901 (1994).

70. K. F. Klein, R. Arndt, G. Hillrichs, M. Ruetting, M. Veidemanis, R. Dreiskemper, J. Clarkin, and G. Nelson, "UV-Fibers For Applications below 200 nm," Proceedings of SPIE **4253**, 42 (2001).

71. S. Unger, J. Kirchhof, S. Schröter, A. Schwuchow, and H. Frost, "Transmission Behaviour of Silica Core - Fluorine Doped Cladding Fibers in the Visible and Ultraviolet Regions," Proceedings of SPIE **4616**, 161 (2002).

72. J. Vydra and G. Schötz, "Improved all silica fibers for deep UV-applications," Proceedings of SPIE **3596**, 165 (1999).

73. D. L. Griscom and M. Mizuguchi, "Determination of the visible range optical absorption spectrum of peroxy radicals in gamma-irradiated fused silica," J. Non-Cryst. Solids **239**, 66 (1998).

74. L. Skuja, K. Tanimura, and N. Itoh, "Correlation between the radiation-induceed intrinsic 4.8 eV optical absorption and 1.9 eV Photoluminescence bands in glassy SiO_2," J. Appl. Phys. **80**, 3518 (3518).

75. L. Skuja, M. Mizuguchi, H. Hosono, and H. Kawazoe, "The Nature of the 4.8 eV optical absorption band induceed by vacuum-ultraviolet irradiation of glassy SiO_2," Nuclear Instruments and Methods in Physics Research B **166**, 711 (2000).

76. E. J. Friebele, D. L. Griscom, and M. J. Marrone, "The optical absorption and luminescence bands near 2 eV in irradiated and drawn synthetic silica," J. Non-Cryst. Solids **71**, 133 (1985).

77. L. Skuja, "Section 2 - Point defects in silica glass Luminescence and optical absorption - The origin of the intrinsic 1.9 eV luminescence band in glassy SiO_2," J. Non-Cryst. Solids **179**, 51 (1994).

78. P. Kaiser, "Drawing-Induced coloration in vitreous silica fibers," J. Opt. Soc. Am. **64**, 475 (1974).

79. Y. Hibino and H. Hanafusa, "Defect structure and formation mechanism of drawing-induced absorption at 630 nm in silica optical fibers," J. Appl. Phys. **60**, 1797 (1986).

80. Y. Hibino and H. Hanafusa, "Formation mechanism of drawing induceed peroxy radicals in pure silica optical fibers," J. Appl. Phys. **62**, 1433 (1987).

81. H. Hanafusa, Y. Hibino, and F. Yamamoto, "Formation mechanism of drawing-induced defects in optical fibers," J. Non-Cryst. Solids **95**, 655 (1987).

82. A. Lino, M. Kuwabara, and K. Kokura, "Mechanisms of Hydrogen-Induced Losses in Silica-Based Optical Fibers," J. Lightwave Technol. **8**, 1675 (1990).

83. Y. Hibino and H. Hanafusa, "Consolidating-Atmosphere influence on Drawing-induced defects in pure silica optical fibers," J. Lightwave Technol. **6**, 172 (1988).

84. T. Niemi, H. Ludvigsen, F. Scholder, M. Legre, M. Wegmüller, N. Gisin, J. R. Jensen, A. Petersson, and P.M.W. Skovgaard, "Polarization Properties of Single-Moded, Large-Mode Area Photonic Crystal Fibers," in Proceedings of 28th European conference on optical communication, Symposium 1.9 (Copenhagen, 2002).

85. T. Kato, M. Hirano, M. Onishi, and M. Nishimura, "Ultra-low nonlinearity low-loss pure silica core fiber for long-haul WDM transmission," Electron. Lett. **35**, 1615 (1999).

86. K. Suzuki, H. Kubota, S. Kawanishi, M. Tanaka, and M. Fujita, "High-speed bi-directional polarization division multiplexed optical transmission in ultra low-loss (1.3 dB/km) polarization maintaining photonic crystal fibre," Electron. Lett. **37**, 1399 (2001).

87. B. Zsigri, C. Peucheret, M. D. Nielsen, and P. Jeppesen, "Transmission over 5.6 km large effective area and low loss (1.7 dB/km) photonic crystal fiber," Electron. Lett. **39**, 796 (2003).

88. P. A. Andersen, B. Zsigri, C. Peucheret, P. Jeppesen, K. P. Hansen, and M. D. Nielsen, "Photonic Crystal Fibers used in a Multi-Wavelength Source and as Transmission Fiber in a WDM System," in Proceedings of Conference on Lasers and Electro Optics, CLEO, (San Francisco, CA, 2004).

89. C. Peucheret, B. Zsigri, P. A. Andersen, K. S. Berg, A. Tersigni, P. Jeppesen, K. P. Hansen, and M. D. Nielsen, "Transmission over photonic crystal fiber at 40 Gbit/s using mid-span spectral inversion in a highly nonlinear photonic crystal fiber," in Proceedings of Conference on Lasers and Electro Optics, CLEO, Post Deadline (Baltimore, MD, USA, 2003).

90. C. Peucheret, B. Zsigri, P. A. Andersen, K. S. Berg, A. Tersigni, P. Jeppesen, K. P. Hansen, and M. D. Nielsen, "40 Gbit/s transmission over photonic crystal fibre using mid-span spectral inversion in a highly nonlinear photonic crystal fibre," Electron. Lett. **39**, 919 (2003).

91. B. Zigri, C. Peucheret, M. D. Nielsen, and P. Jeppesen, "Transmission over 57.6 km of photonic crystal fiber," in Proceedings of 9th OptoElectronics and Communications Conference - OECC, Submitted (2004).

92. T. P. Hansen, J. Broeng, S. E. B. Libori, E. Knudsen, A. Bjarklev, J. R. Jensen, and H. R. Simonsen, "Highly Birefringent Index-Guiding Photonic Crystal Fibers," IEEE Photonic Tech. L. **13**, 588 (2001).

93. M. J. Steel, T. P. White, C. M. de Sterke, R.C. McPhedran, and L.C. Botten, "Symmetry and degeneracy in Microstructured optical fibers," Opt. Lett. **26**, 488 (2001).

94. J. Broeng, G. Vienne, A. Petersson, P. M. W. Skovgaard, J. R. Folkenberg, M. D. Nielsen, C. Jacobsen, H. R. Simonsen, and N. A. Mortensen, "Air-clad photonic crystal fibers for high-power single-mode lasers," Proceedings of SPIE **5335**, 192 (2004).

95. J. C. Knight, J. Broeng, T. A. Birks, and P. S. Russell, "Photonic band gap guidance in optical fibers," Science **282**, 1476 (1998).

96. T. P. Hansen, J. Broeng, and A. Bjarklev, "Solid-core Photonic Bandgap fiber with large anormalous dispersion," in Proceedings of Optical Fiber Communication Conference & Exhibition, OFC, FI6 (Atlanta, Ge, 2003), pp. 700.

97. J. Lægsgaard and A. Bjarklev, "Doped photonic bandgap fibers for short-wavelength nonlinear devices," Opt. Lett. **28**, 783 (2002).

98. K. Saitoh and M. Koshiba, "Single-polarization single-mode photonic crystal fibers," IEEE Photonic. Tech. L. **15**, 1384 (2003).

99. D. A. Nolan, G. E. Berkey, M.-J. Li, X. Chen, W. A. Wood, and L. A. Zenteno, "New single polarization fiber with high extinction ratio," in Proceedings of Optical Fiber Communication Conference & Exhibition, OFC, WI6 (Los Angeles, CA, USA, 2004).

100. A. Ortogosa-Blanch, J. C. Knight, W. J. Wadsworth, J. Arriaga, B. J. Mangan, T. A. Birks, and P. S. Russell, "Highly birefringent photonic crystal fibers," Opt. Lett. **25**, 1325 (2000).

101. M. D. Nielsen, G. Vienne, J. R. Jensen, and A. Bjarklev, "Modeling birefringence in isolated elliptical core photonic crystal fibers," in Proceedings of The Lasers and Electro Optics Society Annual Meeting, ThG4 (San Diego, CA, 2001), pp. 707.

102. K. Suzuki, H. Kubota, S. Kawanishi, M. Tanaka, and M. Fujita, "Optical Properties of a low-loss polarization-maintaining photonic crystal fiber," Opt. Express **9**, 676 (2001).

103. J. Noda, K. Okamoto, and Y. Sasaki, "Polarization-maintaining fibers and their applications," J. Lightwave Technol. **4**, 1071 (1986).

104. P. L. Chu and R. A. Sammut, "Analytical Method for Calculation of Stresses and Material birefringence in Polarization-Maintaining Optical Fiber," J. Lightwave Technol. **2**, 650 (1984).

Paper A

M.D. Nielsen, C. Jacobsen, N.A. Mortensen, J.R. Folkenberg, and H.R. Simonsen

"*Low-loss photonic crystal fibers for data transmission and their dispersion properties*"

Optics Express, Vol. **12**, No. 7, pp. 1372-1376

(2004)

Low-loss photonic crystal fibers for transmission systems and their dispersion properties

M.D. Nielsen[1,2], C. Jacobsen[1], N.A. Mortensen[1], J.R. Folkenberg[1], and H.R. Simonsen[1]

[1] *Crystal Fibre A/S, Blokken 84, DK-3460 Birkerød, Denmark*
[2] *COM, Technical University of Denmark,DK-2800 Kongens Lyngby, Denmark*
mdn@crystal-fibre.com

Abstract: We report on a single-mode photonic crystal fiber with attenuation and effective area at 1550 nm of 0.48 dB/km and 130 μm^2, respectively. This is, to our knowledge, the lowest loss reported for a PCF not made from VAD prepared silica and at the same time the largest effective area for a low-loss (< 1 dB/km) PCF. We briefly discuss the future applications of PCFs for data transmission and show for the first time, both numerically and experimentally, how the group velocity dispersion is related to the mode field diameter.

OCIS codes: (060.2400) Fiber Properties, (060.2430) fibers, Single-mode, (999.999) Photonic crystal fiber

References and Links

1. K. Tajima, K. Nakajima, K. Kurokawa, N. Yoshizawa, and M. Ohashi "*Low-loss photonic crystal fibers,*" Optical fiber communications conference, OFC 2002 (Anaheim, CA, USA)**,** pp. 523-524 (2002).
2. L. Farr, J. C. Knight, B. J. Mangan, and P. J. Roberts "*Low loss photonic crystal fibre,*" 28th European conference on optical communication (Copenhagen, Denmark)**,** PD1-3, (2002).
3. K. Tajima, J. Zhou, K. Nakajima, and K. Sato "*Ultra low loss and long length photonic crystal fiber,*" Optical fiber communications conference, OFC (Anaheim, CA, USA)**,** PD1, (2003).
4. K. Tajima, J. Zhou, K. Kurokawa, and K. Nakajima "*Low water peak photonic crystal fibers,*" 29th European conference on optical communication ECOC'03 (Rimini, Italy)**,** pp. 42-43 (2003).
5. C.M. Smith, N. Venkataraman, M.T. Gallagher, D. Müller, J.A. West, N.F. Borrelli, D.C. Allan, and K.W. Koch, "Low-loss hollw-core silica/air photonic bandgap fibre," Nature **424**, 657-659 (2003).
6. N.A. Mortensen and J.R. Folkenberg, "Low-loss criterion and effective area considerations for photonic crystal fibers," J. Opt. A: Pure Appl. Opt. **5**, 163-167 (2003).
7. O. Humbach, H. Fabian, U. Grzesik, U. Haken, and W. Heitmann, "Analysis of OH absorption bands in synthetic silica," J. Non-Cryst. Solids **203**, 19-26 (1996).
8. M.D. Nielsen and N.A. Mortensen, "Photonic crystal fiber design based on the V-parameter," Opt. Express **11**, 2762-2768 (2003). http://www.opticsexpress.org/abstract.cfm?URI=OPEX-11-21-2762
9. M.D. Nielsen, J.R. Folkenberg, N.A. Mortensen, and A. Bjarklev, "Bandwidth comparison of photonic crystal fibers and conventional single-mode fibers," Opt. Express **12**, 430-435 (2004). http://www.opticsexpress.org/abstract.cfm?URI=OPEX-12-3-430
10. M.D. Nielsen, J.R. Folkenberg, and N.A. Mortensen, "Singlemode photonic crystal fiber with effevtive area of 600 μm^2 and low bending loss," Electron. Lett. **39**, 1802-1803 (2004).
11. S.G. Johnson and J.D. Joannopoulos, "Block-iterative frequency-domain methods for Maxwell's equations in a planewave basis," Opt. Express **8**, 173-190 (2001). http://www.opticsexpress.org/abstract.cfm?URI=OPEX-8-3-173
12. J. Lægsgaard, A. Bjarklev, and S.E.B. Libori, "Chromatic dispersion in photonic crystal fibers: fast and accurate scheme for calculation," J. Opt. Soc. Am. B **20**, 443-448 (2003).
13. G.P. Agrawal, *Fiber-Optic Communication Systems* (John Wiley & Sons, Inc., 1997)
14. T. Kato, M. Hirano, M. Onishi, and M. Nishimura, "Ultra-low nonlinearity low-loss pure silica core fiber for long-haul WDM transmission," Electron. Lett. **35**, 1615-1617 (1999).
15. K. P. Hansen, J. R. Jensen, C. Jacobsen, H. R. Simonsen, J. Broeng, P. M. W. Skovgaard, A. Petersson, and A. Bjarklev "*Highly Nonlinear Photonic Crystal Fiber with Zero-Dispersion at 1.55 μm,*" Optical fiber Communications conference OFC 2002 (Anaheim, CA, USA)**,** (2002).

#3860 - $15.00 US Received 23 February 2004; revised 23 March 2004; accepted 26 March 2004

1. Introduction

In recent years, the typical attenuation level of photonic crystal fibers (PCFs) has been reduced dramatically. This is both true for fibers relying on index guiding [1-4] as well as those based on the photonic bandgab effect [5], although the latter type still needs to improve with almost two orders of magnitude in order to have lower loss than the index guiding fibers.

A few years back, the typical attenuation level for index guiding PCFs was a few dB/km at 1550 nm. In the beginning of 2002 the 1 dB/km limit was reached [1] and during a relatively short period of time, this was improved to the current record level of 0.28 dB/km [4]. The most recent improvements have been obtained by using high purity glass prepared by the vapour-phase axial deposition (VAD) technique and by eliminating the presence of OH contamination. While these advances are indeed both significant and impressing, most of the fibers reported have relative small effective areas no larger than ~80 μm^2 [4], and typically ~20 μm^2 [1-3]. Since the sensitivity towards attenuation caused by structural variations, both in the transverse and longitudinal dimension of the fiber, increases as the effective area is increased, it is interesting to hold up the effective area against the obtained attenuation level [6].

Here we present results on a low-loss PCF with an effective area significantly larger than that of previous reports. Also, we numerically investigate the relation between the mode-field diameter (MFD) and the group velocity dispersion (GVD) at the 1550 nm wavelength and compare the obtained results with measurements performed on a broad range of PCFs with widely different dimensions. All the fibers considered here are index-guiding PCFs with a cladding region consisting of a triangular arrangement of air holes running along the full length of the fiber surrounding a central core region which is formed by omitting a single air hole.

2. Fabricated fiber

An optical micrograph of the fabricated PCF is shown in Fig. 1, indicating the fiber diameter, D = 173 µm, the air-hole diameter, d = 5.15 µm, and the pitch, Λ = 10.6 µm. The fiber has a single-layer acrylate coating (not shown) with a diameter of 315 µm. As seen from the picture, the microstructured cladding region consists of 54 air holes corresponding to 4 periods of which the 6 holes in the corners of the outer ring have been omitted.

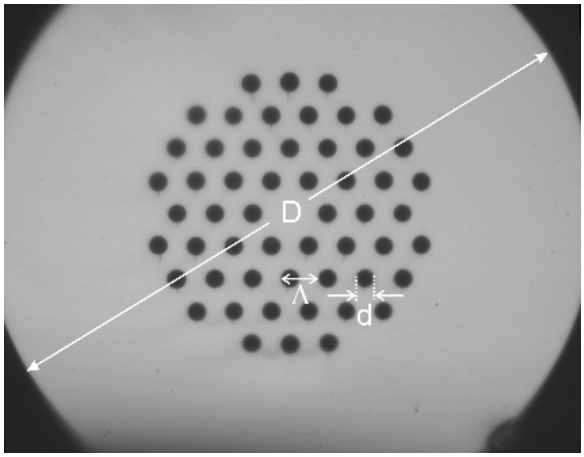

Fig. 1. Optical micrograph of the fabricated PCF.

#3860 - $15.00 US Received 23 February 2004; revised 23 March 2004; accepted 26 March 2004

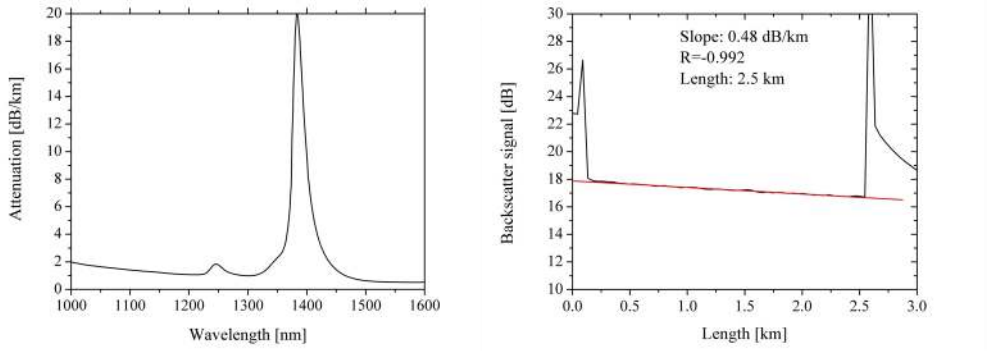

Fig. 2. Measured spectral attenuation (left) and OTDR trace at 1550 nm (right) of the fabricated PCF.

The fiber was fabricated by the stack and pull method where capillary tubes made of pure silica are stacked in a hexagonal pattern around a central silica rod. The surfaces of the elements were polished prior to stacking in order to reduce the influence of surface roughness [1]. The raw materials used for this fiber were commercially available silica rods and tubes with a typical OH content in the order of ~0.5 ppm.

The spectral attenuation of the fiber was measured by the cutback technique using a white light source and an optical spectrum analyzer. The fiber length used for this measurement was 2.5 km and the obtained attenuation spectrum is shown in Fig. 2 (left). In order to check for inhomogeneities, such as scattering points, along the fiber length, the fiber was inspected using an optical time domain reflectometer (OTDR) with an operating wavelength of 1550 nm and pulse duration of 10 ns. The obtained OTDR trace is shown in Fig. 2 (right) as the black solid line. The red line, also shown in Fig. 2 (right), is the result of a linear regression on the measured data yielding a slope of -0.48 dB/km with a Pearson factor, R = -0.992, indicating a highly homogeneous fiber. The agreement between the attenuation at 1550 nm obtained from the spectral measurements and from the OTDR is excellent and well within the measurement uncertainty.

Analyzing the spectral attenuation data shows an OH induced attenuation peak at 1380 nm in the order of 20 dB/km corresponding to an OH concentration of ~0.4 ppm [7] and an attenuation contribution at 1550 nm of 0.15 dB/km [4]. This is in good agreement with the expected values from the raw materials. By extracting the λ^{-4} dependent scattering component, the Rayleigh scattering coefficient was determined to be 1 dB/(km·μm^4), equivalent to a contribution of 0.18 dB/km at 1550 nm. The remaining 0.16 dB/km of the attenuation at 1550 nm is attributed to the absorption from impurities and other imperfections.

From d/Λ and Λ, the effective area of the fundamental mode is calculated to be 130 μm^2 [8] which is equivalent to a Gaussian MFD of ~13 μm. This way of determining the MFD has proven to agree with measured data well within the typical measurement uncertainty [9,10]. This is to our knowledge the largest effective area reported so far for a low loss (< 1dB km) PCF.

3. Dispersion

As the effective area is increased and the strength of the wave guiding decreases, the GVD is expected to approach that of the bulk material [10]. Since the waveguide contribution to the dispersion is always positive when $\lambda << \Lambda$, the GVD must decrease towards the material dispersion for increasing effective area.

#3860 - $15.00 US Received 23 February 2004; revised 23 March 2004; accepted 26 March 2004

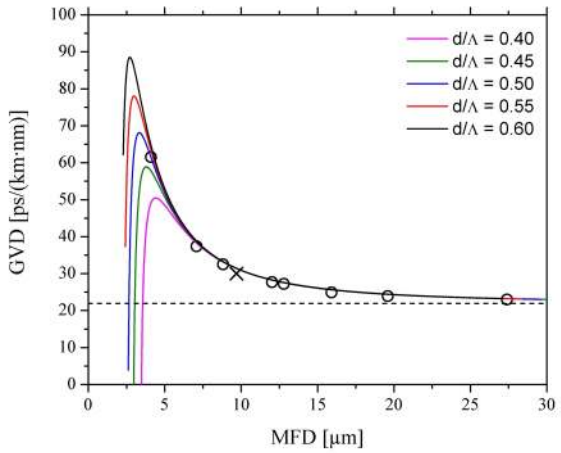

Fig. 3. GVD at 1550 nm as function of the MFD. The solid line indicates numerical results and the dashed line indicates D_M. Measured values at 1550 nm for 8 different PCF are indicated by circles while the cross represents independent data from Ref. [4].

By using the plane-wave expansion method [11], the effective index, n, as function of the free-space optical wavelength, λ, and the effective area of the fundamental mode was calculated for a range of d/Λ values from 0.40 to 0.60 covering the relevant parameter space for possible transmission fibers. In these numerical simulations, the refractive index of silica was taken to have a constant value of 1.444. The GVD is defined as the derivative of v_g^{-1} with respect to λ, where v_g is the group velocity, and can therefore be calculated by the following relation where c is the speed of light and D_M is the material dispersion:

$$GVD = \frac{d}{d\lambda}\left(\frac{1}{v_g}\right) = -\frac{\lambda}{c}\frac{d^2 n}{d\lambda^2} + D_M$$

In this expression it has been assumed that the waveguide contribution to the GVD is independent of D_M which is a good approximation provided that $\lambda << \Lambda$ [12]. The value of D_M for pure silica at 1550 nm was calculated from the Sellmeier relation [13] to be 21.9 ps/(km·nm). In Fig. 3, the calculated GVD at 1550 nm is plotted as function of the MFD for d/Λ = 0.40, 0.45, 0.50, 0.55, and 0.60 indicated by solid lines while D_M is indicated by the dashed horizontal line. As seen from this plot, all the solid curves coincide for MFDs larger than ~5 μm and the GVD is thus in this range given by the MFD regardless of the exact value of d/Λ. To verify whether the calculated relation corresponds with measurements, the group delay as function of wavelength was measured for a broad range of PCFs with widely different MFDs and from these data the GVD at 1550 nm of each fiber was derived. The measured fibers all had the same basic structure although the number of air holes varied from fiber to fiber. The MFDs of all the characterized fibers were calculated from the relation given in Ref. [8] and in Table 1, Λ, d/Λ, calculated MFD and measured GVD are listed. The number in the IDs refers to the approximate size of the core region. The measurements listed in Table 1 are indicated in Fig. 3 by open circles and in general, excellent agreement with numerical results is observed with a typical deviation of 0.5 ps/(km·nm). The deviation for the LMA5 is seen to be slightly larger which is attributed to the exact determination of d/Λ which plays a role for this fiber only and, more importantly, to the fact that the assumption that $\lambda << \Lambda$ is no longer fulfilled. The data point in Fig. 3 indicated by a cross represents independent data from Ref. [4] and also in this case the agreement is very good.

#3860 - $15.00 US Received 23 February 2004; revised 23 March 2004; accepted 26 March 2004

Table 1. Structural parameters, calculated MFD and measured dispersion of the tested PCFs

ID	Λ [μm]	d/Λ	MFD [μm]	GVD [ps/(km·nm)]
LMA-5[1]	2.9	0.44	4.1	61.5
LMA-8[1]	5.6	0.46	7.1	37.4
LMA-10	7.2	0.48	8.8	32.5
LMA-15	10.0	0.50	12.0	27.7
LMA-16	10.6	0.49	12.8	27.2
LMA-20	13.0	0.47	15.9	24.9
LMA-25	16.4	0.50	19.5	23.9
LMA-35[2]	23.2	0.50	27.4	23.0

[1]More information on this fiber is available in Ref. [9]
[2]More information on this fiber is available in Ref.[10]

4. Discussion and conclusion

The recent advances in the reduction of the attenuation level of index-guiding PCFs have left little doubt that these fibers, from an attenuation point of view, will be able to compete with conventional solid fibers for data transmission applications. One can even speculate that the ultimate attenuation level of the PCF might be even lower than that of conventional fibers since the PCF is a single material fiber with no boundary between two types of glass with different thermal expansion coefficients. However, little interest has until now been paid towards the GVD properties of these fibers in the telecom window. As demonstrated here, the GVD for the PCF will always tend to have a higher value than what is typical for a conventional solid fiber with comparable MFD. With proper dispersion compensation, this high GVD could be an advantage since it tends to suppress nonlinear interaction between channels in multi-wavelength transmission systems [14] .

The numerical results in Fig. 3 have a slight offset compared with the measured data in the order of 0.5 ps/(km·nm). Since this offset is independent of both the MFD and the GVD values, we attribute this to a corresponding deviation in calculated material dispersion from the actual material dispersion value of the glass.

For sufficiently small MFDs, the GVD passes through zero and which has been used for realization of nonlinear fibers with zero dispersion at 1550 nm [15]. At some point, a further reduction of the structural scale, the mode will begin to expand relative to the structure and the MFD will increase. The simple behavior outlined here for large-mode area fibers should therefore not be extrapolated to nonlinear fibers.

We have demonstrated a PCF with an effective area of 130μm^2 and attenuation at 1550 nm of 0.48 dB/km and thereby shown that PCFs with effective areas able to compete with conventional solid fibers can be obtained while keeping the attenuation low. A significant contribution to this attenuation level was OH contamination present in the raw materials. We believe that the attenuation can be reduced close to the fundamental limit of pure silica while, at the same time, even larger effective areas than the one reported here, can be obtained.

Acknowledgments

M.D. Nielsen acknowledges financial support from the Danish Academy of Technical Sciences.

#3860 - $15.00 US Received 23 February 2004; revised 23 March 2004; accepted 26 March 2004

Paper B

N.A. Mortensen, J.R. Folkenberg, **M.D. Nielsen**, and K.P. Hansen

"*Modal cut-off and the V-parameter in photonic crystal fibers*"

Optics Letters, Vol. **28**, No. 20, pp.1879-1881

(2003)

Modal cutoff and the V parameter in photonic crystal fibers

Niels Asger Mortensen and Jacob Riis Folkenberg

Crystal Fibre A/S, Blokken 84, DK-3460 Birkerød, Denmark

Martin D. Nielsen and Kim P. Hansen

Crystal Fibre A/S, Blokken 84, DK-3460 Birkerød, Denmark, and
COM, Technical University of Denmark, DK-2800 Kongens Lyngby, Denmark

Received April 1, 2003

We address the long-standing unresolved problem concerning the V parameter in a photonic crystal fiber. In formulating the parameter appropriate for a core defect in a periodic structure, we argue that the multimode cutoff occurs at a wavelength λ^* that satisfies $V_{\mathrm{PCF}}(\lambda^*) = \pi$. By comparing this approach with numerics and recent cutoff calculations we confirm this result. © 2003 Optical Society of America

OCIS codes: 060.2310, 060.2400, 060.2430.

In a photonic crystal fiber (PCF) an arrangement of air holes running along the full length of the fiber provides the confinement and guidance of light. Air holes of diameter d are typically arranged in a triangular lattice[1] with a pitch Λ (see insert in Fig. 1), but, e.g., honeycomb[2] and kagome[3,4] arrangements are other options. By making a defect in the lattice, one can confine light and guide it along the fiber axis. The guidance mechanism depends on the nature of the defect and the air-hole arrangement. For a triangular lattice with a silica core, light is confined by total internal reflection,[1] whereas for an air core a photonic bandgap confines light to the defect.[5] For recent reviews we refer to Ref. 6 and references therein.

Both types of PCF have revealed surprising and novel optical properties. In this Letter we consider the silica-core PCF (see insert in Fig. 1) which was the one first reported.[1] This structure provides the basis of a variety of phenomena, including endlessly single-mode behavior,[7] large-mode-area PCFs,[8] and highly nonlinear PCF with unique dispersion properties.[9–11]

Properties of standard fibers are often parametrized by the so-called V parameter and the entire concept is very close to the heart of the majority of the optical fiber community (see, e.g., Refs. 12 and 13). The cutoff properties and the endlessly single-mode phenomena of PCFs can also be qualitatively understood within this framework.[1,7,14–16] However, the proper choice of the correct length scale for the V parameter has, until now, remained unsolved and so has the value of V^* that marks the second-order cutoff. In this Letter we clarify this problem and also put recent work on multimode cutoff[17,18] into the context of the V parameter.

The tradition of parametrizing the optical properties in terms of the V parameter stems from analysis of the step index fiber (SIF). The SIF is characterized by the core radius ρ, the core index n_c, and the cladding index n_{cl}, which all enter into the parameter V_{SIF}, given by

$$V_{\mathrm{SIF}}(\lambda) = \frac{2\pi\rho}{\lambda}\,(n_c{}^2 - n_{\mathrm{cl}}{}^2)^{1/2}. \tag{1}$$

Because of its inverse dependence on the wavelength λ, $V_{\mathrm{SIF}}(\lambda)$ is often referred to as the normalized frequency. However, in a more general context, this is somewhat misleading [especially if n_c and (or) n_{cl} has a strong wavelength dependence], and in this Letter we emphasize a more physical interpretation. To do this, we first introduce the NA (or the angle of divergence θ), given by

$$\mathrm{NA} = \sin\theta = (n_c{}^2 - n_{\mathrm{cl}}{}^2)^{1/2}, \tag{2}$$

which follows from the use of Snell's law for critical incidence at the interface between the n_c and n_{cl} regions (see, e.g., Refs. 12 and 13). Next, we introduce the free-space wave number $k = 2\pi/\lambda$ and its transverse projection $k_\perp = k\,\sin\theta$. The V parameter can now simply be written as

$$V_{\mathrm{SIF}} = k_\perp \rho\,. \tag{3}$$

From this form it is obvious why the parameter carries information about the number of guided modes: The natural parameter describing the transverse intensity distribution is nothing but $k_\perp\rho$. Furthermore, for the second-order cutoff wavelength, λ^*, the usual value $V_{\mathrm{SIF}}(\lambda^*) = V_{\mathrm{SIF}}{}^* \simeq 2.405$ follows naturally from the solution of the first zero of the Bessel function, i.e., $J_0(V_{\mathrm{SIF}}{}^*) = 0$.

In general, for wave propagation in confined structures the number $k_\perp\rho$ has a very central role. The transmission cross section of a narrow slit[19] is an example, and counterparts of the electromagnetic problem can also be seen in, e.g., electronic systems such as the quantum-point contact, where $k_\perp\rho$ also determines the number of modes (see, e.g., Ref. 20). In the context of PCFs it is also natural to consider a V parameter, which was already done in the seminal work by the Bath group[1] and in the subsequent work on endlessly single-mode properties[7] and effective V values.[14] However, in attempting to adopt Eq. (1) to PCFs, one is faced with the problem of choosing a value for ρ, and in Refs. 7 and 14 it was emphasized that one may choose any transverse dimension. In

0146-9592/03/201879-03$15.00/0

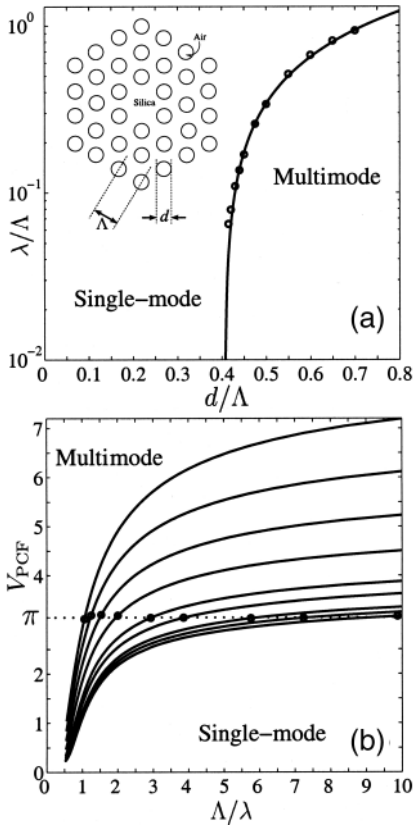

Fig. 1. (a) Single-mode–multimode phase diagram. The solid curve shows the phase boundary of Kuhlmey *et al.*[18] [expression (6)], and the circles indicate solutions to $V_{PCF}(\lambda^*) = \pi$ [Eqs. (4) and (5)]. (b) Numerical results for PCFs with varying hole diameter (from the bottom, $d/\Lambda = 0.43, 0.44, 0.45, 0.475, 0.50, 0.55, 0.60, 0.65, 0.70$). The curves show results for the V parameter [Eq. (4)], the circles indicate the corresponding cutoff wavelengths [expression (6)], and the dotted line shows ${V_{PCF}}^*$ [Eq. (5)].

this Letter we point out that the problem is not a matter of defining a core radius; rather, one should look for the natural length scale of the problem, the air-hole pitch Λ. This choice was also suggested in Ref. 7, although it was considered an arbitrary choice. Regarding the second-order cutoff, it was suggested in Ref. 14 that ${V_{PCF}}^* \approx 2.5$, but it was also concluded that the arbitrary choice of the length scale means that the particular number for ${V_{PCF}}^*$ also becomes somewhat arbitrary. In this Letter we demonstrate that this is not the case and that a very simple and elegant solution exists.

To show this, we introduce the following V parameter for a PCF

$$V_{PCF}(\lambda) = \frac{2\pi\Lambda}{\lambda}[{n_c}^2(\lambda) - {n_{cl}}^2(\lambda)]^{1/2}, \tag{4}$$

where $n_c(\lambda) = c\beta/\omega$ is the "core index" associated with the effective index of the fundamental mode and, similarly, $n_{cl}(\lambda)$ is the effective index of the fundamental space-filling mode in the triangular air-hole lattice. The second-order cutoff occurs at a wavelength λ^*, where the effective transverse wavelength, $\lambda_\perp = 2\pi/k_\perp$, allows a mode with a single node (see the schematic in Fig. 2) to fit into the defect region, i.e., ${\lambda_\perp}^* \simeq 2\Lambda$. When Eq. (4) is written in terms of $k_\perp$ the corresponding value of ${V_{PCF}}^*$ easily follows:

$${V_{PCF}}^* = {k_\perp}^*\Lambda = \frac{2\pi}{{\lambda_\perp}^*}\Lambda = \pi\,. \tag{5}$$

Although this derivation may seem somewhat heuristic, we shall compare it with numerical results and show that the very central number π is indeed the correct value.

For the numerical comparison we need to calculate both $V_{PCF}(\lambda)$ and the second-order cutoff, λ^*. For the V parameter we use a fully vectorial plane-wave method[21] to calculate $n_c(\lambda)$ and $n_{cl}(\lambda)$ for various air-hole diameters. For the material refractive index we use $n = 1$ for the air holes and $n = 1.444$ for the silica. Ignoring the frequency dependence of the latter, the wave equation becomes scale invariant,[22] and all the results to be presented can thus be scaled to the desired value of Λ. Regarding the cutoff, one of us recently suggested a phase diagram for the single-mode and multimode operation regimes,[17] which was subsequently followed up in more detail by Kuhlmey *et al.*[18] From highly accurate multipole solutions of Maxwell's equations, it was numerically found that the single-mode–multimode boundary can be accounted for by the expression[18]

$$\lambda^*/\Lambda \simeq \alpha(d/\Lambda - d^*/\Lambda)^\gamma. \tag{6}$$

Here, $\alpha = 2.80 \pm 0.12$, $\gamma \simeq 0.89 \pm 0.02$, and $d^*/\Lambda \simeq 0.406$. This phase boundary is shown by the solid curve in Fig. 1(a) and was recently confirmed experimentally based on cutoff measurements in various PCFs.[23] For $d/\Lambda < d^*/\Lambda$ the PCF has the remarkable property of being so-called endlessly single mode,[7] and for $d/\Lambda > d^*/\Lambda$ the PCF supports a second-order mode at wavelengths $\lambda/\Lambda < \lambda^*/\Lambda$ and is single mode for $\lambda/\Lambda > \lambda^*/\Lambda$.

In Fig. 1(b) we show numerical results for various values of d/Λ. The solid curves show results for the V parameter, Eq. (4); the circles indicate the corresponding cutoff wavelengths, expression (6); and the dotted line shows ${V_{PCF}}^*$, Eq. (5). First we notice that the cutoff results of Kuhlmey *et al.*,[18] expression (6), agree with a picture of a constant V value ${V_{PCF}}^*$ below which the PCF is single mode. This similarity with SIFs indicates that the cutoff in SIFs and PCFs rely on the same basic physics. Furthermore, it can also be seen that the cutoff points are in excellent agreement with the value ${V_{PCF}}^* = \pi$, Eq. (5), and this also supports the idea of Λ as the natural length scale for the V parameter. We emphasize that the extremely

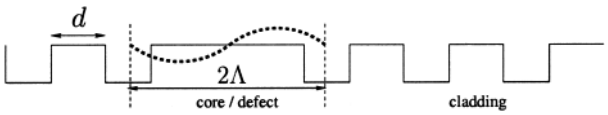

Fig. 2. Schematics of the cross section of a PCF. The dotted curve illustrates the field amplitude of a second-order mode with a single node.

small deviations from this value are within the accuracy of the coefficients in expression (6). In Fig. 1(b) the data points show cutoff results calculated from $V_{\mathrm{PCF}}(\lambda^*) = \pi$, and these results are in perfect agreement with the results of Kuhlmey *et al.*[18]

In conclusion, we have shown that the multimode cutoff in PCFs can be understood from a generalized V parameter and that the single-mode regime is characterized by $V_{\mathrm{PCF}} < V_{\mathrm{PCF}}{}^* = \pi$.

N. A. Mortensen is grateful to B. T. Kuhlmey for stimulating discussions, and M. D. Nielsen and K. P. Hansen acknowledge financial support by the Danish Academy of Technical Sciences. N. A. Mortensen's e-mail address is nam@crystal-fibre.com.

References

1. J. C. Knight, T. A. Birks, P. St. J. Russell, and D. M. Atkin, Opt. Lett. **21,** 1547 (1996).
2. J. C. Knight, J. Broeng, T. A. Birks, and P. St. J. Russell, Science **282,** 1476 (1998).
3. F. Benabid, J. C. Knight, G. Antonopoulos, and P. St. J. Russell, Science **298,** 399 (2002).
4. M. Mekata, Phys. Today **56,** 12 (2003).
5. R. F. Cregan, B. J. Mangan, J. C. Knight, T. A. Birks, P. St. J. Russell, P. J. Roberts, and D. C. Allan, Science **285,** 1537 (1999).
6. P. Russell, Science **299,** 358 (2003).
7. T. A. Birks, J. C. Knight, and P. St. J. Russell, Opt. Lett. **22,** 961 (1997).
8. J. C. Knight, T. A. Birks, R. F. Cregan, P. St. J. Russell, and J.-P. De Sandro, Electron. Lett. **34,** 1347 (1998).
9. D. Mogilevtsev, T. A. Birks, and P. St. J. Russell, Opt. Lett. **23,** 1662 (1998).
10. A. Ferrando, E. Silvestre, J. J. Miret, and P. Andrés, Opt. Lett. **25,** 790 (2000).
11. J. C. Knight, J. Arriaga, T. A. Birks, A. Ortigosa-Blanch, W. J. Wadsworth, and P. St. J. Russell, IEEE Photon. Technol. Lett. **12,** 807 (2000).
12. A. K. Ghatak and K. Thyagarajan, *Introduction to Fiber Optics* (Cambridge U. Press, Cambridge, 1998).
13. A. W. Snyder and J. D. Love, *Optical Waveguide Theory* (Chapman & Hall, New York, 1983).
14. J. C. Knight, T. A. Birks, and P. St. J. Russell, J. Opt. Soc. Am. A **15,** 748 (1998).
15. J. Broeng, D. Mogilevstev, S. E. Barkou, and A. Bjarklev, Opt. Fiber Technol. **5,** 305 (1999).
16. J. C. Knight, T. A. Birks, R. F. Cregan, P. St. J. Russell, and J. P. de Sandro, Opt. Mater. **11,** 143 (1999).
17. N. A. Mortensen, Opt. Express **10,** 341 (2002), http://www.opticsexpress.org.
18. B. T. Kuhlmey, R. C. McPhedran, and C. M. de Sterke, Opt. Lett. **27,** 1684 (2002).
19. E. A. Montie, E. C. Cosman, G. W. 't Hooft, M. B. van der Mark, and C. W. J. Beenakker, Nature **350,** 594 (1991).
20. A. Szafer and A. D. Stone, Phys. Rev. Lett. **62,** 300 (1989).
21. S. G. Johnson and J. D. Joannopoulos, Opt. Express **8,** 173 (2001), http://www.opticsexpress.org.
22. J. D. Joannopoulos, R. D. Meade, and J. N. Winn, *Photonic Crystals: Molding the Flow of Light* (Princeton U. Press, Princeton, N.J., 1995).
23. J. R. Folkenberg, N. A. Mortensen, K. P. Hansen, T. P. Hansen, H. R. Simonsen, and C. Jakobsen, Opt. Lett. **28,** 1882 (2003).

Paper C

M.D. Nielsen and N.A. Mortensen

"*Photonic Crystal Fiber design based on the V-parameter*"

Optics Express, Vol. **11**, No. 21, pp. 2762-2768

(2003)

Photonic crystal fiber design based on the V–parameter

Martin Dybendal Nielsen[1,2*] **and Niels Asger Mortensen**[1]

[1] *Crystal Fibre A/S, Blokken 84, DK-3460 Birkerød, Denmark*
[2] *COM, Technical University of Denmark, DK-2800 Kongens Lyngby, Denmark*

[*] *mdn@crystal-fibre.com*

Abstract: Based on a recent formulation of the V–parameter of a photonic crystal fiber we provide numerically based empirical expressions for this quantity only dependent on the two structural parameters — the air hole diameter and the hole-to-hole center spacing. Based on the unique relation between the V–parameter and the equivalent mode field radius we identify how the parameter space for these fibers is restricted in order for the fibers to remain single mode while still having a guided mode confined to the core region.

OCIS codes: (060.2280) Fiber design and fabrication, (060.2400) Fiber properties, (060.2430) Fibers, single-mode, (999.999) Photonic crystal fiber

References and links

1. S. G. Johnson and J. D. Joannopoulos, "Block-iterative frequency-domain methods for Maxwell's equations in a planewave basis," Opt. Express **8**, 173 (2001), http://www.opticsexpress.org/abstract.cfm?URI=OPEX-8-3-173.
2. T. P. White, B. T. Kuhlmey, R. C. McPhedran, D. Maystre, G. Renversez, C. M. de Sterke, and L. C. Botton, "Multipole method for microstructured optical fibers. I. Formulation," J. Opt. Soc. Am. B **19**, 2322 (2002).
3. J. C. Knight, T. A. Birks, P. S. J. Russell, and D. M. Atkin, "All-silica single-mode optical fiber with photonic crystal cladding," Opt. Lett. **21**, 1547 (1996).
4. A. W. Snyder and J. D. Love, *Optical Waveguide Theory* (Chapman & Hall, New York, 1983).
5. D. Marcuse, "Gaussian approximation of the fundamental modes of graded-index fibers," J. Opt. Soc. Am. **68**, 103 (1978).
6. N. A. Mortensen, J. R. Folkenberg, M. D. Nielsen, and K. P. Hansen, "Modal cut-off and the V–parameter in photonic crystal fibers," Opt. Lett. **28**, 1879 (2003).
7. B. T. Kuhlmey, R. C. McPhedran, and C. M. de Sterke, "Modal cutoff in microstructured optical fibers," Opt. Lett. **27**, 1684 (2002).
8. J. R. Folkenberg, N. A. Mortensen, K. P. Hansen, T. P. Hansen, H. R. Simonsen, and C. Jakobsen, "Experimental investigation of cut-off phenomena in non-linear photonic crystal fibers," Opt. Lett. **28**, 1882 (2003).
9. M. D. Nielsen, N. A. Mortensen, J. R. Folkenberg, and A. Bjarklev, "Mode-Field Radius of Photonic Crystal Fibers Expressed by the V–parameter," Opt. Lett. **28**, 2309 (2003).
10. T. P. White, R. C. McPhedran, C. M. de Sterke, L. C. Botton, and M. J. Steel, "Confinement losses in microstructured optical fibers," Opt. Lett. **26**, 1660 (2001).
11. B. T. Kuhlmey, R. C. McPhedran, C. M. de Sterke, P. A. Robinson, G. Renversez, and D. Maystre, "Microstructured optical fibers: where's the edge?," Opt. Express **10**, 1285 (2002), http://www.opticsexpress.org/abstract.cfm?URI=OPEX-10-22-1285.
12. W. H. Reeves, J. C. Knight, P. S. J. Russell, and P. J. Roberts, "Demonstration of ultra-flattened dispersion in photonic crystal fibers," Opt. Express **10**, 609 (2002), http://www.opticsexpress.org/abstract.cfm?URI=OPEX-10-14-609.
13. N. A. Mortensen and J. R. Folkenberg, "Low-loss criterion and effective area considerations for photonic crystal fibers," J. Opt. A: Pure Appl. Opt. **5**, 163 (2003).
14. T. A. Birks, J. C. Knight, and P. S. J. Russell, "Endlessly single mode photonic crystal fibre," Opt. Lett. **22**, 961 (1997).

#3057 - $15.00 US
Received September 23, 2003; Revised October 14, 2003

1. Introduction

Theoretical descriptions of photonic crystal fibers (PCFs) have traditionally been restricted to numerical evaluation of Maxwell's equations. In the most general case, a plane wave expansion method with periodic boundary conditions is employed [1] while other methods, such as the multipole method [2], take advantage of the localized nature of the guided modes and to some extend the circular shape of the air-holes. The reason for the application of these methods is the relatively complex dielectric cross section of a PCF for which rotational symmetry is absent.

The aim of this work is to provide a set of numerically based empirical expressions describing the basic properties such as cutoff and mode-field radius of a PCF based on the fundamental geometrical parameters only.

2. Fiber geometry and numerical method

We consider the fiber structure first studied by Knight *et al.* [3] and restrict our study to fibers that consist of pure silica with a refractive index of 1.444. The air holes of diameter d are arranged on a triangular grid with a pitch, Λ. In the center an air hole is omitted creating a central high index defect serving as the fiber core. A schematic drawing of such a structure is shown in the inset of the right panel in Fig. 1.

Depending on the dimensions, the structure comprises both single- and multi-mode fibers with large mode area as well as nonlinear fibers. The results presented here cover relative air hole sizes, d/Λ, from 0.2 to 0.9 and normalized wavelengths, λ/Λ, from around 0.05 to 2. The modeling is based on the plane-wave expansion method with periodic boundary conditions [1]. For the calculations of guided modes presented the size of the super cell was 8×8 resolved by 256×256 plane waves while for calculations on the cladding structure only, the super cell was reduced to a simple cell resolved by 32×32 planes waves.

3. The V–parameter and the relative mode-field radius

When attempting to establish a simple formalism for the PCF it is natural to strive for a result similar to the V–parameter known from standard fibers [4, 5]. However, a simple translation is

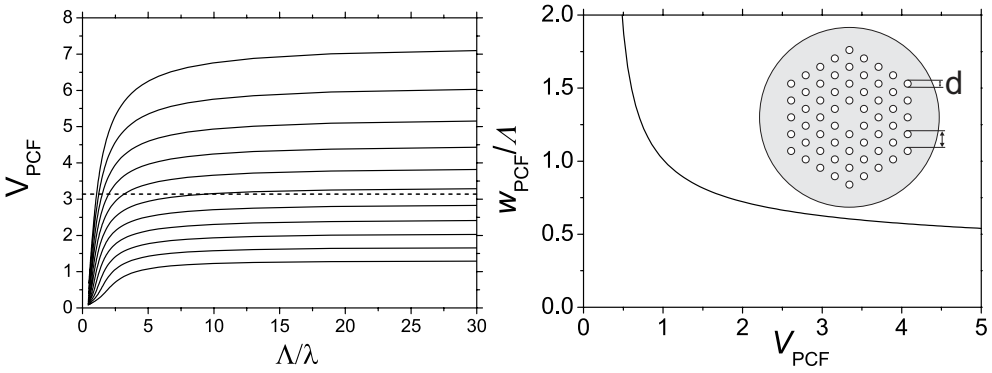

Fig. 1. left panel shows V_{PCF} calculated from Eq. (1) for d/Λ ranging from 0.20 (lowest curve) to 0.70 in steps of 0.05. The dashed line indicates $V_{\mathrm{PCF}} = \pi$. The right panel shows the relative equivalent mode-field radius, w_{PCF}/Λ plotted as function of V_{PCF} for each of the 9 curves in the left panel. The inset shows a schematic drawing of the considered PCF structure.

#3057 - $15.00 US
Received September 23, 2003; Revised October 14, 2003

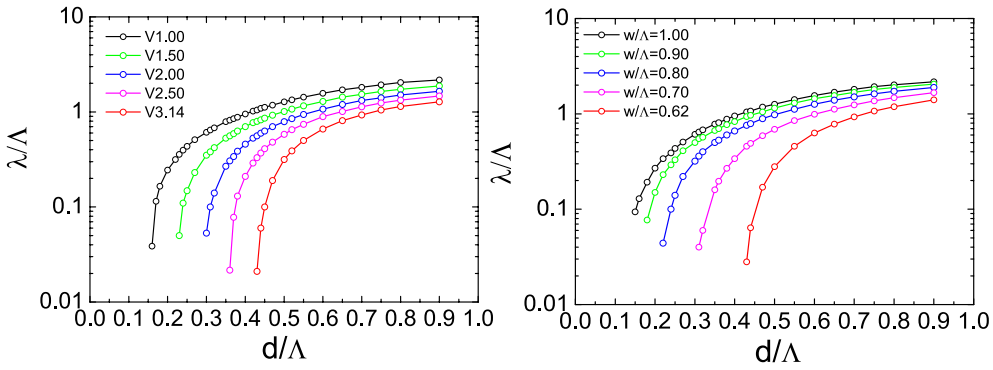

Fig. 2. The left panel shows curves for constant values of V_{PCF} in a normalized wavelength versus relative hole-size plot. The open circles indicate calculated data points with full lines to guide the eye. Similarly, the right panel shows curves for constant relative equivalent mode-field radius.

not straight forward since no wavelength-independent core- or cladding index can be defined. Recently, we instead proposed a formulation of the V–parameter for a PCF given by [6]

$$V_{\mathrm{PCF}} = 2\pi \frac{\Lambda}{\lambda} \sqrt{n_{\mathrm{FM}}^2(\lambda) - n_{\mathrm{FSM}}^2(\lambda)} \tag{1}$$

Although this expression has the same overall mathematical form as known from standard fibers, the unique nature of the PCF is taken into account. In Eq. (1), $n_{\mathrm{FM}}(\lambda)$ is the wavelength dependent effective index of the fundamental mode (FM) and $n_{\mathrm{FSM}}(\lambda)$ is the corresponding effective index of the first cladding mode in the infinite periodic cladding structure often denoted the fundamental space filling mode (FSM). For a more detailed discussion of this expression and its relation to previous work we refer to Ref. [6] and references therein. We have recently argued that the higher-order mode cut-off can be associated with a value of $V_{\mathrm{PCF}} = \pi$ [6] and showed that this criterion is indeed identical to the single-mode boundary calculated from the multipole method [7]. Recently the cut off results have also been confirmed experimentally [8]. Further supporting the definition of V_{PCF} is the recent observation [9] that the relative equivalent mode field radius of the fundamental mode, w_{PCF}/Λ as function of V_{PCF} fold over a single curve independent of d/Λ. The mode field radius w_{PCF} is defined as $A_{\mathrm{eff}} = \pi w_{\mathrm{PCF}}^2$ and corresponds to the $1/e^2$ width of a Gaussian intensity distribution with the same effective area, A_{eff}, as the fundamental mode itself [9].

In the left panel of Fig. 1, calculated curves of V_{PCF} as function of Λ/λ are shown for d/Λ ranging from 0.20 to 0.70 in steps of 0.05. In general, all curves are seen to approach constant levels dependent on d/Λ. The horizontal dashed line indicates the single-mode boundary $V_{\mathrm{PCF}} = \pi$. In the right panel, w_{PCF}/Λ is plotted as function of V_{PCF} for each of the 9 curves in the left panel and as seen all curves fold over a single curve. An empirical expression for w_{PCF}/Λ can be found in Ref. [9]. The mode is seen to expand rapidly for small values of V_{PCF} and the mode-field radius saturates toward a constant value when V_{PCF} becomes large. In fact, it turns out that $w_{\mathrm{PCF}}/\Lambda \simeq 1.00$ for $V_{\mathrm{PCF}} = 1$ and $w_{\mathrm{PCF}}/\Lambda \simeq 0.62$ for $V_{\mathrm{PCF}} = \pi$. In the left panel of Fig. 2, curves corresponding to constant values of V_{PCF} are shown in a λ/Λ versus d/Λ plot. In the right panel, curves of constant w_{PCF}/Λ is shown, also in a λ/Λ versus d/Λ plot. Since there is a unique relation between w_{PCF}/Λ and V_{PCF} [9] the curves naturally have the same shape.

When designing a PCF any combination of d and Λ is in principle possible. However, in

#3057 - $15.00 US
Received September 23, 2003; Revised October 14, 2003

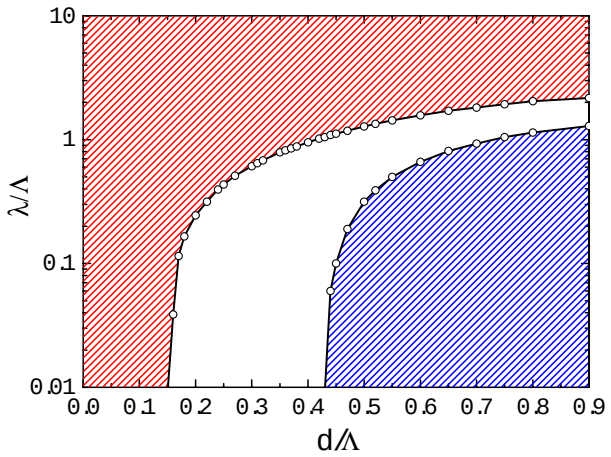

Fig. 3. Plot of the parameter space in terms of relative hole size and normalized wavelength divided into three regions by the boundaries defined by $V_{\mathrm{PCF}} = 1$ and $V_{\mathrm{PCF}} = \pi$. In the upper red area the mode penetrates deeply into the cladding region and in lower blue region the structure supports a higher-order mode.

some cases the guiding will be weak causing the mode to expand beyond the core and into the cladding region [10, 11] corresponding to a low value of V_{PCF}. In the other extreme, the confinement will be too strong allowing for the guiding of higher-order modes [6, 7]. Since both situations are governed by V_{PCF} the design relevant region in a λ/Λ versus d/Λ plot can be defined. This is done in Fig. 3 where the low limit is chosen to be $V_{\mathrm{PCF}} = 1$ where $w_{\mathrm{PCF}}/\Lambda \simeq 1$. How large a mode that can be tolerated is of course not unambiguous. However, for $w_{\mathrm{PCF}} \sim \Lambda$ leakage-loss typically becomes a potential problem in PCFs with a finite cladding structure. In non-linear PCFs it is for dispersion reasons often advantageous operating the PCF at $V_{\mathrm{PCF}} \lesssim 1$ and then a high number of air-hole rings is needed to achieve an acceptable level of leakage loss [12].

Finally, we note that the practical operational regime is also limited from the low wavelength side. In Ref. [13] a low-loss criterion was formulated in terms of the coupling length $z_c = \lambda/[n_{\mathrm{FM}}(\lambda) - n_{\mathrm{FSM}}(\lambda)]$ between the FM and the FSM. In general scattering-loss due to longitudinal non-uniformities increases when z_c increases and a PCF with a low z_c will in general be more stable compared to one with a larger z_c. Using $n_{\mathrm{FM}} + n_{\mathrm{FSM}} \approx 2n_{\mathrm{FM}} \approx 2n_{\mathrm{silica}}$ we can rewrite Eq. (1) as

$$V_{\mathrm{PCF}} \propto \frac{\Lambda}{\lambda}\sqrt{\frac{\lambda}{z_c(\lambda)}} \tag{2}$$

from which it is seen that a high value of the V–parameter is preferred over a smaller value. In Fig. (3) it is thus preferable to stay close to the single-mode boundary ($V_{\mathrm{PCF}} \sim \pi$) but in general there is a practical lower limit to the value of λ/Λ which can be realized because when $\lambda/\Lambda \lesssim 0.1$ one generally has that $z_c \gg \lambda$ [13].

4. V–parameter expression

Although the V–parameter offers a simple way to design a PCF, a limiting factor for using Eq. (1) is that a numerical method is still required for obtaining the effective indices. In analogy

#3057 - $15.00 US
Received September 23, 2003; Revised October 14, 2003

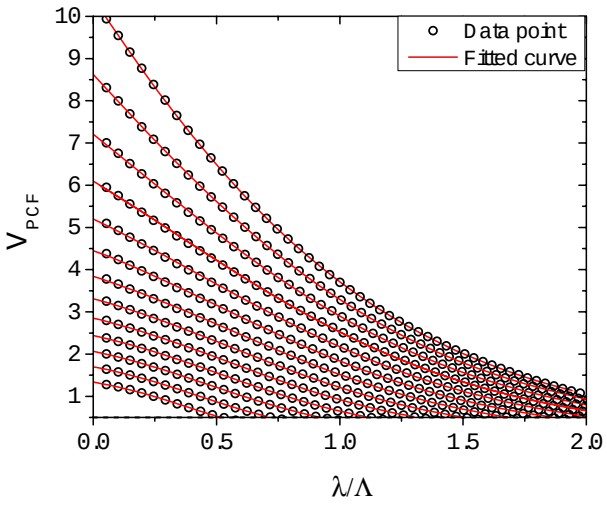

Fig. 4. Plot of V_{PCF} as a function of relative wavelength λ/Λ for d/Λ ranging from 0.20 (lowest curve) to 0.80 in steps of 0.05.

with expressions for standard fibers [5] it would therefore be convenient to have an alternative expression only dependent on the wavelength, λ, and the structural parameters d and Λ. In Fig. 4, we show V_{PCF} as function of λ/Λ (data are shown by open circles) for d/Λ ranging from 0.20 to 0.80 in steps of 0.05. Each data set in Fig. 4 is fitted to a function of the form

$$V_{\mathrm{PCF}}\left(\tfrac{\lambda}{\Lambda},\tfrac{d}{\Lambda}\right)=\frac{\mathscr{A}\left(\frac{d}{\Lambda}\right)}{\mathscr{B}\left(\frac{d}{\Lambda}\right)\times\exp\left[\mathscr{C}\left(\frac{d}{\Lambda}\right)\times\frac{\lambda}{\Lambda}\right]+1} \tag{3a}$$

and the result is indicated by the full red lines. Eq. (3a) is not based on considerations of the physics of the V-parameter but merely obtained by trial and error in order to obtain the best representation of calculated data with the lowest possible number of free parameters. Prior to the fit, the data sets are truncated at $V_{\mathrm{PCF}}=0.5$ since $w_{\mathrm{PCF}}\gtrsim 2\Lambda$ in this region (see left panel in Fig. 1) and the data is thus not practically relevant. In Eq. (3a) the fitting parameters $\mathscr{A}$, $\mathscr{B}$, and $\mathscr{C}$ depend on d/Λ only. In order to extract this dependency, suitable functions (again obtained by trial and error) are fitted to the data sets for $\mathscr{A}$, $\mathscr{B}$, and $\mathscr{C}$. We find that the data are well described by the following expressions

$$\mathscr{A}\left(\tfrac{d}{\Lambda}\right)=\tfrac{d}{\Lambda}+0.457+\frac{3.405\times\frac{d}{\Lambda}}{0.904-\frac{d}{\Lambda}} \tag{3b}$$

$$\mathscr{B}\left(\tfrac{d}{\Lambda}\right)=0.200\times\tfrac{d}{\Lambda}+0.100+0.027\times\left(1.045-\tfrac{d}{\Lambda}\right)^{-2.8} \tag{3c}$$

$$\mathscr{C}\left(\tfrac{d}{\Lambda}\right)=0.630\times\exp\left(\frac{0.755}{0.171+\frac{d}{\Lambda}}\right) \tag{3d}$$

The above set of expressions, Eqs. (3), constitute our empirical expression for the V–parameter in a PCF with λ/Λ and d/Λ being the only input parameters. For $\lambda/\Lambda<2$ and $V_{\mathrm{PCF}}>0.5$ the expression gives values of V_{PCF} which deviates less than 3% from the correct values obtained from Eq. (1).

#3057 - $15.00 US
Received September 23, 2003; Revised October 14, 2003

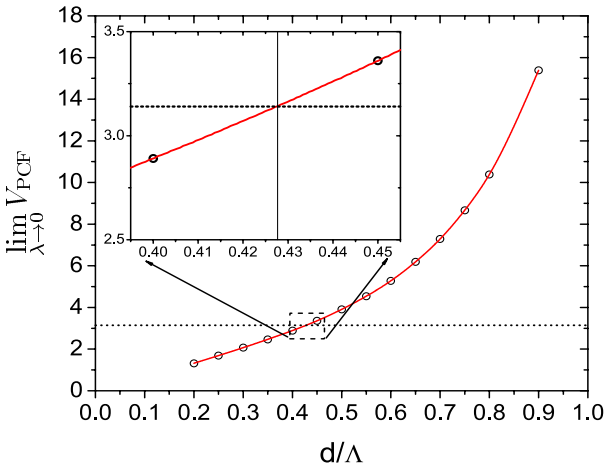

Fig. 5. Plot of V_{PCF} in the $\lambda \to 0$ limit as function of the relative air hole size (open circles). The full red line represents a fit to the data points and the horizontal dash line indicated the ESM limit $V_{\mathrm{PCF}} = \pi$. The insert shows a close-up of the intersection with the vertical line indicating the air hole size $d/\Lambda \simeq 0.43$.

5. Endlessly single-mode criterion

The term endlessly single-mode (ESM) refers to PCFs which regardless of wavelength only support the two degenerate polarization states of the fundamental mode [14]. In the framework of the V–parameter this corresponds to structures for which $V_{\mathrm{PCF}} < \pi$ for any λ/Λ [6]. As seen in the left panel of Fig. 1 this corresponds to sufficiently small air holes. However, from the plot in Fig. 1 it is quite difficult to determine the exact d/Λ value for which $V_{\mathrm{PCF}} = \pi$ for λ approaching 0. From Eq. (3) it is easily seen that the value may be obtained from

$$\lim_{\lambda \to 0} V_{\mathrm{PCF}}\left(\frac{\lambda}{\Lambda}, \frac{d}{\Lambda}\right) = \frac{\mathscr{A}\left(\frac{d}{\Lambda}\right)}{\mathscr{B}\left(\frac{d}{\Lambda}\right) + 1} = \pi. \tag{4}$$

Fig. 5 illustrates this equation graphically where we have extrapolated the data in Fig. 4 to $\lambda = 0$. From the intersection of the full line with the dashed line we find that $d/\Lambda \simeq 0.43$ bounds the ESM regime. Solving Eq. (4) we get $d/\Lambda \simeq 0.44$ and the deviation from the numerically obtained value is within the accuracy of the empirical expression.

6. Conclusion

There are several issues to consider when designing a PCF. In this work we have addressed the single/multi-mode issue as well as those related to mode-field radius/field-confinement, and mode-spacing. We have shown how these properties can be quantified via the V–parameter. Based on extensive numerics we have established an empirical expression which facilitate an easy evaluation of the V-parameter with the normalized wavelength and hole-size as the only input parameters. We believe that this expression provides a major step away from the need of heavy numerical computations in design of solid core PCFs with triangular air-hole cladding.

#3057 - $15.00 US
Received September 23, 2003; Revised October 14, 2003

Acknowledgments

We thank J. R. Folkenberg for stimulating discussion and M. D. Nielsen acknowledges financial support by the Danish Academy of Technical Sciences.

#3057 - $15.00 US Received September 23, 2003; Revised October 14, 2003

Paper D

N.A. Mortensen, **M.D. Nielsen**, J.R. Folkenberg, K.P. Hansen, J. Lægsgaard

"*Small-core photonic crystal fibers with weakly disordered air-hole claddings*"

Journal of Optics A: Pure and Applied optics, Vol. **6**, pp. 221-223

(2004)

INSTITUTE OF PHYSICS PUBLISHING JOURNAL OF OPTICS A: PURE AND APPLIED OPTICS

J. Opt. A: Pure Appl. Opt. **6** (2004) 221–223 PII: S1464-4258(04)68465-0

Small-core photonic crystal fibres with weakly disordered air-hole claddings

Niels Asger Mortensen[1], **Martin D Nielsen**[1,2], **Jacob Riis Folkenberg**[1], **Kim P Hansen**[1,2] **and Jesper Lægsgaard**[2]

[1] Crystal Fibre A/S, Blokken 84, DK-3460 Birkerød, Denmark
[2] COM, Technical University of Denmark, DK-2800 Kongens Lyngby, Denmark

Received 29 August 2003, accepted for publication 26 November 2003
Published 5 December 2003
Online at stacks.iop.org/JOptA/6/221 (DOI: 10.1088/1464-4258/6/2/011)

Abstract
Motivated by recent experimental work by Folkenberg *et al* (2003 *Opt. Lett.* **28** 1882–4) we consider the effect of weak disorder in the air-hole lattice of small-core photonic crystal fibres. We find that the broken symmetry leads to higher-order modes which have generic intensity distributions resembling those found in standard fibres with elliptical cores. This explains why recently reported experimental higher-order mode profiles appear very different from those calculated numerically for ideal photonic crystal fibres with inversion and six-fold rotational symmetry. The splitting of the four higher-order modes into two groups fully correlates with the observation that these modes have different cut-offs.

Keywords: photonic crystal fibre, disorder, degeneracies

(Some figures in this article are in colour only in the electronic version)

The advances in the fabrication techniques and structural control of both index-guiding as well as photonic band-gap photonic crystal fibres (PCFs) are believed to improve the agreement between experiments and theory based on ideal structures (for a recent review of the field we refer to [1] and references therein). The recent investigation of micro-bending induced attenuation in PCFs [2] is an example of the successful merging of experiments and simulations and, similarly, the recent experiments [3] on multi-mode cut-off in small-core PCFs show good agreement with theoretical predictions [4, 5]. On the other hand, in the latter experiments the observed higher-order mode profiles were very different from those of an ideal structure despite the fact that the studied fibres appeared to have highly regular air-hole lattices. However, the relative strength of disorder may still be significant and in this paper we numerically study the effect of such variations on both fields and propagation constants.

We consider the type of PCF first studied by Knight *et al* [6] for which the ideal structure has inversion and six-fold rotational symmetry, see figure 1. In the first row of figure 2 we show the electrical field intensity $|\boldsymbol{E}_m^{(0)}|^2$ (the superscript emphasizes the ideal or 'unperturbed' structure) of the first six ($m = 1, 2, 3, \ldots, 6$) eigenmodes at $\lambda = 780$ nm of an ideal PCF with $\Lambda = 1.4$ μm and $d/\Lambda = 0.67$ corresponding to one of the fibres studied in [3]. The results are based on a numerical

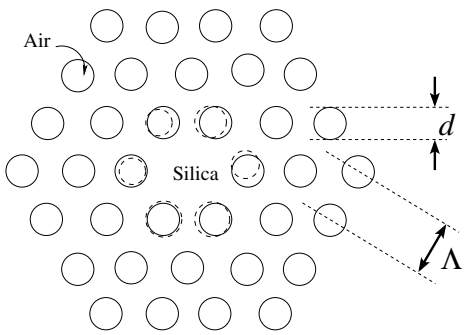

Figure 1. Schematic diagram of the cross-section of a photonic crystal fibre. The dashed circles indicate small random displacements and variations in diameter of the six inner air holes.

fully vectorial solution of Maxwell's equations in a plane-wave basis with periodic boundary conditions [7] and basis vectors which support the inversion and six-fold rotational symmetry of the dielectric structure. For the refractive index n we use $n = 1$ in air and for silica we use a Sellmeier expression with $n = 1.453\,67$. The fundamental modes ($m = 1$ and 2) have close-to-Gaussian profiles [8, 9].

Historically, their degeneracy has been widely debated (see [10, 11] and references therein) but recently it was finally

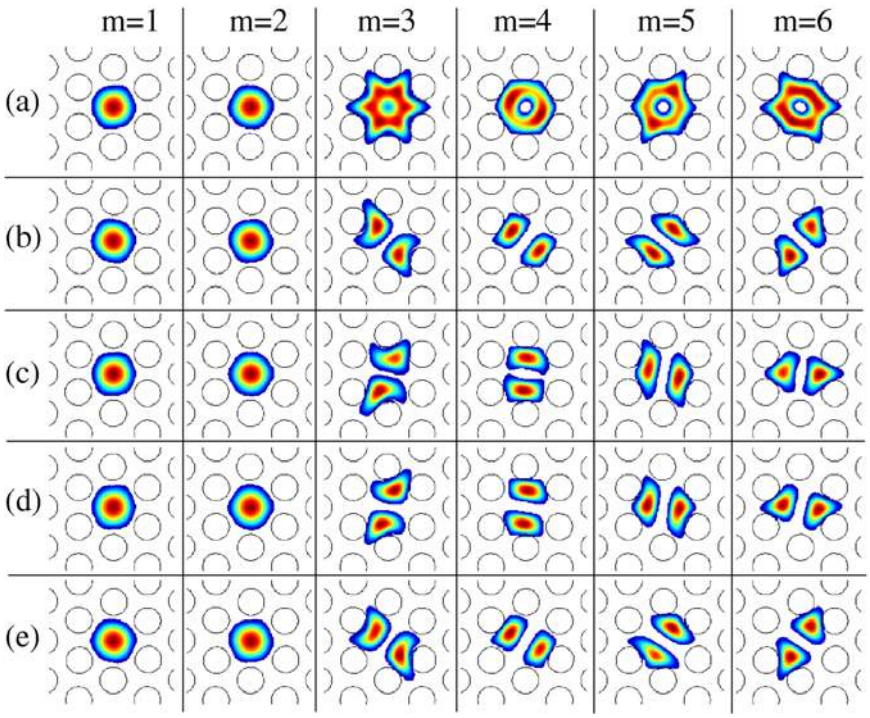

Figure 2. Plot of the electrical field intensity. Row (a) shows results for the ideal structure and rows (b)–(e) are for different random disorders in the inner ring of the air-hole lattice.

proved by Steel *et al* [10] how their degeneracy follows from group theory because $\boldsymbol{E}_1^{(0)}$ and $\boldsymbol{E}_2^{(0)}$ do not support the full symmetry. Recently, the degeneracies of higher-order modes were addressed by Guobin *et al* [12], but only in the case of a PCF supporting 10 eigenmodes. The general picture is quite complicated and the degeneracies and order depend on the number of guided eigenmodes [13]. In a picture of true eigenmodes, this can be understood as follows; for a given number M of guided eigenmodes the eigenvalues are minimized with the constraint that the eigenfields are orthonormal. When the number is changed to, say, $M+1$ the orthogonalization affects all $M+1$ eigenvalues and eigenfields and thus the picture of degeneracies may in general also change compared to the picture for M eigenmodes.

In our case we numerically find that while $\boldsymbol{E}_3^{(0)}$ and $\boldsymbol{E}_4^{(0)}$ support the full symmetry, $\boldsymbol{E}_5^{(0)}$ and $\boldsymbol{E}_6^{(0)}$ do not. Group theory thus predicts that the PCF have a set of modes which are either pair-wise two-fold degenerate ($m = 1, 2$ and 5, 6) or non-degenerate ($m = 3$ and 4). This contrasts with the situation of a step-index fibre (SIF) in the weakly guided approximation where the first higher-order modes are four-fold degenerate. The third and fourth modes are nearly degenerate in the sense that our numerical studies show that the splitting $\beta_4^{(0)} - \beta_3^{(0)}$ is much smaller than the spacings $\beta_5^{(0)} - \beta_4^{(0)}$ and $\beta_3^{(0)} - \beta_2^{(0)}$ to the two neighbouring groups of degenerate modes. The grouping of the four higher-order modes into two groups is experimentally reflected in the different cut-off wavelengths of the two groups [3]. Compared to the picture in the weakly guided approximation, the splitting of the higher-order modes in PCFs originates from the inversion and six-fold rotational symmetry and the magnitude of the splitting is driven by the high index contrast between air and silica. We note that for a

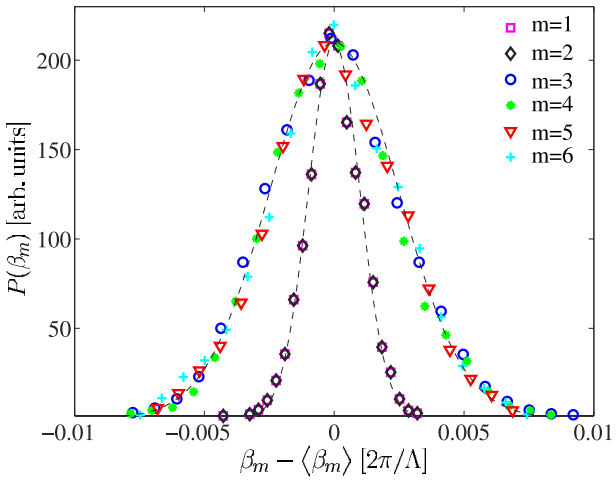

Figure 3. Plot of distribution $P(\beta_m)$ for the first six modes $m = 1$–6. The dashed curves show Gaussian fits.

standard fibre, a sufficiently high index contrast will eventually also split the higher-order modes.

From perturbation theory (for the problem of shifting boundaries see [14]) it is obvious that for guided modes the six inner air-holes are of most importance to the optical properties, whereas disorder in the air-hole lattice further out in the cladding mainly affects the guided modes in terms of e.g. leakage loss [15]. Thus, in the search for over-all qualitative effects of disorder it is sufficient to only let the six inner air-holes (see figure 1) have small random displacements $\Delta\boldsymbol{r}_i$ ($i = 1, 2, \ldots, 6$) with respect to the ideal positions of the air-holes as well as small random deviations Δd_i in their diameters. We consider the situation where the displacements

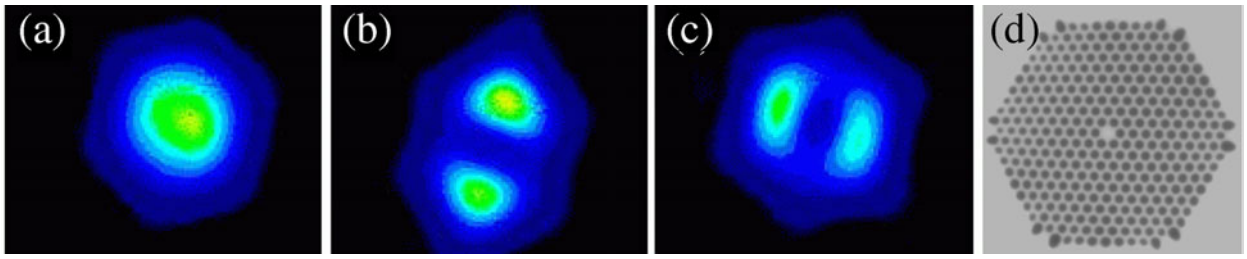

Figure 4. Near field images at $\lambda = 780$ nm recorded at the output of 2.0 m of a PCF. Panels (a)–(c) show the fundamental and higher-order modes. Panel (d) shows a microscope image of the cross-section of the PCF with $\Lambda \simeq 1.41$ μm and $d/\lambda \simeq 0.66$.

and deviations in diameter have a Gaussian distribution (zero mean and widths σ_Λ and σ_d) and are mutually uncorrelated, i.e.

$$\begin{aligned} \langle \Delta \boldsymbol{r}_i \rangle = \langle \Delta d_i \rangle = \langle \Delta \boldsymbol{r}_i \Delta d_j \rangle = 0 \\ \langle \Delta \boldsymbol{r}_i \Delta \boldsymbol{r}_j \rangle = \sigma_\Lambda^2 \delta_{ij}, \qquad \langle \Delta d_i \Delta d_j \rangle = \sigma_d^2 \delta_{ij}. \end{aligned} \tag{1}$$

In the following we study a large ensemble (more than 1000 members) of fibres numerically.

Since the structural imperfection is typically a small perturbation of the ideal structure we have $\langle \beta_m \rangle \simeq \beta_m^{(0)}$. The grouping discussed above thus also holds approximately for the average propagation constants $\langle \beta_m \rangle$ as we also have confirmed numerically (not shown). In figure 3 we show the distribution of the propagation constant for the first six eigenmodes at $\lambda = 780$ nm of a PCF with $\Lambda = 1.4$ μm and $d/\Lambda = 0.67$. For the disorder we have used $\sigma_\Lambda = \sigma_d = 0.02 \times \Lambda$ corresponding to 2% structural variations of the six inner air holes. The fundamental mode only has a small fraction of the field near to the air-hole silica interfaces compared to higher-order modes, see row (a) in figure 2. From perturbation theory one thus expects the fundamental mode to be less sensitive to disorder than the higher-order modes. Indeed, from figure 3 it is seen that the distribution $P(\beta_m)$ has a common width for $m = 1, 2$ which is significantly smaller than the common width for the higher-order modes ($m = 3$–6).

For a non-zero σ, symmetries are broken and symmetry-related degeneracies are in principle lifted. For $m = 1, 2$ this splitting is often referred to as form-birefringence, quantified by $\Delta n_{12} = (\beta_1 - \beta_2)/k$ where k is the free-space wave number. However, since $\langle \boldsymbol{E}_1^{(0)} | \delta\varepsilon | \boldsymbol{E}_1^{(0)} \rangle \simeq \langle \boldsymbol{E}_2^{(0)} | \delta\varepsilon | \boldsymbol{E}_2^{(0)} \rangle$ for a scalar perturbation $\delta\varepsilon$ there is no significant form-birefringence ($\Delta n_{12} \simeq 0$) to lowest order in perturbation theory. Indeed, for the studied disorder strength we numerically find an extremely narrow distribution. The width is vanishing (within our numerical accuracy) corresponding to a delta-function distribution $P(\beta_1 - \beta_2) \simeq \delta(\beta_1 - \beta_2)$.

The effect of disorder on the fields is illustrated in figure 2. Rows (b)–(e) show examples of the electrical field intensity for four random configurations of the inner ring of air holes. In general, we find that the modes in the ideal structure, row (a), deform into profiles having two maxima with a node in between, similarly to the deformation of the modes in elliptical core SIFs [16]. This picture correlates perfectly with the modes observed experimentally in [3]. Figure 4 shows near fields recorded at $\lambda = 780$ nm for a PCF with $\Lambda \simeq 1.41$ μm and $d/\lambda \simeq 0.66$. Here, the fundamental mode, panel (a), corresponds to the linear combination $\boldsymbol{E} \sim \boldsymbol{E}_1 + \boldsymbol{E}_2$ and for the higher-order modes, panels (b) and (c) correspond to $\boldsymbol{E} \sim \boldsymbol{E}_3 + \boldsymbol{E}_4$ and $\boldsymbol{E} \sim \boldsymbol{E}_5 + \boldsymbol{E}_6$, respectively.

In conclusion we have demonstrated how even weak disorder in the air-hole lattice leads to deformation of the higher-order modes in small-core photonic crystal fibres. In the presence of disorder the higher-order modes resemble those in elliptical core standard fibres. Our findings explain why the recently reported higher-order mode profiles and the grouping of higher-order modes correlate with the observation that they have different cut-offs.

Acknowledgments

We acknowledge useful discussions with B T Kuhlmey. M D Nielsen and K P Hansen are financially supported by the Danish Academy of Technical Sciences and J Lægsgaard by the Danish Technical Research Council.

References

[1] Russell P 2003 *Science* **299** 358–62
[2] Nielsen M D, Vienne G, Folkenberg J R and Bjarklev A 2003 *Opt. Lett.* **28** 236–8
[3] Folkenberg J R, Mortensen N A, Hansen K P, Hansen T P, Simonsen H R and Jakobsen C 2003 *Opt. Lett.* **28** 1882–4
[4] Mortensen N A, Folkenberg J R, Nielsen M D and Hansen K P 2003 *Opt. Lett.* **28** 1879–81
[5] Kuhlmey B T, McPhedran R C and de Sterke C M 2002 *Opt. Lett.* **27** 1684–6
[6] Knight J C, Birks T A, Russell P S J and Atkin D M 1996 *Opt. Lett.* **21** 1547–9
[7] Johnson S G and Joannopoulos J D 2001 *Opt. Express* **8** 173–90
[8] Mortensen N A 2002 *Opt. Express* **10** 341–8
[9] Mortensen N A and Folkenberg J R 2002 *Opt. Express* **10** 475–81
[10] Steel M J, White T P, de Sterke C M, McPhedran R C and Botton L C 2001 *Opt. Lett.* **26** 488–90
[11] Koshiba M and Saitoh K 2001 *IEEE Photon. Technol. Lett.* **13** 1313–5
[12] Guobin R, Zhi W, Shuqin L and Shuisheng J 2003 *Opt. Express* **11** 1310–21
[13] Kuhlmey B T and Mortensen N A 2003 unpublished
[14] Johnson S G, Ibanescu M, Skorobogatiy M A, Weisberg O, Joannopoulos J D and Fink Y 2002 *Phys. Rev.* E **65** 066611
[15] White T P, McPhedran R C, de Sterke C M, Botton L C and Steel M J 2001 *Opt. Lett.* **26** 1660–2
[16] Snyder A W and Love J D 1983 *Optical Waveguide Theory* (New York: Chapman and Hall)

Paper E

M.D. Nielsen, N.A. Mortensen, J.R. Folkenberg, and A. Bjarklev

"*Mode Field Radius of Photonic Crystal Fibers Expressed by the V-parameter*"

Optics Letters, Vol. **28**, No. 23, pp. 2309-2311

(2003)

Mode-field radius of photonic crystal fibers expressed by the V parameter

Martin Dybendal Nielsen

Crystal Fibre A/S, Blokken 84, DK-3460 Birkerød, Denmark, and
COM, Technical University of Denmark, Orsteds Plads 349, DK-2800 Kgs. Lyngby, Denmark

Niels Asger Mortensen and Jacob Riis Folkenberg

Crystal Fibre A/S, Blokken 84, DK-3460 Birkerød, Denmark

Anders Bjarklev

COM, Technical University of Denmark, Orsteds Plads 349, DK-2800 Kgs. Lyngby, Denmark

Received June 19, 2003

We numerically calculate the equivalent mode-field radius of the fundamental mode in a photonic crystal fiber (PCF) and show that this is a function of the V parameter only and not the relative hole size. This dependence is similar to what is found for graded-index standard fibers, and we furthermore show that the relation for the PCF can be excellently approximated with the same general mathematical expression. This is to our knowledge the first semianalytical description of the mode-field radius of a PCF. © 2003 Optical Society of America

OCIS codes: 060.2280, 060.2310, 060.2400, 060.2430.

Theoretical descriptions of photonic crystal fibers (PCFs) have traditionally been based on numerical methods such as the plane-wave expansion method,[1,2] methods employing localized functions,[3,4] or the multipole method.[5,6] A numerical approach is generally required because of the complex dielectric cross section of PCF, which makes analytical approaches very difficult and results in the fact that no closed-form analytical descriptions of propagation constants or mode fields are available. In this Letter we investigate the relation between the equivalent mode-field radius of the fundamental mode and a recently proposed formulation of the V parameter for a PCF.[7] We show that the equivalent mode-field radius is a function of the V parameter only and provide an empirical expression describing this relation that has the same mathematical form as that known from the description of graded-index standard fibers.[8]

The PCF analyzed in this work is an all-silica fiber that has a triangular arrangement of circular voids with diameter d running along the full length of the fiber. The voids are placed symmetrically around a central defect that acts as the fiber core, consisting of a solid silica region, i.e., an omitted air hole. The air-hole matrix, which has a lattice constant Λ, functions as a cladding region, and the fiber structure is invariant in the longitudinal direction. Such a fiber was first proposed in Ref. 9 and was shown to possess unique properties such as endlessly single-mode operation.[10] The endlessly single-mode operation is a consequence of the fact that the number of guided modes is finite regardless of wavelength and that the upper limit for this number decreases with the air-filling fraction of the structure, i.e., with the value of d/Λ. Sufficiently small air holes will result in only two supported modes, namely, the two degenerate polarization states of the fundamental mode.[10]

In the case of graded-index standard fibers, of which the step-index fiber (SIF) can be considered a special case, the V parameter plays a central role in the description of the number of guided modes, the cutoff criterion,[11] and the mode-field radius.[8] In an attempt to obtain an expression for a V parameter that is adequate for PCFs, approximations based on an equivalent SIF have generally been employed.[10,12] Although these approximations contain the overall correct physics they fail to describe the cutoff properties and have difficulty when it comes to determining an appropriate equivalent core radius. Recently, we proposed a definition of the V parameter for a PCF,[7] V_{PCF}, rejecting the SIF approximation [see Ref. 7 for a more detailed discussion of Eq. (1)]:

$$V_{\mathrm{PCF}}(\lambda) = \frac{2\pi}{\lambda}\,\Lambda[n_{\mathrm{co}}{}^2(\lambda) - n_{\mathrm{cl}}{}^2(\lambda)]^{1/2}, \qquad (1)$$

In Eq. (1), λ is the free-space wavelength and $n_{\mathrm{co}}(\lambda)$ and $n_{\mathrm{cl}}(\lambda)$ are the effective indices of the fundamental mode and the first eigenmode in the perfect infinite cladding structure, respectively. The last-named item is often denoted the fundamental space-filling mode and can be interpreted as the refractive index of the cladding material in the absence of the core.[10] With this definition it can be shown that the condition for the higher-order mode cutoff can be formulated as $V_{\mathrm{PCF}} = \pi$.[7] Both effective indices in Eq. (1) are strongly wavelength dependent and cannot be approximated by constants as in the case of standard fibers. It is due to the strong dispersion of the effective indices that the PCF can be attributed many of its

0146-9592/03/232309-03$15.00/0

unique properties. In Fig. 1, V_{PCF} calculated with the plane-wave expansion method[13] is plotted as a function of normalized frequency Λ/λ for values of d/Λ ranging from 0.30 to 0.70 in steps of 0.05. The horizontal dashed line in the plot indicates $V_{\mathrm{PCF}} = \pi$ and thereby the single-mode boundary. Since the variation of the refractive index of silica, n_{silica}, over the transparent wavelength region is of the order of a few percent, the effect of material dispersion will result in only a small shift in the effective indices $n_{\mathrm{co}}(\lambda)$ and $n_{\mathrm{cl}}(\lambda)$. Furthermore, such a perturbation will shift both indices by the same value, further reducing the effect on V_{PCF} [see Eq. (1)]. In the calculations we therefore used a fixed value of $n_{\mathrm{silica}} = 1.444$, thereby preserving the scale invariance of Maxwell's equations.

V_{PCF} approaches a constant value, dependent on d/Λ for increasing Λ/λ (Ref. 10), and, since the number of modes generally increases with the V parameter, the asymptotic behavior of V_{PCF} is consistent with the endlessly single-mode property. In the framework of standard fibers, the weak wavelength dependence of the V parameter will lead to a mode-field radius that is also only weakly dependent on the wavelength.

For a graded-index standard fiber, the index profile can be described by a power law, in which case the shape of the index profile is governed by an exponent, g. For $g = 1$ the index profile is triangular, for $g = 2$ the profile is parabolic, and in the limit of large values of g the profile approaches that of a SIF. For this type of fiber the mode field is generally very close to a Gaussian distribution, provided that the field does not penetrate too deeply into the cladding region. The agreement between the actual mode and a Gaussian distribution has a weak dependence on g and is a perfect match in the case of a parabolic index profile. The mode-field radius, w, is a function of the V parameter and can be fitted by use of the expression[8]

$$\frac{w}{a} = \frac{A}{V^{2/(2+g)}} + \frac{B}{V^{3/2}} + \frac{C}{V^{6}}. \tag{2}$$

A, B, and C are fitting parameters that are dependent on the index profile, while a denotes the core radius. In the case of a SIF the first term in Eq. (2) is constant and the values of A, B, and C are 0.65, 1.619, and 2.879, respectively. The deviation of the fits provided by Eq. (2) is less than 2% in the range $1.5 < V < 7$, and the relation is therefore extremely useful when one is designing and working with SIFs or graded-index fibers in general.

To investigate a similar relation for the PCF, we first introduce an equivalent mode-field radius of the fundamental mode, w_{PCF}, as the mode-field radius of the Gaussian distribution with the same effective area, A_{eff}, as the fundamental mode itself, yielding the simple relation $A_{\mathrm{eff}} = \pi w^2$. The effective area is calculated as

$$A_{\mathrm{eff}} = \left[\int \mathrm{d}\mathbf{r}_{\perp} I(\mathbf{r}_{\perp})\right]^2 \left[\int \mathrm{d}\mathbf{r}_{\perp} I^2(\mathbf{r}_{\perp})\right]^{-1}. \tag{3}$$

In Eq. (3), $I(\mathbf{r}_{\perp})$ is the transverse intensity distribution of the mode. Although the intensity distribution of the fundamental mode in a PCF is not rotational symmetric but rather has the sixfold symmetry of the triangular cladding structure, a Gaussian approximation is in fact very good and was previously employed in the description of various PCF properties.[14–16] By numerical calculation of A_{eff} as a function of the normalized wavelength, λ/Λ, the normalized mode-field radius, w_{PCF}/Λ, can be plotted as a function of V_{PCF}, as shown in Fig. 2. The normalization with Λ is chosen since Λ is the natural length scale of the problem in the same sense as the core radius, a, is for the graded-index fiber. The plot in Fig. 2 represents data for $d/\Lambda = 0.30$ and $d/\Lambda = 0.70$. The data points for these two calculations overlap in the entire range where the values of V_{PCF} overlap and data for calculations with $d/\Lambda = 0.35$, 0.40, 0.45, 0.50, 0.55, 0.60, 0.65 (not shown) fall on the same curve, indicating that w_{PCF}/Λ is in fact a function of V_{PCF} only. Also included in Fig. 2 is the corresponding curve for the SIF (dashed curve) showing w_{SIF}/a as function of V_{SIF} calculated from Eq. (2).

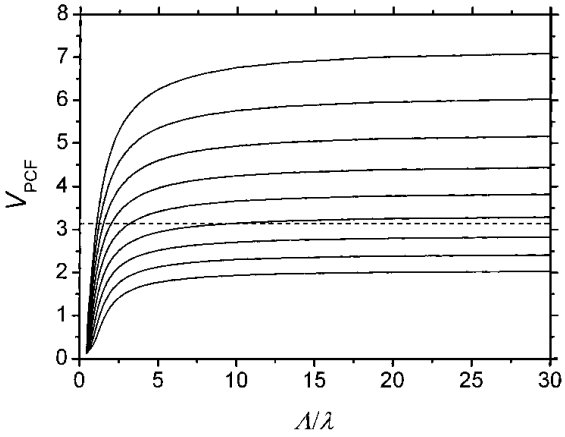

Fig. 1. Calculated V_{PCF} [from Eq. (1)] as a function of the normalized frequency, Λ/λ, for $d/\Lambda = 0.30$, 0.35, 0.40, 0.45, 0.50, 0.55, 0.60, 0.65, 0.70 (from bottom curve to top). The dashed line indicates the single-mode boundary, $V_{\mathrm{PCF}} = \pi$.

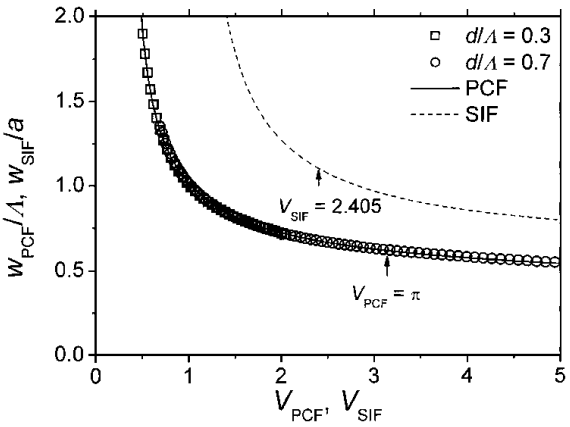

Fig. 2. Normalized mode-field radius for the PCF, w_{PCF}/Λ, as a function of V_{PCF} for $d/\Lambda = 0.3$ and $d/\Lambda = 0.7$, along with a numerical fit through these points (solid curve). The corresponding expression for the normalized mode-field radius, w_{SIF}/a for the SIF as a function of V_{SIF} is also shown (dashed curve). The two arrows indicate the higher-order mode cutoffs of the SIF and PCF.

The functional dependence of w_{PCF}/Λ on V_{PCF} is seen to follow the same overall behavior as w_{SIF}/a as a function of V_{SIF}. For increasing values of V_{PCF}, w_{PCF}/Λ must saturate at a constant value corresponding to the minimum obtainable mode size, whereas it grows dramatically for sufficiently small values of V_{PCF}, indicating that the mode is weakly confined to the core and begins to penetrate into the cladding region. This is in good agreement with the fact that small values of V_{PCF} are realized either for small values of d/Λ or if the optical wavelength is similar to the structural dimensions, $\lambda \sim \Lambda$.

Because of the similar functional dependence of the mode-field radii on the respective V parameters it is reasonable to use the same fitting function for the PCF as was used for graded-index standard fibers. However, assuming the simplest case of a SIF, it is not possible to obtain a good fit, and the more general expression, for which g can assume any positive value, was therefore employed. This results in parameters $A = 0.7078$, $B = 0.2997$, and $C = 0.0037$ in the case of $g = 8$. The fits based on these parameters are plotted in Fig. 2 (solid curve) and can be seen to be very good for small as well as for large values of V_{PCF}. The maximal deviation between values predicted by the fit and the data points is determined to be less than 1%.

An important difference between the PCF and the SIF can be learned from the curves in Fig. 2 on which the higher-order mode cutoff are indicated at $V_{PCF} = \pi$ and $V_{SIF} = 2.405$. While the cutoff for the PCF is located at a point where the curve is relatively flat the SIF cutoff is located on a point where the curve is relatively steep. Also, V_{SIF} depends on the wavelength as λ^{-1}, further increasing the wavelength dependence of the mode size in the single-mode region of the SIF. For the PCF, not only the mode-size dependence on V_{PCF} close to cutoff but also the dependence of V_{PCF} itself on λ is weak, provided that Λ is a few times larger than λ or more (see Fig. 1). This results in a mode-field size that is essentially wavelength independent for the PCF compared with the SIF.

In conclusion, we have shown that the recently proposed expression for the V parameter of a PCF uniquely determines the normalized mode-field radius. Furthermore, we have presented a simple analytical expression describing this relation that is based on the same general expression used for graded-index standard fibers and have thereby further closed the gap between standard fibers and PCFs in terms of available tools describing their properties.

M. D. Nielsen (e-mail address mdn@crystal-fibre.com) acknowledges financial support by the Danish Academy of Technical Sciences.

References

1. J. Broeng, S. E. Barkou, A. Bjarklev, J. C. Knight, T. A. Birks, and P. St. J. Russell, Opt. Commun. **156,** 240 (1998).
2. A. Ferrando, E. Silvestre, J. J. Miret, and P. Andrés, Opt. Lett. **24,** 276 (1999).
3. D. Mogilevtsev, T. A. Birks, and P. St. J. Russell, Opt. Lett. **23,** 1662 (1998).
4. T. M. Monro, D. J. Richardson, N. G. R. Broderick, and P. J. Bennett, J. Lightwave Technol. **17,** 1093 (1999).
5. T. P. White, B. T. Kuhlmey, R. C. McPhedran, D. Maystre, G. Renversez, C. M. de Sterke, and L. C. Botten, J. Opt. Soc. Am. B **19,** 2322 (2002).
6. B. T. Kuhlmey, T. P. White, G. Renversez, D. Maystre, L. C. Botten, C. M. de Sterke, and R. C. McPhedran, J. Opt. Soc. Am. B **19,** 2331 (2002).
7. N. A. Mortensen, J. R. Folkenberg, M. D. Nielsen, and K. P. Hansen, Opt. Lett. **28,** 1879 (2003).
8. D. Marcuse, J. Opt. Soc. Am. **68,** 103 (1978).
9. J. C. Knight, T. A. Birks, P. St. J. Russel, and D. M. Atkin, Opt. Lett. **21,** 1547 (1996).
10. T. A. Birks, J. C. Knight, and P. St. J. Russell, Opt. Lett. **22,** 961 (1997).
11. W. A. Gambling, D. N. Payne, and H. Matsumyra, Electron. Lett. **13,** 139 (1977).
12. J. C. Knight, T. A. Birks, and P. St. J. Russell, J. Opt. Soc. Am. A **15,** 748 (1998).
13. S. G. Johnson and J. D. Joannopoulos, Opt. Express **8,** 173 (2001), http://www.opticsexpress.org.
14. N. A. Mortensen and J. R. Folkenberg, Opt. Express **10,** 475 (2002), http://www.opticsexpress.org.
15. N. A. Mortensen, Opt. Express **10,** 342 (2002), http://www.opticsexpress.org.
16. N. A. Mortensen, J. R. Folkenberg, P. M. W. Skovgaard, and J. Broeng, IEEE Photon. Technol. Lett. **14,** 1094 (2002).

Paper F

M.D. Nielsen, G. Vienne, J.R. Folkenberg, and A. Bjarklev

"Investigation of micro deformation induced attenuation spectra in a photonic crystal fiber"

Optics Letters, Vol. **28**, No. 4, pp. 236-238

(2003)

Investigation of microdeformation-induced attenuation spectra in a photonic crystal fiber

Martin Dybendal Nielsen, Guillaume Vienne, and Jakob Riis Folkenberg

Crystal Fibre A/S, Blokken 84, DK-3460 Birkerod, Denmark

Anders Bjarklev

Research Center COM, Technical University of Denmark, Orsteds Plads 349, DK-2800 Kgs. Lyngby, Denmark

Received September 3, 2002

We investigate both theoretically and experimentally the induced spectral attenuation in an all-silica photonic crystal fiber subjected to periodic axial microdeformations. The induced attenuation spectra show discrete attenuation peaks with a spectral position that is dependent on the period of the induced deformation. The peaks are assumed to be the result of mode coupling between the fundamental mode and a highly lossy higher-order mode. This assumption is verified through numerical calculation of the beat length between these two modes. Excellent agreement between experiment and numerical predictions of the spectral position of the attenuation peaks is obtained. © 2003 Optical Society of America

OCIS codes: 060.2270, 060.2400, 060.2430.

The development of the photonic crystal fiber (PCF) has opened up a wide range of possibilities for the realization of optical fibers with unique properties. Among the most significant achievements are the demonstration of the photonic bandgap effect through the realization of the air-guiding fiber[1] and the utilization of the large index contrast between air and glass to obtain highly nonlinear fibers.[2] The latter has, along with the possibility of shifting the zero-dispersion wavelength below 1.3 μm all the way to visible wavelengths,[3] formed the basis for generation of broadband supercontinuum spectra.[4] Another unique possibility that has arisen from the development of PCF is the design of fibers with novel cutoff properties based on the strong wavelength dependence of the effective index of microstructured cladding, allowing for the realization of endlessly single-mode fibers.[5] Such fibers can be designed to support only the fundamental mode regardless of wavelength and consequently have properties that are attractive in the context of future broadband multiwavelength transmission systems.[6]

In this Letter we study this type of PCF in the context of axial-deformation-induced attenuation, both experimentally and theoretically. Such attenuation was previously reported for standard optical fibers,[7,8] and it was shown to consist of discrete peaks with a spectral shape that could be described by the period of the deformation along with the deformation spectrum of the fiber. Furthermore, a strictly theoretical approach comparing standard fibers and PCFs indicated that similar behavior is to be expected in the case of PCFs.[9]

In this Letter the obtained attenuation spectra are explained through the mode spacing between the fundamental mode and the first higher-order mode, expressed as the beat length. Since only the beat length is considered, no assumptions regarding the deformation spectrum of the fiber are made, and consequently no predictions of the spectral shape or the amplitude of the attenuation peaks are given.

The beat length, L_B, between two modes with propagation constants β_1 and β_2 can generally be expressed as

$$L_B = \frac{2\pi}{\beta_1 - \beta_2} = \frac{2\pi}{n_1 2\pi/\lambda - n_2 2\pi/\lambda} = \frac{\lambda}{n_1 - n_2}, \qquad (1)$$

where λ is the free-space wavelength and n_1 and n_2 are the mode indices relating to β_1 and β_2, respectively. When an axial periodic deformation is applied, phase matching is obtained when L_B equals an integer times the deformation period, provided that the modal field overlap integral is nonzero.[10] Hence, if light is launched in the fundamental mode of the fiber and passed through a periodically deformed region, power will be lost to the other mode at a wavelength where the phase-matching condition is fulfilled, giving rise to strong attenuation at this wavelength.

To verify this theory for a PCF, we determine the beat length between the fundamental mode and the first higher-order mode numerically for a fabricated fiber. The fiber consists of a triangular arrangement of air holes in a pure silica background and is fabricated by the stack-and-pull method.[11] A picture of the cleaved facet of the fiber taken with an optical microscope is shown in Fig. 1. The fiber has an outer diameter of 125 μm and an acrylate coating, yielding a total diameter of 240 μm. Furthermore, it has five periods of air holes around the core, equal to a total of 90 air holes with a hole-to-hole spacing, referred to as the pitch, Λ, of 10.1 μm. The relative size of the air holes, d/Λ, where d is the diameter of the hole, is 0.51. The structure exhibits a high degree of uniformity indicated by a relative standard deviation of Λ equal to 1.2% and a relative standard deviation of d equal to 1.7%, both calculated on the basis of the 60 holes in the inner four rings. To adapt the hexagonal structure to the circular geometry, the holes in the outer ring are designed with a varying size.

For such a fiber to support only the fundamental mode at any given wavelength, the air-filling fraction

0146-9592/03/040236-03$15.00/0

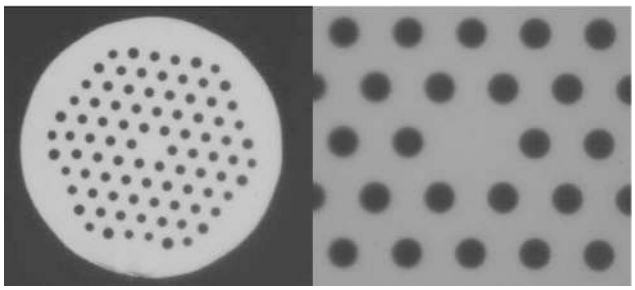

Fig. 1. Left, microscope picture of the cleaved end facet of the investigated fiber (outer diameter, 125 μm). Right, close up of the core region of the investigated fiber.

has to be sufficiently low. In this case the mode index of the first higher-order mode can stay below the cladding index of an infinite structure at any wavelength, causing only the fundamental mode to be guided.[5] In a real fiber, even with moderate air-filling fractions, a higher-order mode will in fact always be allowed at sufficiently low wavelengths because of the finite size of the structure. However, such a mode will typically be much less confined to the core and will have propagation loss that is many orders of magnitude larger than that of the fundamental mode, causing the fiber effectively to act as a single-mode fiber. Consequently, when we used a fiber length of 60 cm and inspected the near field at 635 nm, it was not possible to excite any higher-order modes, regardless of coupling conditions.

Assuming a perfectly uniform structure with the structural parameters obtained from the picture in Fig. 1 and assuming the refractive index of silica to be 1.444, the allowed frequencies for the first three eigenvalues as a function of propagation constant are calculated with a full vectorial mode solver based on the plane-wave method.[12] The first two eigenvalues, representing the two orthogonal polarization states of fundamental mode of the fiber, are degenerate in the case of a perfect structure[13] and the third represents the first higher-order mode. The mode indices for the first and third eigenvalues are shown in Fig. 2. The difference in mode index is tending toward zero as the wavelength decreases and becomes short relative to Λ, causing the influence of the holes to decrease, and the mode index tends toward the refractive index of silica. In the other extreme, where the wavelength is large compared with Λ, the index difference will also decrease, since the structure will no longer be resolved and the mode index will approach an average value between the refractive indices of silica and air, weighted with the air-filling fraction. This behavior of the index difference is observed when one is considering macrobending loss, for which loss edges occur at both short and long wavelengths.[14]

L_B between the two modes is calculated from Eq. (1), and the result is shown in Fig. 3. At short wavelengths, L_B increases drastically because of the vanishing index difference, indicating an increasingly unstable fiber in which mode coupling and thereby loss is caused by deformations on a millimeter scale.

The calculations indicate that mode coupling can be expected in the spectral range from approximately 400 to 1700 nm for deformations corresponding to beat lengths from 600 to 2500 μm. The fiber is characterized by use of a white-light source, a deformation device that is compliant with standard IEC 62221-3C,[15] and an optical spectrum analyzer. The deformation device consists of two metal plates with a mat of vulcanized rubber and a wire mesh in between. The wire mesh is quadratic woven with a well-defined mesh size, wire diameter, and hence period. The fiber is placed between the mesh and the rubber mat and oriented parallel to one of the orientations in the mesh, giving a total deformation length of 18 cm. We can replace the mesh with other meshes to obtain different deformation periods. Finally, we can apply weight on the upper metal plate to increase the deformation force, which has a typically value of ~35 N. To obtain an attenuation spectrum, we record a transmission spectrum with applied deformation, along with a reference spectrum with the mesh and the top plate removed. Subtracting these spectra simply yields the induced attenuation. Recorded attenuation peaks are shown in

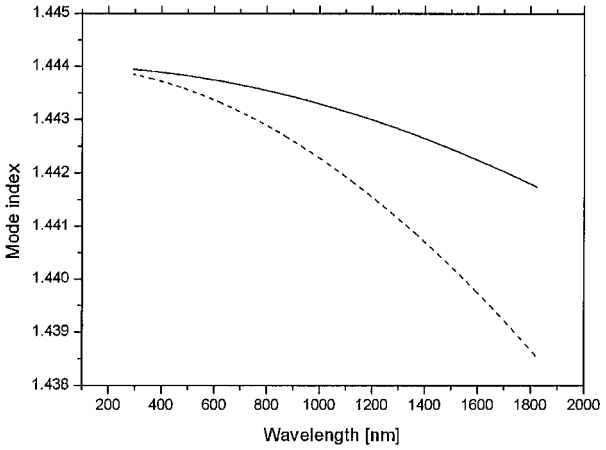

Fig. 2. Calculated mode index as a function of wavelength for the first and third eigenvalues (solid and dashed curves, respectively) in the case of a perfectly uniform structure with Λ and d as the fabricated fiber.

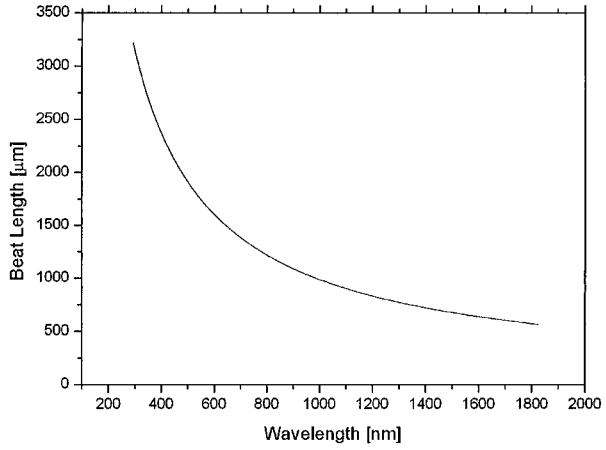

Fig. 3. Calculated beat length between the fundamental mode and first higher-order mode for a perfect structure with parameters as the fabricated fiber.

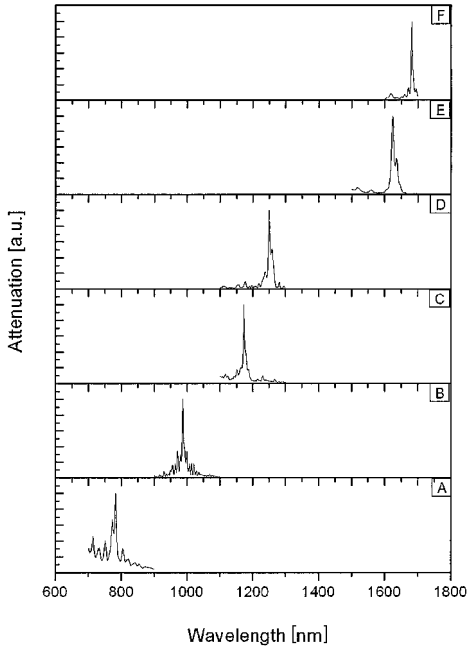

Fig. 4. Measured attenuation peaks A–F, sorted by wavelength. The spectra are given in arbitrary units.

Table 1. Calculated and Measured Data for the Attenuation Peaks shown in Fig. 3

Peak	Calculated Wavelength (nm)	Grating Period (μm)	Order	Measured Wavelength (nm)	Deviation (%)
A	786.5	620	2	782.8	0.5
B	987.3	500	2	986.4	0.1
C	1174.2	850	1	1173.2	0.1
D	1220.5	410	2	1249.6	2.4
E	1571.6	325	2	1624.0	3.3
F	1655.7	620	1	1681.2	1.5

Fig. 4. All spectra are recorded with a spectral resolution of 2 nm. In general, the peaks are very sharp, although there is a slight tendency that peaks at lower wavelengths have more side peaks. This tendency is attributed to the fact that the index difference in this region decreases rapidly, causing the confinement of the mode to decrease.

To investigate whether the calculated beat length can explain the spectral positions of the peaks, we use the calculation represented in Fig. 3 to translate the period, or the double period, of a given mesh to a phase-matching wavelength. When the double period is used, the peak is said to be of the order of 2, whereas the direct use of the period corresponds to the order of 1. These results are summarized in Table 1 for all calculated phase-matching wavelengths, along with the measured spectral positions of the peaks within the spectral range 700–1700 nm.

In general, very good agreement between the measured and calculated wavelengths is observed. The deviation is seen to increase slightly at longer wavelengths since the beat length becomes less wavelength dependent in this region. Also, the peaks showing the largest deviation (peaks D and E) correspond to the use of a wire mesh with a mesh size of 250 and 200 μm, respectively. These sizes are close to and less than the diameter of the coated fiber, respectively, making it difficult to ensure that the deformations are strictly periodic and axial.

In conclusion, we have demonstrated the existence of discrete spectral attenuation peaks for a PCF subjected to periodic axial deformations. The spectral positions of these peaks were correlated to the beat length between the fundamental mode and the first higher-order mode. The results show that simple description of the modal properties based on the perfectly uniform fiber structure may explain the microdeformation properties of the investigated fiber with high accuracy.

M. D. Nielsen's e-mail address is mdn@crystal-fibre.com.

References

1. R. F. Cregan, B. J. Mangan, J. C. Knight, T. A. Birks, P. St. J. Russel, P. J. Roberts, and D. C. Allan, Science **285,** 1537 (1999).
2. K. P. Hansen, J. R. Jensen, C. Jacobsen, H. R. Simonsen, J. Broeng, P. M. W. Skovgaard, A. Petersson, and A. Bjarklev, in *Optical Fiber Communications Conference,* Vol. 70 of OSA Trends in Optics and Photonics Series (Optical Society of America, Washington, D.C., 2002), paper FA9.
3. J. K. Ranka, R. S. Windeler, and A. J. Stentz, Opt. Lett. **25,** 25 (2000).
4. K. P. Hansen, J. J. Larsen, J. R. Jensen, S. Keiding, J. Broeng, H. R. Simonsen, and A. Bjarklev, presented at the LEOS 14th Annual Meeting, San Diego, Calif., November 11–15, 2001.
5. T. A. Birks, J. C. Knight, and P. St. J. Russell, Opt. Lett. **22,** 961 (1997).
6. M. D. Nielsen, A. Petersson, C. Jacobsen, H. R. Simonsen, G. Vienne, and A. Bjarklev, paper 03.4.2 presented at the 28th European Conference on Optical Communication (ECOC 2002), Copenhagen, Denmark, September 8–12, 2002.
7. C. B. Probst, A. Bjarklev, and S. B. Andersen, J. Lightwave Technol. **7,** 55 (1989).
8. A. Bjarklev and S. B. Andersen, Electron. Lett. **25,** 417 (1989).
9. A. Bjarklev, T. P. Hansen, K. Hougaard, S. E. B. Libori, E. Knudsen, and J. Broeng, paper We.L.2.4 presented at the 27th European Conference on Optical Communication (ECOC 2001), Amsterdam, The Netherlands, September 30–October 4, 2001.
10. V. Arya, K. A. Murphy, A. Wang, and R. O. Claus, J. Lightwave Technol. **13,** 1998 (1995).
11. T. A. Birks, J. C. Knight, B. J. Mangan, and P. St. J. Russell, IEICE Trans. Electron. **E84-C,** 585 (2001).
12. S. G. Johnson and J. D. Joannopoulos, Opt. Express **8,** 173 (2001), http://www.opticsexpress.org.
13. M. J. Steel, T. P. White, C. Martijn de Sterke, R. C. McPhedran, and L. C. Botten, Opt. Lett. **26,** 488 (2001).
14. T. Sørensen, J. Broeng, A. Bjarklev, E. Knudsen, and S. E. B. Libori, Electron. Lett. **37,** 287 (2001).
15. IEC Tech. Rep. TR 62221, 1.0 (International Electrotechnical Commission, Geneva, Switzerland, 2001).

Paper G

M.D. Nielsen, N.A. Mortensen, and J.R. Folkenberg

"Reduced micro-deformation attenuation in large-mode area photonic crystal fibers for visible applications"

Optics Letters, Vol. **28**, No. 18, pp. 1645-1647

(2003)

Reduced microdeformation attenuation in large-mode-area photonic crystal fibers for visible applications

Martin D. Nielsen

Crystal Fibre A/S, Blokken 84, DK-3460 Birkerød, Denmark, and
Research Center COM, Technical University of Denmark, DK-2800 Kongens Lyngby, Denmark

Niels Asger Mortensen and Jacob Riis Folkenberg

Crystal Fibre A/S, Blokken 84, DK-3460 Birkerød, Denmark

Received March 113, 2003

We consider large-mode-area photonic crystal fibers for visible applications in which microdeformation-induced attenuation becomes a potential problem when the effective area A_{eff} is sufficiently large compared to λ^2. We argue that a slight increase in fiber diameter D can be used in screening the high-frequency components of the microdeformation spectrum mechanically, and we confirm this experimentally for both 15- and 20-μm core fibers. For typical bending radii ($R \sim 16$ cm) the operating bandwidth increases by approximately 3–400 nm to the low-wavelength side. © 2003 Optical Society of America

OCIS codes: 060.2280, 060.2300, 060.2310, 060.2400, 060.2430.

In all-silica photonic crystal fibers (PCFs), light is guided by an arrangement of airholes running along the full length of the fiber. Typically, airholes of diameter d are arranged in a triangular lattice with a pitch Λ of the same length scale as free-space wavelength λ. The core can be either a solid-silica core (see Fig. 1) with total-internal-reflection guidance[1] or an air core with photonic-bandgap guidance.[2] For recent reviews we refer the reader to Ref. 3 and references therein.

Although air-core PCFs probably have the most extraordinary guidance mechanisms, silica-core PCFs also have remarkable properties, such as an endlessly single-mode nature[4] that in principle leads to unlimited, large effective areas.[5] These properties are often greatly desirable for high-power delivery, and thus PCFs are obvious candidates for many of these applications. For single-mode PCFs there is of course another side of the coin that is common to the physics in standard-fiber technology: As effective area A_{eff} is increased, the mode becomes increasingly susceptible to longitudinal fiber variations, microdeformations, and macrobending.[6] Nevertheless, the PCF technology has a clear advantage because of its endlessly single-mode properties and the relative ease by which small effective core–cladding index steps Δn_{eff} can be achieved through control of d and Λ. In standard fibers such control is difficult because extremely small, well-controlled doping levels are required for $\Delta n_{\text{eff}} \ll 10^{-3}$.

Even though the general physics causes Δn_{eff} to decrease if A_{eff} is increased, there is still room for improvement by optimal choice of the microstructured cladding and the core's shape and size. Recently we demonstrated an improved large-mode-area (LMA) design with a three-rod core[7] instead of the usual one-rod core.[1] Compared to fibers of the one-rod design, this new LMA PCF offers a larger Δn_{eff} for the same A_{eff} and vice versa in the limit $\lambda \ll \Lambda$.

The general view has been that the operation of LMA PCFs is limited by macrobending loss,[5,8,9] but, by pushing the technology to still larger effective areas, limitations can be set by, e.g., microbending deformations as well.[6] Microbending deformations may be caused by external perturbations, as was shown recently,[10] but even when there are no external perturbations there may still be residual microdeformations caused by frozen-in mechanical stress in, e.g., the coating material. When performance is not limited by macrobending it is obvious to look into properties of the screening of microbending deformations. Recently, results for the attenuation of a PCF with a 15-μm core diameter and an outer diameter $D = 125$ μm were reported.[6] In the visible regime the performance of this PCF was clearly found to suffer from microdeformation-induced attenuation. In this Letter we suggest a simple way to screen the effect of microdeformations and demonstrate a considerable reduction of the loss level in LMA PCFs for visible applications.

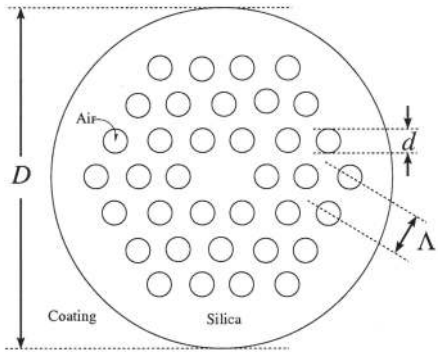

Fig. 1. Schematic of the cross section of a PCF with a triangular airhole cladding and a silica core in which light is effectively confined by a total-internal-reflection mechanism. D, outer fiber diameter; d, airhole diameter; Λ, airhole pitch.

0146-9592/03/181645-03$15.00/0

We emphasize that the actual loss level arises from competing effects[6] and, once the effect of microbending has been suppressed below the macrobending-induced attenuation level, the operation of the fiber may of course still be limited by macrobending attenuation.

The Fourier spectrum of naturally occurring microbending deformations will typically be quite broadband, although sharp distinct features may also be exhibited, e.g., for periodic deformations.[10] In either case the high-frequency components of the externally applied deformation spectrum do not affect the optical waveguide, because of the stiffness of the fiber. In other words, it is practically impossible to deform the fiber on a length scale comparable to or shorter than the fiber diameter. In terms of the effective index step, microdeformations will be screened if $\Delta n_{\mathrm{eff}} > \Delta n_{\mathrm{micro}}$. For a simple fiber model it can be shown that[11]

$$\Delta n_{\mathrm{micro}} = (\lambda/\pi D)\,(E_c/\pi E_f)^{1/4}, \qquad (1)$$

where D is the fiber diameter, E_c is the Young modulus of the coating, and E_f is the effective Young modulus of the air–silica composite material. In this Letter we focus on the D dependence of $\Delta n_{\mathrm{micro}}$. The use of coating materials with special mechanical properties for improving the screening properties of the fiber is an alternative direction not addressed here.

From Eq. (1) it is obvious that the property that $\Delta n_{\mathrm{micro}} \propto 1/D$ can be used as a simple way to screen microdeformations. In the optical-fiber community it is a longstanding tradition and standard to use $D \simeq 125\ \mu$m, but, as we demonstrate here, there is a clear advantage in increasing the diameters of LMA PCFs (for, e.g., visible applications) similarly to what is often done for standard technology specialty fibers; e.g., Ref. 12.

When values for E_f and E_c are used for silica and typical polymer coatings, respectively, Eq. (1) suggests that $\Delta n_{\mathrm{micro}} \sim 0.1 \times \lambda/D$. For typical fiber diameters and wavelengths this expression gives numbers that differ only slightly in order of magnitude from typical mode spacings.[10] For the PCFs that we compare here we have two versions, with $D = 125\ \mu$m and with $D = 175\ \mu$m, but with otherwise similar dielectric cross sections in terms of core size, pitch, and airhole diameter. Though the change in diameter may seem like a modest change, it has an important effect on $\Delta n_{\mathrm{micro}}$, which is decreased by ~30%, and for the PCFs studied here we shall see that this change is enough to bring the PCF from the $\Delta n_{\mathrm{eff}} < \Delta n_{\mathrm{micro}}$ regime to the $\Delta n_{\mathrm{eff}} > \Delta n_{\mathrm{micro}}$ regime. For PCFs Δn_{eff} decreases when the wavelength decreases (opposite the case for standard fibers); thus microbending loss will increase with decreasing wavelength.

In Fig. 2 we show the experimentally observed spectral attenuation for two endlessly single-mode PCFs with a core diameter $2\Lambda - d$ of 15 μm and with an airhole diameter $d/\Lambda \sim 0.44$, i.e., close to the theoretical endlessly single-mode limit.[13] The fibers were drawn from similar preforms fabricated by the stack-and-pull method,[1] but different thicknesses of overcladding were used for the two drawings, which yielded two fibers with similar microstructures but with the different values of D, as mentioned above. The fibers have five and seven rings of air holes, respectively, but because $\lambda \ll \Lambda$ the different numbers are of no importance in terms of leakage loss,[14] and thus the different thicknesses of overcladding do not influence the optical properties of the guided modes. The two fibers were both found to be single mode (in both the visible and the near-infrared regimes), and they have similar mode-field diameters (~12 μm) and otherwise differ only in their mechanical properties. For each of the fibers the attenuation was characterized with a cutback technique that used a fiber length of >100 m on a spool of 16-cm radius, a white-light source, and an optical spectrum analyzer. Comparing the two curves in Fig. 2, we can see the effect of a larger outer diameter D to be quite dramatic, and for the PCF with the largest diameter the spectral dependence has a typical Rayleigh dependence, although there is a wavelength-independent offset compared with the ultimate Rayleigh limit, which is indicated by the dashed curve. This wavelength-independent offset indicates the absence of both macrobending- and microdeformation-induced attenuation. The slightly higher loss of $D = 175\ \mu$m for $\lambda \gtrsim 1100$ nm is due to contamination.

In Fig. 3 we consider two PCFs with a 20-μm core diameter and $d/\Lambda \sim 0.44$; we compare two versions, one with $D = 125\ \mu$m for which the effect of microdeformations is pronounced and one with $D = 230\ \mu$m for which the effect of the deformation is screened. The fibers have three and seven rings of airholes, respectively, but we emphasize that this difference has no importance in terms of leakage loss because $\lambda \ll \Lambda$.[14] Again the version with a larger outer diameter has a significantly lower attenuation level (cf. Figs. 3A and 3B). By changing the macrobending radius (Fig. 3B) we actually find evidence that the effect of microdeformations is fully screened even 200 nm below the O–H attenuation peak at $\lambda \sim 1.24\ \mu$m and that macrobending limitations become more apparent. For the PCF with the smallest outer diameter the attenuation level caused by microdeformations is too high to make macrobending a limiting effect (Fig. 3A), whereas for the large-diameter version we observe a clear bend edge, which,

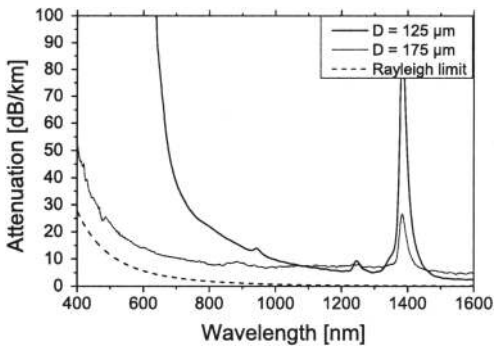

Fig. 2. Spectral attenuation for two PCFs, both with a 15-μm core diameter, characterized on a spool of 16-cm radius.

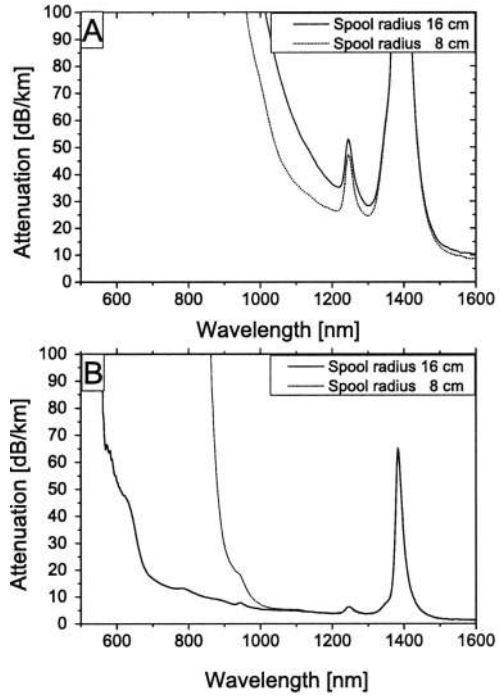

Fig. 3. Spectral attenuation for different macrobending for two PCFs with a 20-μm core diameter. In A and B the outer diameter of the PCF is $D = 125$ μm and $D = 230$ μm, respectively.

as expected, shifts toward longer wavelengths when the bend radius is decreased. One can see from Fig. 3A that the attenuation is actually higher on the 16-cm spool, further indicating that microdeformation is the limiting factor. The difference is caused by different spooling conditions, e.g., variations in the tension or in the physical surface topography of the spool.

In conclusion, we have shown how microdeformation-induced loss in LMA PCFs can be suppressed by a slight increase in fiber diameter D compared with the standard of $D \sim 125$ μm. The suppression can be understood as a simple mechanical screening of the high-frequency components of the microdeformation spectrum. For a PCF with a 20-μm core we have demonstrated a significant reduction of the loss level by going from $D \simeq 125$ μm to $D \simeq 230$ μm. For a bend radius $R \simeq 16$ cm this improved PCF guides light with a loss level that does not exceed ~20 dB/km down to $\lambda \sim 650$ nm, where macrobending attenuations sets in. We believe that the present findings have important implications for prospects of utilizing LMA PCFs for high-power delivery in the visible regime and for use of the PCF technology in fiber-laser applications.

M. D. Nielsen acknowledges financial support by the Danish Academy of Technical Sciences. M. D. Nielsen's e-mail address is mdn@crystal-fibre.com.

References

1. J. C. Knight, T. A. Birks, P. St. J. Russell, and D. M. Atkin, Opt. Lett. **21,** 1547 (1996).
2. R. F. Cregan, B. J. Mangan, J. C. Knight, T. A. Birks, P. St. J. Russell, P. J. Roberts, and D. C. Allan, Science **285,** 1537 (1999).
3. P. Russell, Science **299,** 358 (2003).
4. T. A. Birks, J. C. Knight, and P. St. J. Russell, Opt. Lett. **22,** 961 (1997).
5. J. C. Knight, T. A. Birks, R. F. Cregan, P. St. J. Russell, and J.-P. De Sandro, Electron. Lett. **34,** 1347 (1998).
6. N. A. Mortensen and J. R. Folkenberg, J. Opt. A Pure Appl. Opt. **5,** 163 (2003).
7. N. A. Mortensen, M. D. Nielsen, J. R. Folkenberg, A. Petersson, and H. R. Simonsen, Opt. Lett. **28,** 393 (2003).
8. J. C. Baggett, T. M. Monro, K. Furusawa, and D. J. Richardson, Opt. Lett. **26,** 1045 (2001).
9. T. Sørensen, J. Broeng, A. Bjarklev, E. Knudsen, and S. E. B. Libori, Electron. Lett. **37,** 287 (2001).
10. M. D. Nielsen, G. Vienne, J. R. Folkenberg, and A. Bjarklev, Opt. Lett. **28,** 236 (2003).
11. A. Bjarklev and S. B. Andreasen, Electron. Lett. **25,** 417 (1989).
12. M. E. Fermann, Opt. Lett. **23,** 52 (1998).
13. B. T. Kuhlmey, R. C. McPhedran, and C. M. de Sterke, Opt. Lett. **27,** 1684 (2002).
14. T. P. White, R. C. McPhedran, C. M. de Sterke, L. C. Botton, and M. J. Steel, Opt. Lett. **26,** 1660 (2001).

Paper H

M.D. Nielsen, N.A. Mortensen, M. Albertsen, J.R. Folkenberg, A. Bjarklev, and C. Dominica

"*Predicting macrobending-loss for large-mode area photonic crystal fibers*"

Optics Express, Vol. **12**, No. 8, pp. 1775-1779

(2004)

Predicting macrobending loss for large-mode area photonic crystal fibers

M. D. Nielsen,[1,2,*] **N. A. Mortensen,**[1,3] **M. Albertsen,**[2,4]
J. R. Folkenberg,[1] **A. Bjarklev,**[2] **and D. Bonacinni**[4]

[1]*Crystal Fibre A/S, Blokken 84, DK-3460 Birkerød, Denmark*
[2]*COM, Technical University of Denmark, DK-2800 Kongens Lyngby, Denmark*
[3]*Department of Micro and Nanotechnology, Technical University of Denmark, DK-2800 Kongens Lyngby, Denmark*
[4]*European Southern Observatory, Karl-Swarzschildstrasse 2, D-85748 Garching bei München, Germany*

[*]*mdn@crystal-fibre.com*

Abstract: We report on an easy-to-evaluate expression for the prediction of the bend-loss for a large mode area photonic crystal fiber (PCF) with a triangular air-hole lattice. The expression is based on a recently proposed formulation of the V-parameter for a PCF and contains no free parameters. The validity of the expression is verified experimentally for varying fiber parameters as well as bend radius. The typical deviation between the position of the measured and the predicted bend loss edge is within measurement uncertainty.

OCIS codes: (060.2280) Fiber design and fabrication, (060.2400) Fiber properties, (060.2430) Fibers, single-mode, (999.999) Photonic crystal fiber

References and links

1. J. C. Knight, "Photonic crystal fibres," Nature **424**, 847–851 (2003).
2. T. A. Birks, J. C. Knight, and P. S. J. Russell, "Endlessly single mode photonic crystal fibre," Opt. Lett. **22**, 961–963 (1997).
3. T. Sørensen, J. Broeng, A. Bjarklev, E. Knudsen, and S. E. B. Libori, "Macro-bending loss properties of photonic crystal fibre," Electron. Lett. **37**, 287–289 (2001).
4. T. Sørensen, J. Broeng, A. Bjarklev, T. P. Hansen, E. Knudsen, S. E. B. Libori, H. R. Simonsen, and J. R. Jensen, "Spectral Macro-bending loss considerations for photonic crystal fibres," IEE Proc.-Opt. **149**, 206 (2002).
5. N. A. Mortensen and J. R. Folkenberg, "Low-loss criterion and effective area considerations for photonic crystal fibers," J. Opt. A: Pure Appl. Opt. **5**, 163–167 (2003).
6. J. C. Baggett, T. M. Monro, K. Furusawa, V. Finazzi, and D. J. Richardson, "Understanding bending losses in holey optical fibers," Opt. Commun. **227**, 317–335 (2003).
7. J. Sakai and T. Kimura, "Bending loss of propagation modes in arbitrary-index profile optical fibers," Appl. Opt. **17**, 1499–1506 (1978).
8. J. Sakai, "Simplified bending loss formula for single-mode optical fibers," Appl. Opt. **18**, 951–952 (1979).
9. A. W. Snyder and J. D. Love, *Optical Waveguide Theory* (Chapman & Hall, New York, 1983).
10. N. A. Mortensen, "Effective area of photonic crystal fibers," Opt. Express **10**, 341–348 (2002). URL http://www.opticsexpress.org/abstract.cfm?URI=OPEX-10-7-341.
11. N. A. Mortensen, J. R. Folkenberg, M. D. Nielsen, and K. P. Hansen, "Modal cut-off and the V–parameter in photonic crystal fibers," Opt. Lett. **28**, 1879–1881 (2003).
12. M. D. Nielsen, N. A. Mortensen, J. R. Folkenberg, and A. Bjarklev, "Mode-Field Radius of Photonic Crystal Fibers Expressed by the V–parameter," Opt. Lett. **28**, 2309–2311 (2003).
13. M. D. Nielsen and N. A. Mortensen, "Photonic crystal fiber design based on the V–parameter," Opt. Express **11**, 2762–2768 (2003). URL http://www.opticsexpress.org/abstract.cfm?URI=OPEX-11-21-2762.

#4007 - $15.00 US
Received 9 March 2004; revised 7 April 2004; accepted 9 April 2004

1. Introduction

In solid-core photonic crystal fibers (PCF) the air-silica microstructured cladding (see Fig. 1) gives rise to a variety of novel phenomena [1] including large-mode area (LMA) endlessly-single mode operation [2]. Though PCFs typically have optical properties very different from that of standard fibers they of course share some of the overall properties such as the susceptibility of the attenuation to macro-bending.

Macrobending-induced attenuation in PCFs has been addressed both experimentally as well as theoretically/numerically in a number of papers [2, 3, 4, 5, 6]. However, predicting bending-loss is no simple task and typically involves a full numerical solution of Maxwell's equations as well as use of a phenomenological free parameter, *e.g.* an effective core radius. In this paper we revisit the problem and show how macro-bending loss measurements on high-quality PCFs can be predicted with high accuracy using easy-to-evaluate empirical relations.

2. Predicting macro-bending loss

Predictions of macro-bending induced attenuation in photonic crystal fibers have been made using various approaches including antenna-theory for bent standard fibers [3, 4], coupling-length criteria [2, 5], and phenomenological models within the tilted-index representation [6]. Here, we also apply the antenna-theory of Sakai and Kimura [7, 8], but contrary to Refs. [3, 4] we make a full transformation of standard-fiber parameters such as Δ, W, and V [9] to fiber parameters appropriate to high-index contrast PCFs with a triangular arrangement of air holes. In the large-mode area limit we get (see Appendix)

$$\alpha\Lambda \simeq \frac{1}{8\sqrt{6\pi}}\frac{1}{n_S}\frac{\Lambda^2}{A_{\text{eff}}}\frac{\lambda}{\Lambda}F\left(\frac{1}{6\pi^2}\frac{1}{n_S^2}\frac{R}{\Lambda}\left(\frac{\lambda}{\Lambda}\right)^2 V_{\text{PCF}}^3\right),\ F(x)=x^{-1/2}\exp(-x), \tag{1}$$

for the power-decay, $P(z)=P(0)\exp(-2\alpha z)$, along the fiber. For a conversion to a dB-scale α should be multiplied by $20\times\log_{10}(e)\simeq 8.686$. In Eq. (1), R is the bending radius, A_{eff} is the effective area [10], n_S is the index of silica, and

$$V_{\text{PCF}}=\Lambda\sqrt{\beta^2-\beta_{cl}^2} \tag{2}$$

is the recently introduced effective V-parameter of a PCF [11]. The strength of our formulation is that it contains no free parameters (such as an arbitrary core radius) and furthermore empirical expressions, depending only on λ/Λ and d/Λ, have been given recently for both A_{eff} and V_{PCF} [12, 13].

From the function $F(x)$ we may derive the parametric dependence of the critical bending radius R^*. The function increases dramatically when the argument is less than unity and thus we may define a critical bending radius from $x\sim 1$ where $F\sim 1/e$. Typically the PCF is operated close to cut-off where $V_{\text{PCF}}^*=\pi$ [11] so that the argument may be written as

	LMA-20	LMA-25	LMA-35
Core Diameter [μm]	20.0	24.5	34.7
Λ [μm]	13.20	16.35	23.15
d/Λ	0.485	0.500	0.500

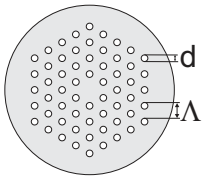

Fig. 1. Structural data for the LMA fibers which all have a cross-section with a triangular arrangement of air-holes running along the full length of the fiber.

#4007 - $15.00 US
Received 9 March 2004; revised 7 April 2004; accepted 9 April 2004

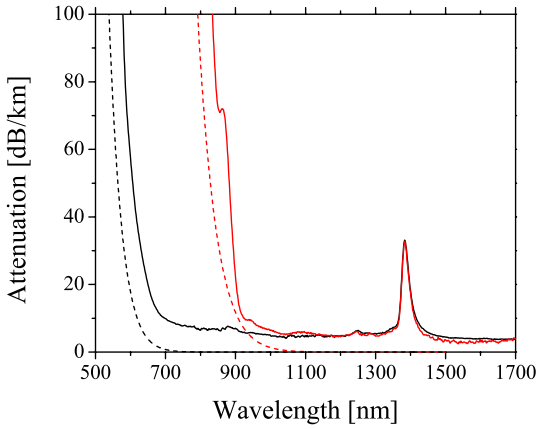

Fig. 2. Macro-bending loss for the LMA-20 fiber for bending radii of R=8 cm (red, solid curve) and R=16 cm (black, solid curve). Predictions of Eq. (1) are also included (dashed curves).

$$\underbrace{\pi^3 \frac{1}{6\pi^2}\frac{1}{n_S^2}}_{\sim 1/4}\frac{R^*}{\Lambda}\left(\frac{\lambda}{\Lambda}\right)^2 \sim 1 \Rightarrow R^* \propto \frac{\Lambda^3}{\lambda^2} \tag{3}$$

This dependence was first reported and experimentally confirmed by Birks *et al.* [2] and recently a pre-factor of order unity was also found experimentally in Ref. [5].

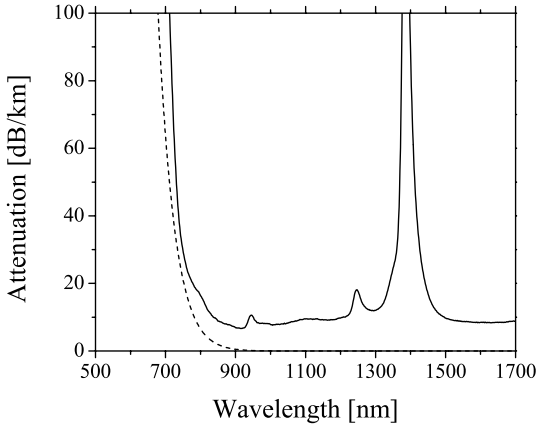

Fig. 3. Macro-bending loss for the LMA-25 fiber for bending radius of R=16 cm (solid curve). Predictions of Eq. (1) are also included (dashed curve).

#4007 - $15.00 US
Received 9 March 2004; revised 7 April 2004; accepted 9 April 2004

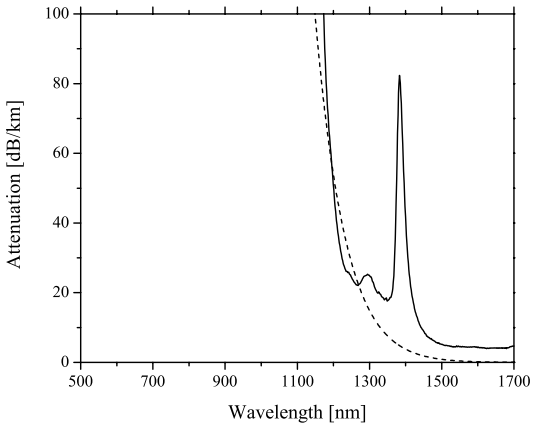

Fig. 4. Macro-bending loss for the LMA-35 fiber for bending radius of R=16 cm (solid curve). Predictions of Eq. (1) are also included (dashed curve).

3. Experimental results

We have fabricated three LMA fibers by the stack-and-pull method and characterized them using the conventional cut-back technique. All three fibers have a triangular air-hole array and a solid core formed by a single missing air-hole in the center of the structure, see Fig. 1.

For the LMA-20 macro-bending loss has been measured for bending radii of R=8 cm and R=16 cm and the results are shown in Fig. 2. The predictions of Eq. (1) are also included. It is emphasized that the predictions are based on the empirical relations for A_{eff} and V_{PCF} provided in Refs. [12] and [13] respectively and therefore do not require any numerical calculations. Similar results are shown in Figs. 3 and 4 for the LMA-25 and LMA-35 fibers, respectively.

4. Discussion and conclusion

The PCF, in theory, exhibits both a short and long-wavelength bend-edge. However, the results presented here only indicate a short-wavelength bend-edge. The reason for this is that the long-wavelength bend-edge occurs for $\lambda \gg \Lambda/2$ [3]. For typical LMA-PCFs it is therefor located in the non-transparent wavelength regime of silica.

In conclusion we have demonstrated that macro-bending loss measurements on high-quality PCFs can be predicted with good accuracy using easy-to-evaluate empirical relations with only d and Λ as input parameters. Since macro-bending attenuation for many purposes and applications is the limiting factor we believe that the present results will be useful in practical designs of optical systems employing photonic crystal fibers.

Appendix

The starting point is the bending-loss formula for a Gaussian mode in a standard-fiber [7, 8]

$$\alpha = \frac{\sqrt{\pi}}{8}\frac{1}{A_{\text{eff}}}\frac{\rho}{W}\frac{\exp\left(-\frac{4}{3}\frac{R}{\rho}\frac{\Delta}{V^2}W^3\right)}{\sqrt{W\frac{R}{\rho}+\frac{V^2}{2\Delta W}}} \tag{4}$$

#4007 - $15.00 US
Received 9 March 2004; revised 7 April 2004; accepted 9 April 2004

where A_{eff} is the effective area, ρ is the core radius, R is the bending radius, and the standard-fiber parameters are given by [7, 9]

$$\Delta = \frac{sin^2\theta_c}{2}\ ,\ V = \beta\,\rho\,sin\theta_c\ ,\ W = \rho\sqrt{\beta^2 - \beta_{cl}^2}. \tag{5}$$

Substituting these parameters into Eq. (4) we get

$$\alpha\Lambda \simeq \frac{1}{8}\sqrt{\frac{2\pi}{3}}\frac{\Lambda^2}{A_{\text{eff}}}\frac{1}{\beta\Lambda}F\left(\frac{2}{3}\frac{R}{\Lambda}\frac{V_{\text{PCF}}^3}{(\beta\Lambda)^2}\right) \tag{6}$$

in the relevant limit where $R \gg \rho$. Here, F and V_{PCF} in Eqs. (1) and (2) have been introduced. For large-mode area fibers we make a further simplification for the isolated propagation constant; using that $\beta = 2\pi n_{\text{eff}}/\lambda \simeq 2\pi n_S/\lambda$ we arrive at Eq. (1).

Acknowledgments

M. D. Nielsen acknowledges financial support by the Danish Academy of Technical Sciences.

#4007 - $15.00 US
Received 9 March 2004; revised 7 April 2004; accepted 9 April 2004

Paper I

M.D. Nielsen, J.R. Folkenberg, N.A. Mortensen, and A. Bjarklev

"*Bandwidth comparison of photonic crystal fibers and conventional single-mode fibers*"

Optics Express, Vol. **12**, No. 3, pp. 430-435

(2004)

Bandwidth comparison of photonic crystal fibers and conventional single-mode fibers

M.D. Nielsen[1,2], J.R. Folkenberg[1], N.A. Mortensen[1], and A. Bjarklev[2]

[1] *Crystal Fibre A/S, Blokken 84, DK-3460 Birkerød, Denmark*
[2] *COM, Technical University of Denmark, DK-2800 Kongens Lyngby, Denmark*

mdn@crystal-fibre.com

Abstract: We experimentally compare the optical bandwidth of a conventional single-mode fiber (SMF) with 3 different photonic crystal fibers (PCF) all optimized for visible applications. The spectral attenuation, single-turn bend loss, and mode-field diameters (MFD) are measured and the PCF is found to have a significantly larger bandwidth than the SMF for an identical MFD. It is shown how this advantage can be utilized for realizing a larger MFD for the PCF while maintaining a bending resistant fiber.

OCIS codes: (060.2400) Fiber Properties, (060.2430) fibers, Single-mode, (999.999) Photonic crystal fiber

References and Links

1. T.A. Birks, J.C. Knight, and P.St.J. Russel, "Endlessly single-mode photonic crystal fiber," Opt. Lett. **22**, 961-963 (1997).
2. N.A. Mortensen and J.R. Folkenberg, "Low-loss criterion and effective area considerations for photonic crystal fibers," J. Opt. A: Pure Appl. Opt. **5**, 163-167 (2003).
3. M.D. Nielsen, N.A. Mortensen, and J.R. Folkenberg, "Reduced microdeformation attenuation in large-mode-area photonic crystal fibers for visible applications," Opt. Lett. **28**, 1645-1647 (2003).
4. W.A. Gambling, D.N. Payne, and H. Matsumyra, "Cut-off frequency in radially inhomogeneous single-mode fibre," Electron. Lett. **13**, 139-140 (1977).
5. D. Marcuse, "Gaussian approximation of the fundamental modes of graded-index fibers," J. Opt. Soc. Am. **68**, 103-109 (1978).
6. N.A. Mortensen, J.R. Folkenberg, M.D. Nielsen, and K.P. Hansen, "Modal Cut-off and the V-parameter in Photonic Crystal Fibers," Opt. Lett. **28**, 1879-1881 (2003).
7. M.D. Nielsen, N.A. Mortensen, J.R. Folkenberg, and A. Bjarklev, "Mode-field radius of photonic crystal fibers expressed by the V-parameter," Opt. Lett. **28**, 2309-2311 (2003).
8. M.D. Nielsen and N.A. Mortensen, "Photonic crystal fiber design based on the V-parameter," Opt. Express **11**, 2762-2768 (2003), http://www.opticsexpress.org/abstract.cfm?URI=OPEX-11-21-2762
9. T. Sørensen, J. Broeng, A. Bjarklev, E. Knudsen, and S.E.B. Libori, "Macro-bending Loss Properties of Photonic Crystal Fibre," Electron. Lett., **37**, 287-289 (2001).
10. O. Humbach, H. Fabian, U. Grzesik, U. Haken, and W. Heitmann, "Analysis of OH absorption bands in synthetic silica," J. Non-Cryst. Solids **203**, 19-26 (1996).

1. Introduction

In conventional single-mode fibers (SMF), the single-mode optical bandwidth is typically limited by a higher-order mode cutoff at short wavelengths and macro-bend loss at long wavelengths. The characteristics of the photonic crystal fiber (PCF) are fundamentally different from this picture. Most important is the fact that the PCF can be designed to be endlessly single-mode (ESM), a term first coined by Birks *et al.* [1] referring to the fact that no higher-order modes are supported regardless of the wavelength. The ESM property has the specious consequence that the waveguide can be scaled to an arbitrary dimension while remaining single mode. However, as the scale of the structure is increased, the susceptibility

#3660 - $15.00 US Received 13 January 2004; revised 26 January 2004; accepted 26 January 2004

towards attenuation induced by variations in structural parameters as well as external perturbations such as bending increases [2,3] limiting the practical dimensions that can be realized.

Often the question of which fiber type is most bend insensitive is raised: A PCF or a conventional SMF? The problem when trying to answer this question is that it is not very precise because the fibers to be compared need to be identical in terms of other optical properties in order for the comparison to be meaningful. Most relevant is to compare fibers with the same mode-field diameter (MFD) since bend loss in general increases with increasing MFD. Even though one should have a PCF and a SMF with identical MFD at a given wavelength, another problem arises from the fact that the MFD of the two fibers vary quite differently as function of wavelength making comparison difficult. Also, the MFD of one or both of the fibers might not necessarily result from an optimal choice of parameters and, finally, the spectral dependency of the bend loss is quite different for the two types of fibers. In this paper, we address these issues and attempt to make the comparison of the optical bandwidth taking the mentioned difficulties above into account. For the comparison we use fibers that are single mode at visible wavelengths and focus on their applicability red, green, and blue light (RGB) applications. The considered PCFs are all made of pure silica with a triangular arrangement of air holes of diameter, d, pitch, Λ, and a core formed by omitting the central air hole of the structure.

2. Theory

A good way to illustrate the differences in the spectral properties of the SMF and the PCF is through the V-parameter. The V-parameter for the SMF, V_{SMF}, has traditionally been applied to derive the higher-order mode cutoff [4] as well as the MFD [5]. Recently, we suggested a V-parameter for the PCF [6], V_{PCF}, and showed that this also held the property of uniquely determining both the higher-order mode cutoff [6] as well as the MFD [7]. The expressions for V_{SMF}, and V_{PCF}, are given by:

$$V_{SMF} = 2\pi \frac{a}{\lambda} \sqrt{n_{co}^2 - n_{cl}^2} \tag{1a}$$

$$V_{PCF} = 2\pi \frac{\Lambda}{\lambda} \sqrt{n_{FM}^2(\lambda) - n_{FSM}^2(\lambda)} \tag{1b}$$

In Eq. (1a), a is the core radius and n_{co} and n_{cl} are the refractive indices of the core and the cladding, respectively. In Eq. (1b), $n_{FM}(\lambda)$ and $n_{FSM}(\lambda)$ are the wavelength dependent effective indices of the fundamental mode (FM) and the fundamental space filling mode (FSM), respectively (see ref. [6] for a detailed discussion on V_{PCF}). In the expression for V_{SMF}, the refractive indices are taken to be constants and V_{SMF}, therefore, depends on the wavelength as $1/\lambda$. The spectral dependency of V_{PCF} is very different from that of V_{SMF}, since the effective indices are strongly wavelength dependent resulting in the fact that the index difference counteracts the effect of the $1/\lambda$ dependency and results in $V_{PCF} \to V_0$ for $\lambda \to 0$, where V_0 is a constant dependent on d/Λ [8]. It is, thus, the decreasing effective index difference with decreasing wavelength that limits the number of modes and also has the effect that bend loss is observed at short wavelengths for the PCF [9]. From a MFD point of view, the increasing index difference as function of the wavelength ensures a close to constant strength of the guiding resulting in a MFD that can be almost constant over a broad wavelength range [7]. This is in contrast to conventional fibers, where the constant index difference becomes insufficient, when the wavelength is increased, causing the mode to expand until guiding is lost and, thereby, limiting the bandwidth at longer wavelengths.

When attempting to compare two different types of fibers as in the case of the SMF and the PCF, ensuring identical MFD are not sufficient. As an example, a PCF with a MFD of 10 μm at an operating wavelength of 1μm can both be realized with the parameters $d/\Lambda = 0.19$,

#3660 - $15.00 US Received 13 January 2004; revised 26 January 2004; accepted 26 January 2004

Λ = 5 µm and with d/Λ = 0.45, Λ = 8µm. In the first case, V_{PCF} = 1.0, whereas the other example yields V_{PCF} = 3.1, and since a high V_{PCF} value is preferred from a robustness point of view [8], these two designs will have a very different bending loss properties. Basing a comparison on PCFs with relative small values of d/Λ, therefore, holds limited relevance. Thus, in order to ensure a fair comparison, both fibers should be designed and operated where they are most robust, i.e., close to cutoff, and it should, furthermore, be insured that the MFDs are identical.

3. Experimental

The experimental investigation is based on a commercially available conventional SMF and 3 different PCFs. The SMF has a Ge-doped core region, a numerical aperture of 0.13, a MFD of 3.5 µm +/-0.5 µm, a cladding diameter of 125 µm, and a long term minimum bend radius of 13 mm. The PCFs all have a cladding diameter of 125 µm, and the structural parameters are listed in table 1.

Table 1. Characteristics of the tested PCFs

ID	Λ [µm]	d/Λ
LMA-5	2.9	0.44
LMA-8	5.6	0.49
LMA-11	7.0	0.44

The spectral attenuation characteristics of the investigated fibers were measured using a white light source and the cutback technique. In Fig. 1, the attenuation spectra from 400 nm to 1700 nm for the conventional SMF and the LMA-5 PCF are shown. The attenuation spectra of LMA-8 and LMA-11 are very similar to that of the LMA-5 and, therefore, left out for the sake of simplicity.

For the conventional SMF (red curve) a sharp peak is observed at 430 nm originating from the higher-order mode cutoff. At a wavelength of around 820 nm the fiber no longer guides and a steep loss edge is observed. For the LMA-5 PCF (black curve), no cutoff is observed (the peaks at 1380 nm, 1245 nm, and 945 nm results from OH contamination [10]), and the fiber, thus, guides a single mode in the entire spectral range investigated. Although the attenuation level of the LMA-5 PCF is slightly higher than what can be realized, it is actually lower than or comparable to that of the conventional SMF for wavelengths lower than around 600 nm. This is due to the benefit of the pure-silica core, which does not suffer from attenuation bands from defect centers at short wavelengths to the same degree as Ge-doped silica. When comparing the curves shown in Fig. 1, a significantly larger single-mode bandwidth is apparently available for the PCF than for the conventional SMF. In order to check, if this large bandwidth comes at a price, the bend loss properties and the MFDs are compared.

#3660 - $15.00 US Received 13 January 2004; revised 26 January 2004; accepted 26 January 2004

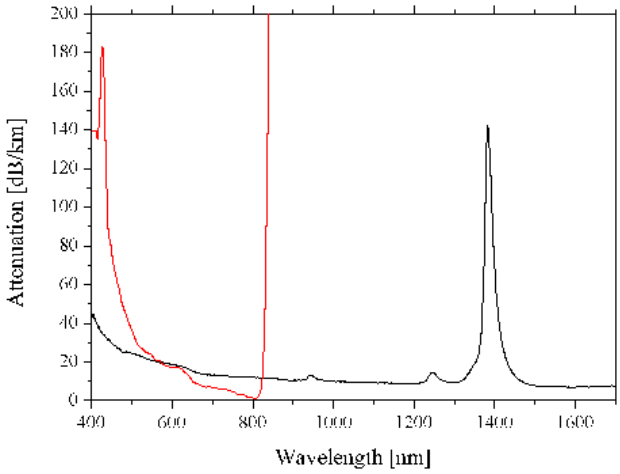

Fig. 1. The red and the black curve show the measured attenuation spectra of the conventional SMF and the LMA-5 PCF, respectively. The peak at 430 nm on the red curve indicates the higher order mode cutoff.

The bend loss properties of the investigated fibers were characterized by measuring the induced attenuation from 360° bends (single-turn bends) while varying bend radius, R. First, white light was coupled into the fiber and a reference spectrum was recorded with an optical spectrum analyzer, while ensuring $R > 80$ mm. The fiber was then given a single turn around a cylinder and a new transmission spectrum was recorded. This procedure was repeated for cylinders with R from 10 to 80 mm (10 mm increments) and the attenuation was taken relative to the initial reference spectrum. The shortest bend radius of 10 mm is below the specified long term minimum bend radius for the conventional SMF and, therefore, not a value, which should be considered for most practical situations. It is, however, useful in order to test how far from the operational limit a fiber with good properties at $R = 20$ mm is. For this investigation the spectral range from 400 nm to 1000 nm was chosen since the conventional SMF, based on Fig. 1, will not operate at longer wavelengths.

In Fig. 2, the measured attenuation spectra are shown in panels A to D. Panel A shows the measurements for the conventional SMF. The shifting peaks in the spectral region between 400 and 450 nm results from bending induced shifting of the cutoff wavelength of the higher-order mode. It is, furthermore, observed, how the single-mode operating bandwidth decreases from the long wavelength side. At the smallest tested bend radius of 10 mm, the bandwidth extends from approximately 430 nm to 700 nm.

Panel B shows the corresponding measurements for the LMA-5 PCF and in this case no influence of the bending is observed. The LMA-5 PCF is, therefore, more robust than it needs to be for RGB applications and this unutilized potential could, therefore, preferably be used for realizing a larger MFD in the case where improved power handling is an issue. When increasing the structural scale by switching to the LMA-8 PCF, the sensitivity towards bending in increased as shown in Panel C. For the smallest applied bending radius of 10 mm, light is completely lost at wavelengths just below 500 nm. However, increasing the bend radius to 20 mm again results in the entire bandwidth being available with only a small indication of attenuation levels around 1 dB at 400 nm.

#3660 - $15.00 US Received 13 January 2004; revised 26 January 2004; accepted 26 January 2004

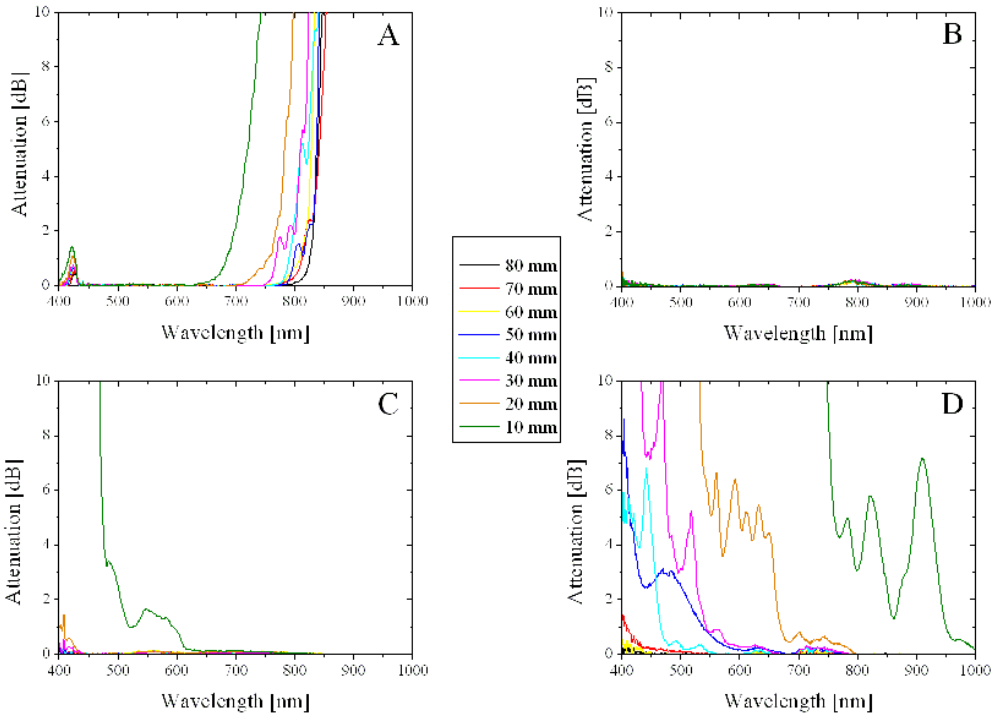

Fig. 2. Attenuation spectra from 400 nm – 1000 nm for single-turn bends with diameters as specified in the legend. Panels A, B, C, and D represent the conventional SMF, LMA-5, LMA-8, and LMA-11, respectively.

The measurements shown in panel C indicate that the structural parameters of the LMA-8 are in fact very close to being optimum in terms of having a fiber with the largest possible structure that is still robust towards any practical bend radius at any RGB wavelength. Bends of 10 mm are as mentioned not suited for long term operation. However, if the requirements for the robustness are less strict, further scaling of the structure is of course feasible. This point is illustrated in panel D, showing measurements for the LMA-11 PCF. In this case, the attenuation at 400 nm reaches 1 dB for R = 70 mm, and the fiber becomes dark for the shortest RBG wavelengths at R = 30 mm.

For investigation of the MFDs, we used a CCD camera to record an image of the fundamental mode at a number of wavelengths for each fiber. Light from light-emitting diodes (LEDs) at 470 nm, 525 nm, 570 nm, and 660 nm is coupled in and out of the fiber using microscope objectives. For each of the obtained images, a Gaussian function is fitted to the mode profile to yield a measure of the MFD. In order to calibrate the absolute scale of the profile, light is coupled into a short piece of PCF (~10 cm), which is kept as straight as possible. By defocusing the coupling at the input, it is possible to guide light in the cladding region over this relatively short distance and to record the spatial distribution with the CCD camera. Since light is guided by the high-index silica regions of the cladding, the image will be an image of the fiber structure with a pattern of dark regions resembling the air holes. By measuring the period along such a line of dark regions, the pitch given in pixels can be determined. From an optical- or an electron micrograph, the pitch can afterwards accurately be determined and the absolute MFD of the near fields determined.

#3660 - $15.00 US Received 13 January 2004; revised 26 January 2004; accepted 26 January 2004

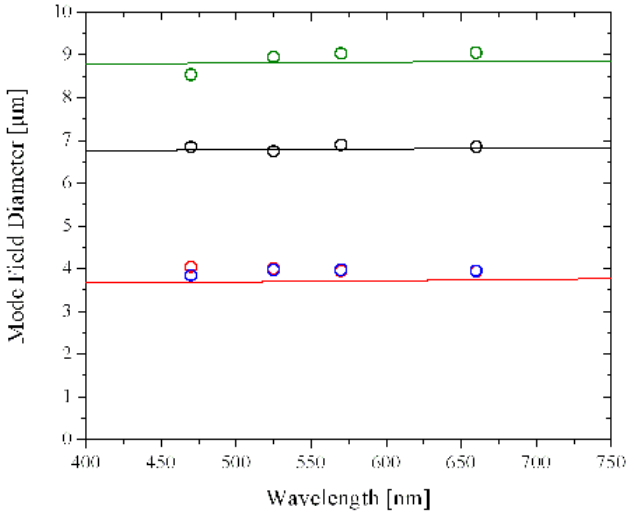

Fig. 3. MFD data for the investigated fibers. The green, black, and red solid curves show the theoretical MFD calculated from the V-parameter of the LMA-11, LMA-8, and LMA-5, respectively. The green, black, red, and blue circles indicate measured values of the MFD for the LMA-11, LMA-8, LMA-5, and the conventional SMF, respectively.

In Fig. 3, measured and calculated MFD data are shown. The green, black, and red solid lines represent calculated data for LMA-11, LMA-8, and LMA-5, respectively. The calculations are based on the relations given in ref. [8] and the structural parameters listed in Table 1. The open green, black, red, and blue circles indicate measured data for the LMA-11, LMA-8, LMA-5, and the conventional SMF, respectively. Good agreement between calculated and measured data is observed showing the strength of the relatively simple expressions given in [8]. It is actually possible to accurately extract the MFD as function of wavelength from an image of the fiber cross section, which is in contrast to the conventional fiber. The MFDs of the LMA-11 and LMA-8 are close to 9.0 and 6.9 µm, respectively, while the MFDs of the LMA-5 and the conventional SMF are both very close to 3.9 µm at the inspected wavelengths. The measurements of the MFDs and the fact that both fibers are operated close to their cutoff wavelength, where robustness is optimum, make it possible to conclude that a direct comparison of the bandwidth from Fig. 1 and panels A and B from Fig. 2 can be justified.

4. Conclusion

We have compared the optical bandwidth of a conventional SMF and 3 different PCFs intended for RGB applications. The MFDs of the LMA-5 PCF and the conventional SMF were identical at the inspected wavelengths. The PCF showed to be more robust towards bending at any of the investigated wavelengths from 400 nm to 1000 nm compared to the conventional SMF. The enhanced properties of the PCF are explained through the strong wavelength dependency of the effective index difference between the guided mode and the cladding modes and can be utilized for realizing a larger MFD with the benefit of improved power handling properties.

Acknowledgments

M.D. Nielsen acknowledges financial support from the Danish Academy of Technical Sciences.

#3660 - $15.00 US Received 13 January 2004; revised 26 January 2004; accepted 26 January 2004

Paper J

M.D. Nielsen, J.R. Folkenberg and N.A. Mortensen

"*Photonic Crystal Fiber with an effective area of 600 μm^2 and low bending loss*"

Electronics Letters, Vol. **39**, No. 25, pp. 1802-1803

(2003)

Singlemode photonic crystal fibre with effective area of 600 μm^2 and low bending loss

M.D. Nielsen, J.R. Folkenberg and N.A. Mortensen

A singlemode all-silica photonic crystal fibre with an effective area of 600 μm^2 and low bending loss is reported. The fibre is characterised in terms of attenuation, chromatic dispersion and modal properties.

Introduction: The photonic crystal fibre (PCF) has, since it was first proposed [1], attracted growing attention owing to its many unique properties. One of the first special characteristics to be reported for the PCF was its potential to be endlessly singlemode (ESM) [2], referring to the absence of higher-order modes regardless of the optical wavelength. For conventional fibres, the effective area is limited by the fact that an increasing core size requires a correspondingly decreasing index step between the core and the cladding in order to maintain singlemode operation. This imposes requirements on the control of the index profile, which is difficult to realise with index-raising doping of the glass. A PCF which is ESM can, in principle, be scaled to an arbitrary dimension and remain singlemode. However, since the numerical aperture (NA) decreases with increasing mode size, the scaling of the PCF is in general limited by macro-bending loss and micro-deformation loss due to the decreasing mode spacing between the guided mode and leaky cladding modes [3, 4]. In contrast to conventional fibres, the bend-loss edge for the PCF is located at lower wavelengths compared to the transmission window [2], because the mode spacing decreases with decreasing wavelength.

In solid core Bragg fibres, effective areas of more than 500 μm^2 at 1550 nm have been demonstrated, but with attenuation levels in the order of dB/m [5]. PCFs with large mode-area have also been demonstrated [6, 7], but only for structures which are intrinsically susceptible to loss caused by bending and other perturbations. In this Letter, we present a singlemode PCF with an effective area of 600 μm^2 and low bending loss.

Fibre design and properties: The considered PCF is an all silica fibre with a number of air holes, of diameter d, running along the length of the fibre, placed on a triangular lattice arrangement with a pitch Λ. The central air hole in the structure is omitted, creating a high-index defect allowing for guidance of light by total internal reflection. For the relative hole size, d/Λ, below a value of 0.41, the propagation loss of the higher-order mode (HOM) increases drastically and it is not considered to be guided [8]. For d/Λ larger than this value the propagation loss decreases and the structure now supports an HOM, although the actual propagation loss might be significantly larger than that of the fundamental mode, causing the fibre in practice to act as a singlemode fibre. Pushing d/Λ to larger values has the benefit of increasing the mode spacing and, in order to investigate these properties, a number of fibres with a fixed cladding diameter of 280 μm and $\Lambda = 23$ μm were fabricated, with d/Λ ranging from 0.45 to 0.53. All fibres were drawn from the same preform built using the stack and pull technique. The value of the cladding diameter was chosen to screen the waveguide from micro-deformations [4]. The air-hole structure had five periods around the core and the fibres were coated with a single-layer actylate coating with a diameter of 426 μm.

Characterisation: All fabricated fibres were characterised in terms of spectral attenuation from 1100 to 1700 nm using the cutback technique. When characterised on a spool with a radius of 8 cm, all fibres showed varying degrees of bending induced attenuation at 1550 nm. However, on a spool of 16 cm radius the bend-loss edge of most fibres had moved to wavelengths lower than 1550 nm, although fibres with $d/\Lambda < 0.48$ were still influenced by the tail of the bend-loss edge. The fibres with the largest d/Λ value of 0.53 showed indication of supporting a high-order mode, which was confirmed by inspecting the near field on a 50 cm sample. The fibre with d/Λ of 0.50 was single-mode in the inspected wavelength region and not influenced by the bend-loss edge. Fig. 1 shows the attenuation spectrum of this fibre, measured on a 150 m sample. The steep bend-loss edge is located at ~1200 nm with a loss tail extending to the position of the OH absorption peak at 1.38 μm. The attenuation is 5 dB/km at 1550 nm, which is in good agreement with the recorded OTDR trace shown in the inset in Fig. 1. The low backscatter intensity observed in the OTDR measurement results from the low NA of the fibre, which is estimated to be 0.04. The attenuation level at 1550 nm is mainly attributed to absorption caused by contamination introduced during the fabrication process, such as OH and other impurities on the surfaces on the capillary tubes used to construct the preform. The attenuation level is similar to that observed in fibres with significantly smaller Λ when using the same fabrication process, and may be drastically improved by applying surface polish of the capillaries and dehydration techniques.

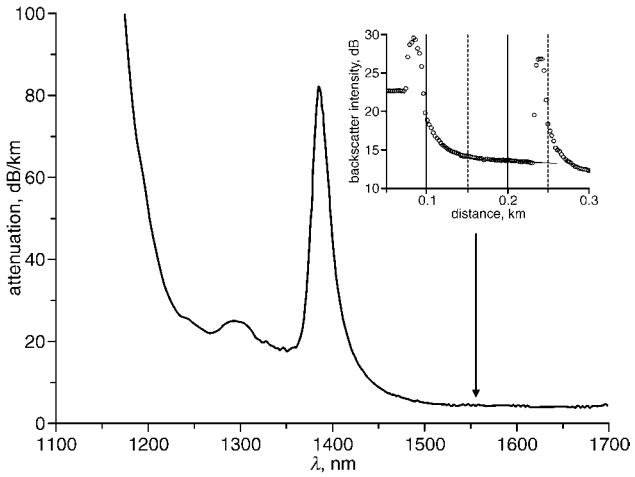

Fig. 1 *Measured spectral attenuation from 1100 to 1700 nm yielding a value of 5 dB/km at 1550 nm*
Inset: OTDR trace at 1550 nm

In Fig. 2, the measured chromatic dispersion from 1520 to 1640 nm (solid line) and the material dispersion of pure silica (dotted line) are shown, along with the waveguide dispersion (dashed line) obtained from a numerical simulation using the planewave expansion method. The waveguide dispersion is almost constant with a value of 1 ps/km nm and the chromatic dispersion is consequently dominated by the material dispersion with a value of 23.3 ps/km nm at 1550 nm.

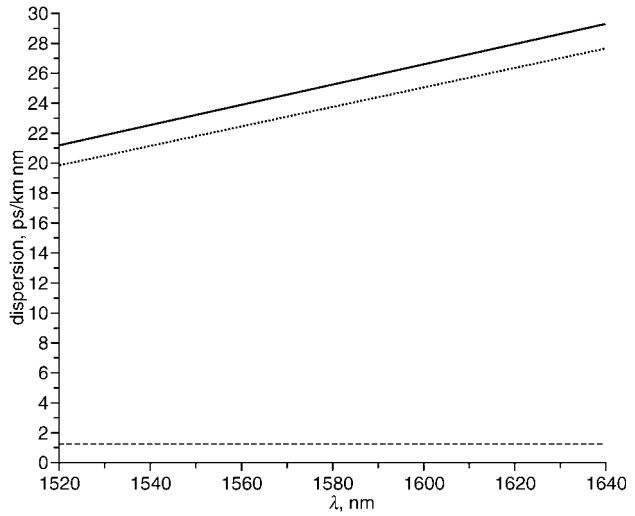

Fig. 2 *Measured chromatic dispersion (solid line), material dispersion of pure silica (dotted line) and calculated waveguide dispersion (dashed line) from 1520 to 1640 nm*

Based on the values of d/Λ and Λ, the effective area, A_{eff}, can be simulated yielding a value of 591 μm^2, which corresponds to an equivalent Gaussian $1/e^2$ modefield diameter (MFD) of 27.4 μm. To verify this experimentally, we studied the near field at 1550 nm, shown as a contour plot in the inset in Fig. 3, which also defines the two orthogonal directions x and y. In Fig. 3, the intensity profile of the near field along the x and y direction is shown (open circles and triangles, respectively). As seen from these profiles, the mode has a close to

Gaussian shape, which is indicated by the two fitted Gaussian functions (represented by the solid and dashed lines for the x and y directions, respectively). However, the near field is not rotational symmetric in the transverse plane but has a hexagonal shape leading to a difference in the $1/e^2$ MFD, which can be extracted from the fits along the two directions. For the x direction, the MFD of the fitted Gaussian is 27.9 μm and for the y direction it is 29.8 μm. The $1/e^2$ width obtained directly from the raw data yields 25.5 and 29.2 μm for the x and y directions, respectively, corresponding to an average value of 27.2 μm. All measures of the MFD can thus be given as $27.7 \pm 8\%$, which is in good agreement with the calculated value for A_{eff}. For $A_{eff} = 600\ \mu m^2$, the nonlinear coefficient, $\gamma = 2\pi n_2/\lambda A_{eff}$, yields a value of 0.16 W km^{-1}, where $n_2 = 2.4 \times 10^{-20}$ m^2/W is the nonlinear refractive index of pure silica.

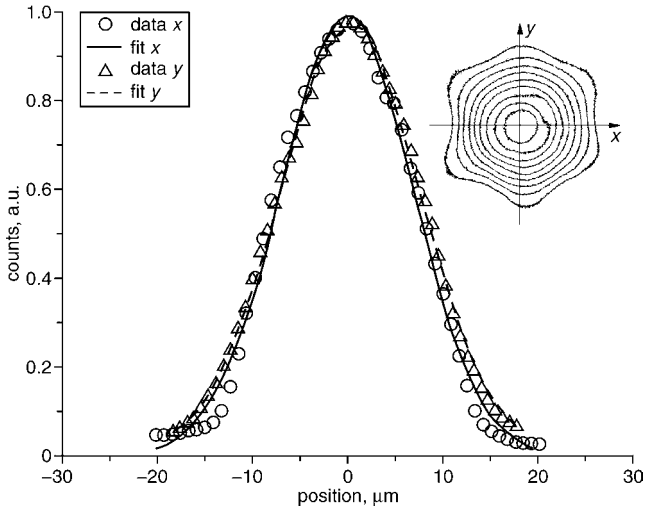

Fig. 3 *Intensity profiles along x and y directions (circles and triangles, respectively) and fitted Gaussian profiles (solid and dashed lines, respectively)*

Inset: Contour plot of measured near-field profile and definition of x and y directions

Conclusion: We have demonstrated a PCF with an effective area of 600 μm^2 at 1550 nm by optimising d/Λ to a value of 0.50 and thereby achieving both singlemode operation and low bending loss.

8 October 2003
Electronics Letters Online No: 20031155
DOI: 10.1049/el:20031155

M.D. Nielsen, J.R. Folkenberg and N.A. Mortensen (*Crystal Fibre A/S, Blokken 84, DK-3460 Birkerød, Denmark*)

E-mail: mdn@crystal-fibre.com

M.D. Nielsen: Also with COM, Technical University of Denmark, Building 345V, DK-2800 Kgs. Lyngby, Denmark

References

1 KNIGHT, J.C., *et al.*: 'All-silica single-mode optical fiber with photonic crystal cladding', *Opt. Lett.*, 1996, **21**, p. 1547
2 BIRKS, T.A., KNIGHT, J.C., and RUSSEL, P.ST.J.: 'Endlessly single-mode photonic crystal fiber', *Opt. Lett.*, 1997, **22**, p. 961
3 MORTENSEN, N.A., and FOLKENBERG, J.R.: 'Low-loss criterion and effective area considerations for photonic crystal fibers', *J. Opt. A, Pure Appl. Opt.*, 2003, **5**, p. 163
4 NIELSEN, M.D., MORTENSEN, N.A., and FOLKENBERG, J.R.: 'Reduced microdeformation attenuation in large-mode-area photonic crystal fibers for visible applications', *Opt. Lett.*, 2003, **28**, p. 1645
5 FÉVRIER, S., *et al.*: 'Very large effective area singlemode photonic bandgap fibre', *Electron. Lett.*, 2003, **39**, p. 1240
6 KNIGHT, J.C., *et al.*: 'Large mode area photonic crystal fibre', *Electron. Lett.*, 1998, **34**, p. 1347
7 BAGGETT, J.C., *et al.*: 'Comparative study of large-mode holey and conventional fibers', *Opt. Lett.*, 2001, **26**, p. 1045
8 KUHLMEY, B.T.: 'Modal cutoff in microstructured optical fibers', *Opt. Lett.*, 2002, **27**, p. 1684

Paper K

N.A. Mortensen, **M.D. Nielsen**, J.R. Folkenberg, A. Petersson, and H.R. Simonsen

"Improved large-mode area endlessly single-mode photonic crystal fibers"

Optics Letters, Vol. **28**, No. 6, pp. 393-395

(2003)

Improved large-mode-area endlessly single-mode photonic crystal fibers

N. A. Mortensen

Crystal Fibre A/S, Blokken 84, DK-3460 Birkerød, Denmark

M. D. Nielsen

Crystal Fibre A/S, Blokken 84, DK-3460 Birkerød, Denmark and
Research Center COM, Technical University of Denmark, DK-2800 Kongens Lyngby, Denmark

J. R. Folkenberg, A. Petersson, and H. R. Simonsen

Crystal Fibre A/S, Blokken 84, DK-3460 Birkerød, Denmark

Received October 28, 2002

We numerically study the possibilities for improved large-mode-area endlessly single-mode photonic crystal fibers for use in high-power delivery applications. By carefully choosing the optimal hole diameter, we find that a triangular core formed by three missing neighboring air holes considerably improves the mode area and loss properties compared with the case with a core formed by one missing air hole. In a realized fiber we demonstrate an enhancement of the mode area by ~30% without a corresponding increase in the attenuation.

OCIS codes: 060.2280, 060.2300, 060.2310, 060.2400, 060.2430.

Applications requiring high-power delivery call for single-mode large-mode-area (LMA) optical fibers. Although standard fiber technology has difficulties in meeting these requirements, the new class[1] of all-silica photonic crystal fibers (PCFs) has a large potential in this area because of their endlessly single-mode properties[2] combined with (in principle) unlimited large effective areas.[3] For recent reviews we refer to Refs. 4 and 5.

The cladding structure of these PCFs consists of a triangular array of air holes of diameter d and pitch Λ corresponding to an air-filling fraction $f = \pi/(2\sqrt{3})(d/\Lambda)^2$. The presence of the air holes results in a strongly wavelength-dependent effective index n_{eff} of the cladding, and in the short- and long-wavelength limits we have

$$\lim_{\lambda \ll \Lambda} n_{\mathrm{eff}} = n_{\mathrm{si}}, \qquad \lim_{\lambda \gg \Lambda} n_{\mathrm{eff}} = f n_{\mathrm{air}} + (1 - f) n_{\mathrm{si}} \equiv \bar{n}. \tag{1}$$

The numerical results in the intermediate regime can be reasonably fitted by, e.g.,

$$n_{\mathrm{eff}} \approx \bar{n} + (n_{\mathrm{si}} - \bar{n}) \cosh^{-2}(\alpha \lambda/\Lambda), \tag{2}$$

where α has order unity and is only weakly dependent on d/Λ; see Fig. 1. It is these unusual dispersion properties of the cladding that facilitate the design of LMA endlessly single-mode optical fibers.[2,3]

To confine the light to a core region of high index a defect in the triangular air-hole array is introduced. Normally one does this by leaving out one of the air holes. In the stack-and-pull approach[1] one of the capillaries is replaced with a silica rod (see the left-hand inset of Fig. 3, below). By choice the index of the defect can be raised by different doping, and the case with a depressed-index core was also studied recently.[6]

The single-rod PCF can in principle be kept endlessly single mode no matter how large the core diameter.[3] However, when the fiber structure is scaled up, the mode area is increased, at the cost of increased susceptibility to longitudinal modulations[7] such as scattering loss induced by, e.g., microbending[8] and

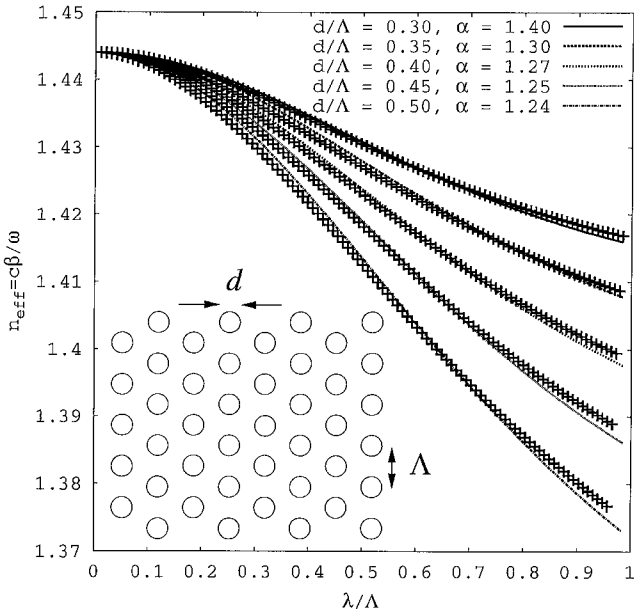

Fig. 1. Effective cladding index for the triangular cladding structure with different hole diameters. The crosses show numerical results from a fully vectorial calculation, and the solid curves are fits to Eq. (2) with α as the fitting parameter.

0146-9592/03/060393-03$15.00/0

macrobending.[9] The reason for this behavior is that to increase the mode area one must scale the pitch Λ to a large value, but this also implies that $\lambda/\Lambda \ll 1$, and in this limit the core index approaches the cladding index; see Eqs. (1). Figure 1 suggests that one may compensate for the decreasing index step by increasing the air-hole diameter, which can be done up to $d/\Lambda \sim 0.45$, the upper limit for endlessly single-mode operation. For a discussion of the particular limit see, e.g., Refs. 10–12. For LMA PCFs working in the UV and the visible regimes this sets an upper limit on the mode areas that can be realized with a reasonable loss, and many applications call for an improved LMA PCF design.

The inclusion of more than a single solid rod in the stacking has been used to form multiple-core[13] and highly birefringent[14] PCFs. In this Letter we demonstrate how inclusion of more neighboring solid rods can be used for improved LMA endlessly single-mode PCFs. Intuitively, this may not seem to be a promising direction, since a reduced value of d/Λ is needed to keep the PCF endlessly single mode. For the birefringent case with two neighboring rods[14] the limit is $d/\Lambda \sim 0.30$, and for a triangular core formed by three neighboring rods (see the right-hand inset of Fig. 3, below) we found $d/\Lambda \sim 0.25$ as the upper limit for endlessly single-mode operation. However, for a given desired mode area this decrease in d/Λ is compensated for by a corresponding smaller value of Λ. In fact, the edge-to-edge separation $\Lambda - d$ of the holes, rather than the pitch Λ itself, turns out to be the important length scale.

In introducing multiple rods an important question about possible birefringence arises. The structure with a single rod has a sixfold symmetry and though group theory clearly excludes any intrinsic birefringence[15] there has been quite some debate based on numerical studies; see, e.g., Ref. 16 and references therein. More generally, group theory predicts that for m-fold rotational symmetry and $m > 2$ a mode with a preferred direction is one of a pair; see Ref. 15 and references therein. PCFs with a triangular core formed by three neighboring rods have a threefold symmetry and thus no intrinsic birefringence. The nonbirefringent property is also confirmed numerically with a fully vectorial plane-wave method,[17] and any small numerical birefringence originates from a numerical grid with symmetry different from the dielectric structure being studied.

To compare the single- and three-rod PCFs, we study two quantities: (i) the mode-field diameter (MFD) and (ii) the coupling length ζ to the cladding. We relate the MFD to the effective area,[11]

$$A_{\mathrm{eff}} = \left[\int \mathrm{d}\mathbf{r}_\perp I(\mathbf{r}_\perp)\right]^2 \left[\int \mathrm{d}\mathbf{r}_\perp I^2(\mathbf{r}_\perp)\right]^{-1}, \qquad (3)$$

by $A_{\mathrm{eff}} = \pi(\mathrm{MFD}/2)^2$. Here, $I(\mathbf{r}_\perp)$ is the transverse intensity distribution of the fundamental mode. For a Gaussian mode of width w, Eq. (3) gives a MFD of $2w$, and the intensity distribution in the types of PCF studied in this Letter can be considered close to Gaussian,[11,18] as we also confirm experimentally.

The coupling length (beat length)

$$\zeta = 2\pi/(\beta - \beta_{\mathrm{cl}}) \qquad (4)$$

between the fundamental mode and the cladding (radiation field) can be used in formulating a low-loss criterion.[19] The additional competing length scales consist of the wavelength and the length scale L_n (or a set $\{L_n\}$ of length scales) for nonuniformity along the fiber and loss will be significant when

$$\lambda \lesssim L_n \lesssim \zeta\,, \qquad (5)$$

and otherwise loss can be expected to be small. Thus, the shorter a coupling length, the lower the susceptibility to longitudinal modulations. We emphasize that this criterion does not quantify loss, but it gives a correct parametric dependence of loss for various loss mechanisms. For PCFs the relevance of this criterion was recently confirmed experimentally in the case of nonuniformities induced by macrobending[7] and microbending[8] and also in a study of PCFs with structural long-period gratings.[20]

In Fig. 2 we compare the single- and three-rod PCFs with $d/\Lambda = 0.45$ and $d/\Lambda = 0.25$, respectively. All numerical results are based on a fully vectorial solution of the Maxwell equations in a plane-wave basis,[17] and for silica we used $n_{\mathrm{si}} = 1.444$ for simplicity. Figure 2(a)

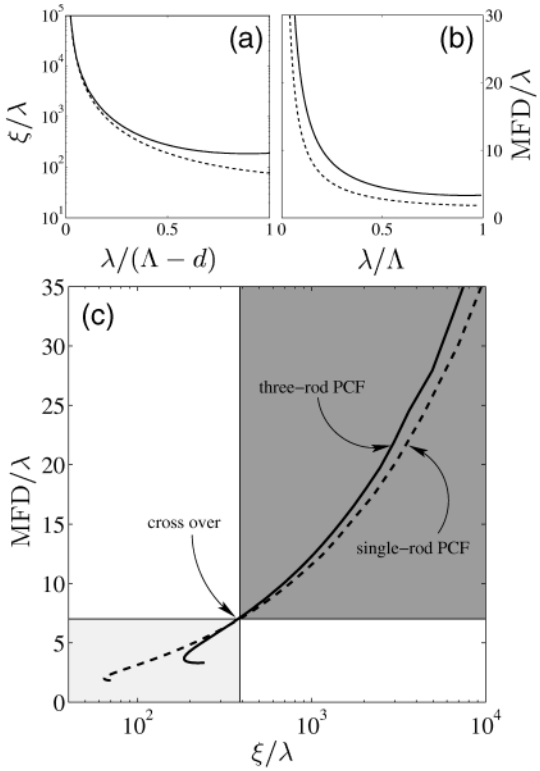

Fig. 2. Comparison of the single-rod (dashed curves) and three-rod (solid curves) PCFs with $d/\Lambda = 0.45$ and $d/\Lambda = 0.25$, respectively. (a) Coupling length versus wavelength, (b) MFD as a function of wavelength. (c) Results of (a) and (b) combined in a plot of MFD versus coupling length.

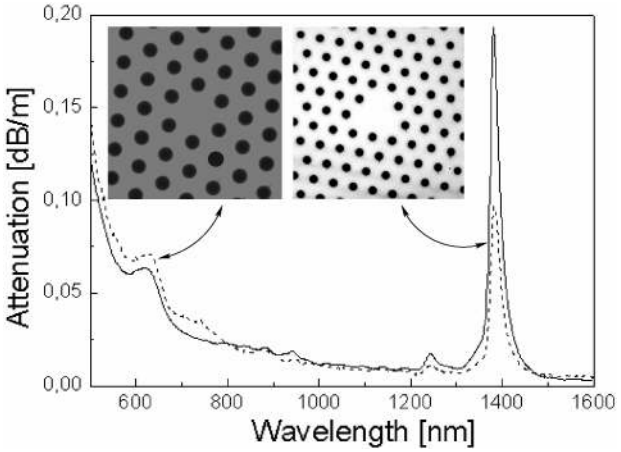

Fig. 3. Attenuation for a single-rod PCF (left-hand inset) and three-rod PCF (right-hand inset) fabricated under comparable conditions and both measured with a bend radius of 16 cm. The single-rod PCF has $\Lambda \simeq 10\ \mu$m, $d/\Lambda \simeq 0.45$, and a MFD of $\sim 10.5\ \mu$m, whereas the three-rod PCF has $\Lambda \simeq 6\ \mu$m, $d/\Lambda \simeq 0.25$, and a MFD of $\sim 12\ \mu$m. Although the mode area of the three-rod PCF is enhanced by $\sim 30\%$ compared with the single-rod PCF the two types of PCF have very similar attenuation.

shows the coupling length versus wavelength. The normalization by the edge-to-edge separation $\Lambda - d$ of the air holes makes the two curves coincide at short wavelengths ($\lambda \ll \Lambda - d$), which clearly demonstrates that $\Lambda - d$ is the length scale of the fiber structure, which determines the susceptibility of the PCF to longitudinal modulations. Figure 2(b) shows the MFD as a function of wavelength, and as can be seen from the figure, the three-rod PCF provides a larger MFD than the single-rod PCF for fixed λ/Λ. Figure 2(c) combines the results of Figs. 2(a) and 2(b) in a plot of MFD versus coupling length. For a MFD of $\sim 7\lambda$ there is a clear cross over, and for a MFD $\gg \lambda$ the three-rod PCF is thus seen to be less susceptible to longitudinal modulations than the single-rod PCF.

Figure 3 shows experimental results for the attenuation of both a single- and a three-rod PCF with hole diameters $d/\Lambda \simeq 0.45$ and $d/\Lambda \simeq 0.25$, respectively, close to the endlessly single-mode limits. The pitches are $\Lambda \simeq 10\ \mu$m and $\Lambda \simeq 6\ \mu$m, respectively, so the core sizes are approximately the same. The two PCFs were fabricated with the aid of the stack-and-pull method under comparable conditions and both PCFs were found to be endlessly single mode in a wavelength range of at least 400 to 1600 nm. As can be seen from the figure, the two PCFs have similar spectral attenuation, even though the mode area of the three-rod PCF is enhanced by $\sim 30\%$ compared with the single-rod PCF. This demonstrates the improvement by the three-rod PCF.

In conclusion, we have found that a triangular core formed by three missing neighboring air holes considerably improves the mode area and (or) loss properties compared with the case in which a core is formed by one missing air hole. This new, improved large-mode area endlessly single-mode PCF is important for high-power delivery applications, and in a realized fiber we have been able to demonstrate an enhancement of the mode area by $\sim 30\%$ without a corresponding change in the loss level.

We thank A. Bjarklev (Research Center COM, Technical University of Denmark) and J. Broeng (Crystal Fibre A/S) for useful discussions. M. D. Nielsen is financially supported by the Danish Academy of Technical Sciences. N. A. Mortensen's e-mail address is nam@crystal-fibre.com.

References

1. J. C. Knight, T. A. Birks, P. St. J. Russell, and D. M. Atkin, Opt. Lett. **21,** 1547 (1996).
2. T. A. Birks, J. C. Knight, and P. St. J. Russell, Opt. Lett. **22,** 961 (1997).
3. J. C. Knight, T. A. Birks, R. F. Cregan, P. St. J. Russell, and J.-P. De Sandro, Electron. Lett. **34,** 1347 (1998).
4. J. C. Knight and P. St. J. Russell, Science **296,** 276 (2002).
5. T. A. Birks, J. C. Knight, B. J. Mangan, and P. St. J. Russell, IEICE Trans. Electron. **E84-C,** 585 (2001).
6. B. J. Mangan, J. Arriaga, T. A. Birks, J. C. Knight, and P. St. J. Russell, Opt. Lett. **26,** 1469 (2001).
7. N. A. Mortensen and J. R. Folkenberg are preparing a manuscript called "Low-loss criterion and effective area considerations for photonic crystal fibers."
8. M. D. Nielsen, G. Vienne, J. R. Folkenberg, and A. Bjarklev, Opt. Lett. **28,** 236 (2003).
9. T. Sørensen, J. Broeng, A. Bjarklev, E. Knudsen, and S. E. B. Libori, Electron. Lett. **37,** 287 (2001).
10. J. Broeng, D. Mogilevstev, S. E. Barkou, and A. Bjarklev, Opt. Fiber Technol. **5,** 305 (1999).
11. N. A. Mortensen, Opt. Express **10,** 341 (2002), http://www.opticsexpress.org.
12. B. T. Kuhlmey, R. C. McPhedran, and C. M. de Sterke, Opt. Lett. **27,** 1684 (2002).
13. B. J. Mangan, J. C. Knight, T. A. Birks, and P. St. J. Russell, Electron. Lett. **36,** 1358 (2000).
14. T. P. Hansen, J. Broeng, S. E. B. Libori, E. Knudsen, A. Bjarklev, J. R. Jensen, and H. Simonsen, IEEE Photon. Technol. Lett. **13,** 588 (2001).
15. T. P. White, R. C. McPhedran, C. M. de Sterke, L. C. Botton, and M. J. Steel, Opt. Lett. **26,** 1660 (2001).
16. M. Koshiba and K. Saitoh, IEEE Photon. Technol. Lett. **13,** 1313 (2001).
17. S. G. Johnson and J. D. Joannopoulos, Opt. Express **8,** 173 (2001), http://www.opticsexpress.org.
18. N. A. Mortensen and J. R. Folkenberg, Opt. Express **10,** 475 (2002), http://www.opticsexpress.org.
19. J. D. Love, IEE Proc. J **136,** 225 (1989).
20. G. Kakarantzas, T. A. Birks, and P. St. J. Russell, Opt. Lett. **27,** 1013 (2002).

Paper L

N.A. Mortensen, **M.D. Nielsen**, J.R. Folkenberg, C. Jacobsen, and H.R. Simonsen

"*Photonic Crystal Fiber with a Hybrid honeycomb cladding*"

Optics Express, Vol. **12**, No. 3, pp. 468-472

(2004)

Photonic crystal fiber with a hybrid honeycomb cladding

Niels Asger Mortensen
Crystal Fibre A/S, Blokken 84, DK-3460 Birkerød, Denmark
asger@mailaps.org

Martin Dybendal Nielsen
Crystal Fibre A/S, Blokken 84, DK-3460 Birkerød, Denmark
COM, Technical University of Denmark, DK-2800 Kongens Lyngby, Denmark

Jacob Riis Folkenberg, Christian Jakobsen, and Harald R. Simonsen
Crystal Fibre A/S, Blokken 84, DK-3460 Birkerød, Denmark

http://www.crystal-fibre.com

Abstract: We consider an air-silica honeycomb lattice and demonstrate a new approach to the formation of a core defect. Typically, a high or low-index core is formed by adding a high-index region or an additional air-hole (or other low-index material) to the lattice, but here we discuss how a core defect can be formed by manipulating the cladding region rather than the core region itself. Germanium-doping of the honeycomb lattice has recently been suggested for the formation of a photonic band-gap guiding silica-core and here we experimentally demonstrate how an index-guiding silica-core can be formed by fluorine-doping of the honeycomb lattice.

OCIS codes: (060.2280) Fiber design and fabrication; (060.2400) Fiber properties; (060.2430) Fibers, single-mode; (999.999) Photonic crystal fiber

References and links

1. J. C. Knight, "Photonic crystal fibres," Nature **424**, 847–851 (2003).
2. J. C. Knight, T. A. Birks, P. S. J. Russell, and D. M. Atkin, "All-silica single-mode optical fiber with photonic crystal cladding," Opt. Lett. **21**, 1547–1549 (1996).
3. J. C. Knight, J. Broeng, T. A. Birks, and P. S. J. Russell, "Photonic Band Gap Guidance in Optical Fibers," Science **282**, 1476–1478 (1998).
4. J. Lægsgaard and A. Bjarklev, "Doped photonic bandgap fibers for short-wavelength nonlinear devices," Opt. Lett. **28**, 783–785 (2003).
5. B. J. Mangan, J. Arriaga, T. A. Birks, J. C. Knight, and P. S. J. Russell, "Fundamental-mode cutoff in a photonic crystal fiber with a depressed-index core," Opt. Lett. **26**, 1469–1471 (2001).
6. J. C. Knight, T. A. Birks, R. F. Cregan, P. S. J. Russell, and J.-P. de Sandro, "Large mode area photonic crystal fibre," Electron. Lett. **34**, 1347–1348 (1998).
7. N. A. Mortensen, M. D. Nielsen, J. R. Folkenberg, A. Petersson, and H. R. Simonsen, "Improved large-mode area endlessly single-mode photonic crystal fibers," Opt. Lett. pp. 393–395 (2003).
8. M. D. Nielsen, J. R. Folkenberg, and N. A. Mortensen, "Single-mode photonic crystal fiber with an effective area of 600 μm^2 and low bending loss," Electron. Lett. **39**, 1802–1803 (2003).
9. M. J. Steel, T. P. White, C. M. de Sterke, R. C. McPhedran, and L. C. Botton, "Symmetry and degeneracy in microstructured optical fibers," Opt. Lett. **26**, 488–490 (2001).
10. M. D. Nielsen, J. R. Folkenberg, and N. A. Mortensen, "Reduced microdeformation attenuation in large-mode-area photonic crystal fibers for visible applications," Opt. Lett. **28**, 1645–1647 (2003).

#3655 - $15.00 US
Received 13 January 2004; revised 30 January 2004; accepted 30 January 2004

11. M. D. Nielsen, G. Vienne, J. R. Folkenberg, and A. Bjarklev, "Investigation of micro deformation induced attenuation spectra in a photonic crystal fiber," Opt. Lett. **28**, 236–238 (2003).
12. K. Saitoh and M. Koshiba, "Full-vectorial imaginary-distance beam propagation method based on finite element scheme: Application to photonic crystal fibers," IEEE J. Quantum Electron. **38**, 927–933 (2002).
13. T. A. Birks, J. C. Knight, and P. S. J. Russell, "Endlessly single mode photonic crystal fibre," Opt. Lett. **22**, 961–963 (1997).
14. S. G. Johnson, M. Ibanescu, M. A. Skorobogatiy, O. Weisberg, J. D. Joannopoulos, and Y. Fink, "Perturbation theory for Maxwell's equations with shifting material boundaries," Phys. Rev. E **65**, 066,611 (2002).
15. B. T. Kuhlmey, R. C. McPhedran, and C. M. de Sterke, "Modal cutoff in microstructured optical fibers," Opt. Lett. **27**, 1684–1686 (2002).
16. N. A. Mortensen, J. R. Folkenberg, M. D. Nielsen, and K. P. Hansen, "Modal cut-off and the V–parameter in photonic crystal fibers," Opt. Lett. **28**, 1879–1881 (2003).
17. J. R. Folkenberg, N. A. Mortensen, K. P. Hansen, T. P. Hansen, H. R. Simonsen, and C. Jakobsen, "Experimental investigation of cut-off phenomena in non-linear photonic crystal fibers," Opt. Lett. **28**, 1882–1884 (2003).
18. N. A. Mortensen, M. D. Nielsen, J. R. Folkenberg, K. P. Hansen, and J. Lægsgaard, "Small-core photonic crystal fibers with weakly disordered air-hole claddings," J. Opt. A: Pure Appl. Opt. **6**, 221–223 (2004).
19. T. T. Larsen, A. Bjarklev, D. S. Hermann, and J. Broeng, "Optical devices based on liquid crystal photonic bandgap fibres," Opt. Express **11**, 2589 – 2596 (2003). http://www.opticsexpress.org/abstract.cfm?URI=OPEX-11-20-2589.

1. Introduction

In their basic form photonic crystal fibers (PCF) typically consist of fused silica with an arrangement of air-holes running along the full length of the fiber (for a recent review we refer the reader to Ref. [1] and references therein). Traditionally, triangular [2] or honeycomb [3] cladding arrangements of the air-holes have been considered with the core defect formed by removing or adding an additional air-hole in the lattice, respectively. This is of course the most obvious way to form a defect in a regular lattice. However, for the honeycomb lattice (see Fig. 1) there is at least one alternative approach which involves additional use of index-altering dopants. Recently, Lægsgaard and Bjarklev [4] suggested how a low-index band-gap guiding core could be formed in a germanium doped honeycomb lattice by absence of doping

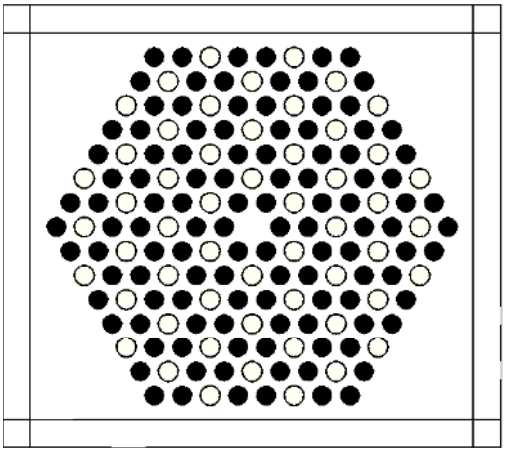

Fig. 1. Cross-section of the PCF with air-holes indicated by filled circles and the fluorine doped regions indicated by open circles. The perfectly-matched layers employed in finite-element simulations are also indicated.

#3655 - $15.00 US Received 13 January 2004; revised 30 January 2004; accepted 30 January 2004

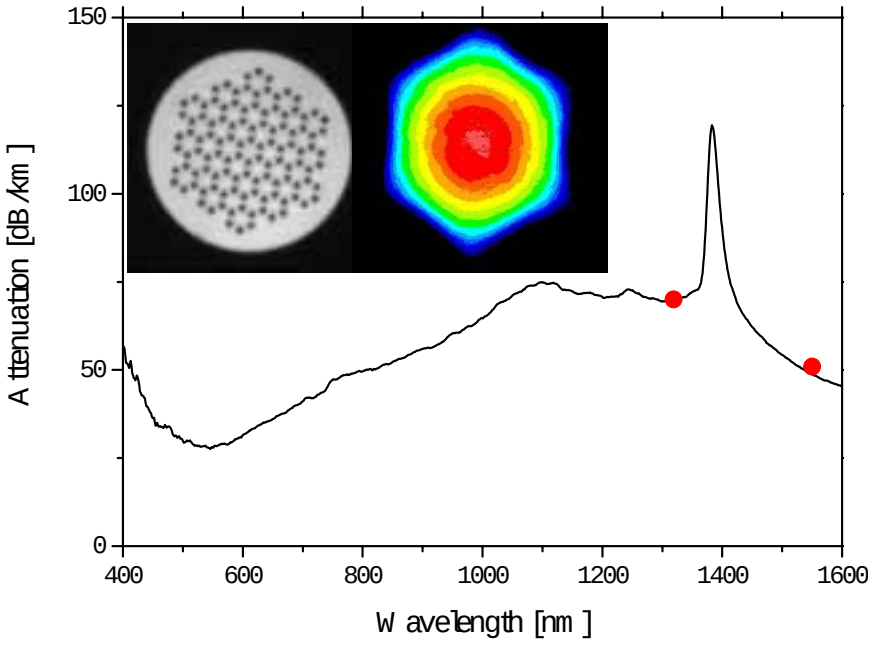

Fig. 2. Spectral loss measured by a standard white-light cut-back technique. OTDR measurements at $\lambda = 1319$ nm and 1550 nm are also indicated by red dots. The measurements are performed with 200 m of fiber on a spool with a radius of 8 cm. The left insets show an optical micrograph of the fiber end-facet with the dark circular regions showing the air holes and the light regions showing the fluorine-doping in the silica background. The right inset shows a near-field image of the fundamental mode at $\lambda = 635$ nm.

in the core region. Here, we suggest doping by fluorine which results in an index-guiding core. Fluorine-doped PCFs have previously been considered by Mangan *et al.* [5] who fabricated a triangular air-hole cladding PCF with a fluorine-doped silica core region. At sufficiently short wavelengths the core index is lower than the effective index of the cladding and the PCF is anti-guiding, but as the wavelength is increased the effective index of the cladding decreases and eventually becomes lower than the core index so that light is guided in the core region. In the present work we use fluorine doping to form a novel large-mode area PCF and the proposed fiber structure may be an alternative to existing large-mode area designs employing a triangular air-hole arrangement in the cladding [6, 7, 8].

2. Fiber design and fabrication

We consider the structure in Fig. 1 where fluorine doped regions (of diameter d_f) are incorporated in a honeycomb lattice of air-holes (of diameter d and nearest-neighbor spacing Λ). The core region is formed by the absence of doping in the central region of the structure. At sufficiently short wavelengths the cladding states will avoid the fluorine-doped regions and the effective cladding index will in some sense resemble that for a triangular arrangement of holes whereas at longer wavelengths the field averages over the fluorine-doped and pure silica regions so that the effective index resembles that of a honeycomb lattice (with a slightly down-shifted background index). The defect region has six-fold rotational symmetry and thus supports a doubly degenerate fundamental mode [9].

#3655 - $15.00 US
Received 13 January 2004; revised 30 January 2004; accepted 30 January 2004

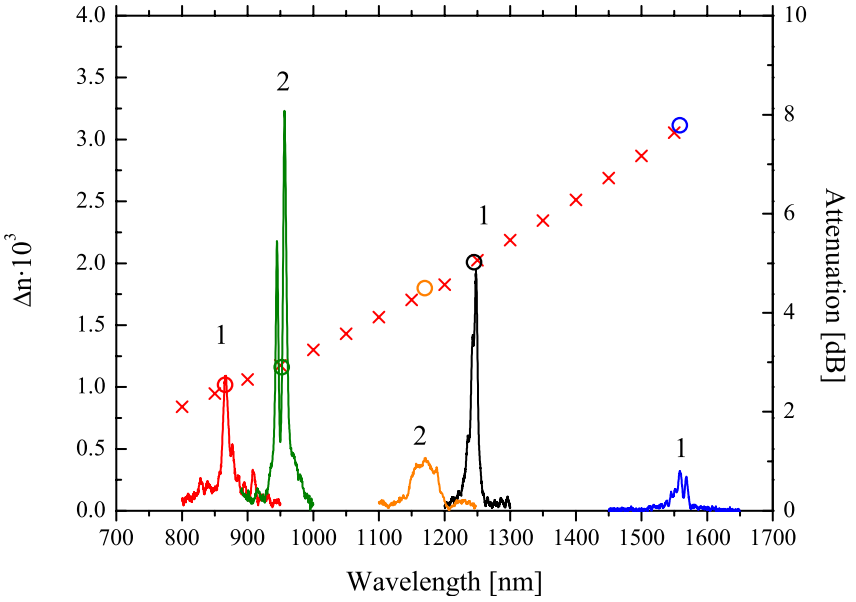

Fig. 3. Mode-spacing (left axis) derived from periodic micro-deformation spectra (right axis). Red crosses indicate values of Δn from numerical simulations while the solid curves are the measured attenuation peaks induced by periodic micro-deformations. The number above each peak indicate if the peak is of 1st or 2nd order and the open circles represent the corresponding mode spacing calculated from the measurements.

We have fabricated the proposed fiber by the stack-and-pull method [2] with hexagonal stacking of fluorine-doped rods (step-index like doping profile) and fused silica tubes and rods. The inset in Fig. 2 shows an optical micrograph of a typical fiber cross section. The fiber has an outer diameter of 175 ∝m in order to reduce micro-bending deformations at short wavelengths [10] and it is coated with a standard single layer acrylate coating. The fluorine-doped regions are of diameter $d_f/\Lambda \sim 0.7$ with an index n_f suppressed by $\delta n \sim 5 \times 10^{-3}$ relative to the index n_s of silica. The pitch is $\Lambda \simeq 10.1$ ∝m and the relative air-hole diameter is $d/\Lambda = 0.64$.

3. Fiber characterization

To facilitate coupling of light to the core region a SMF28 was spliced to 200 m of the PCF. The spectral attenuation was measured by the cut-back technique using a white-light source and an optical spectrum analyzer. Fig. 2 shows the spectral attenuation of the PCF. Data from OTDR measurements at $\lambda = 1319$ nm and 1550 nm are also included and good agreement with the cut-back data is observed. Cut-back transmission experiments on a short length of PCF have revealed no signatures of high-order modes.

The fiber has a low loss regime at short wavelengths and a regime with high loss above 1000 nm extending to the O-H absorption peak. In order to further analyze the modal properties we have studied the mode-spacing which can be derived from micro-deformation measurements. For a detailed description of the method and the interpretation of experimental data we refer the reader to Ref. [11] and references therein. Fig. 3 shows loss spectra (right axis) for various periodic micro-deformations and the derived mode-spacings, Δn are also included (left axis).

#3655 - $15.00 US
Received 13 January 2004; revised 30 January 2004; accepted 30 January 2004

The figure also includes numerical data calculated with the finite-element method incorporating perfectly matched layers [12], see Fig. 1. In agreement with the experimental observations, our simulations also suggest that the PCF is broad-band single mode [13] in the sense that high-order modes have a negligible spacing ($\ll 10^{-4}$) to cladding modes.

In order to understand the spacing between guided modes and cladding modes we apply first-order perturbation theory to the guided modes. Treating the absence of fluorine-doping in the core as a perturbation, $\delta\varepsilon = n_s^2 - n_f^2 \simeq 2n_s\delta n$, we may estimate the shift Δn in mode-index with respect to the cladding modes. From standard perturbation theory (see *e.g.* Ref. [14]) we get

$$\Delta n = \frac{c}{2v_g}\frac{\langle E|\delta\varepsilon|E\rangle}{\langle E|\varepsilon|E\rangle} \simeq \frac{cn_s}{v_g}\frac{\langle E|\delta n|E\rangle}{\langle E|\varepsilon|E\rangle} \tag{1}$$

where c is the velocity of light, E is the unperturbed electrical field, and v_g is the group velocity. For a high-order mode the field-intensity is strongly suppressed at the center of the core region [15, 16, 17, 18] and since d_f/Λ is not too large the mode has a very small overlap with the region where fluorine is absent. This results in a negligible increase in effective index Δn with respect to the cladding modes. In other words, localization in the core is no big energetic advantage for the high-order modes. For the fundamental mode the situation is opposite since it has a large field-intensity at the center of the core and indeed we find a mode-spacing Δn comparable to δn.

The mode-spacing picture in Fig. 3 suggests that the overall loss has little relation to bending-induced scattering loss (we have also verified this by changing the bending radius R) and since confinement loss can be excluded (we have verified this numerically) it is likely that the overall high background originates from various contamination added during the stack-and-pull fabrication process. We believe that the background loss level can be lowered similarly to the recent achievements in triangular cladding large-mode area PCFs [8].

4. Conclusion

We have studied a new approach to the formation of a core defect in the honeycomb structure by fluorine-doped regions added to the cladding. At sufficiently short wavelengths the cladding states will avoid the fluorine-doped regions and the effective cladding index will in some sense resemble that for a triangular arrangement and light will be confined to the core region where fluorine-doping is absent.

We believe that hybrid cladding designs could be an interesting direction which allows a higher degree of modal/dispersion engineering and the particular structure studied in this paper could also be interesting for photonic band-gap fiber devices employing liquid crystals [19].

Acknowledgments

N. A. Mortensen thanks J. Lægsgaard (COM, Technical University of Denmark) for stimulating discussions and L. Gregersen (Comsol A/S) for technical support. M. D. Nielsen acknowledges financial support by the Danish Academy of Technical Sciences.

#3655 - $15.00 US Received 13 January 2004; revised 30 January 2004; accepted 30 January 2004

Paper M

J.R. Folkenberg, **M.D. Nielsen**, N.A. Mortensen, C. Jacobsen, and H.R. Simonsen

"*Polarization Maintaining Large-mode area Photonic Crystal Fiber*"

Optics Express, Vol. **12**, No. 5, pp. 956-960

(2004)

Polarization maintaining large mode area photonic crystal fiber

J.R. Folkenberg[1], M.D. Nielsen[1,2], N.A. Mortensen[1], C. Jakobsen[1], and H.R. Simonsen[1]

[1]Crystal Fibre A/S, Blokken 84, DK-3460 Birkerød, Denmark
[2]COM, Technical university of Denmark, DK-2800 Kongens Lyngby, Denmark
jrf@crystal-fibre.com

Abstract: We report on a polarization maintaining large mode area photonic crystal fiber. Unlike, previous work on polarization maintaining photonic crystal fibers, birefringence is introduced using stress applying parts. This has allowed us to realize fibers, which are both single mode at any wavelength and have a practically constant birefringence for any wavelength. The fibers presented in this work have mode field diameters from about 4 to 6.5 micron, and exhibit a typical birefringence of $1.5 \cdot 10^{-4}$.

OCIS codes: (060.2270) Fiber characterization; (060.2280) Fiber Design and Fabrication; (060.2420) Fibers, polarization maintaining; (999.999) Photonic crystal fibers.

Reference and Links

1. T.A. Birks, J.C. Knight, and P.S.J. Russell, "Endlessly single-mode photonic crystal fiber," Opt. Lett. **22**, 961-963 (1997).
2. J.C. Knight, "Photonic crystal fibres," Nature **424**, 847-851 (2003).
3. A. Ortigosa-Blanch, J.C. Knight, W.J. Wadsworth, J. Arriaga, B.J. Mangan, T.A. Birks, and P.S.J. Russell, "Highly birefringent photonic crystal fibers," Opt. Lett. **25**, 1325-1327 (2000).
4. T.P. Hansen, J. Broeng, S.E.B. Libori, E. Knudsen, A. Bjarklev, J.R. Jensen, and H. Simonsen, "Highly birefringent index-guiding photonic crystal fibers", IEEE. Phot. Technol. Lett. **13**, 588-590 (2001).
5. M.D. Nielsen, J.R. Folkenberg, N.A. Mortensen, and A. Bjarklev, "Bandwidth comparison of photonic crystal fibers and conventional single-mode fibers," Opt. Express **12**, 430-435 (2004), http://www.opticsexpress.org/abstract.cfm?URI=OPEX-12-3-430
6. K. Suzuki, H. Kubota, S. Kawanishi, M. Tanaka, and M. Fujita, "Optical properties of a low-loss polarization-maintaining photonic crystal fiber," Opt. Express **9**, 676-680 (2001), http://www.opticsexpress.org/abstract.cfm?URI=OPEX-9-13-676
7. J. Noda, K. Okamoto, and Y. Sasaki, "Polarization-Maintaining Fibers and Their Applications," J. Lightwave Technol. **LT-4**, 1071-1088 (1986).
8. T.P. White, R.C. McPhedran, C.M. de Sterke, L.C. Botten, and M.J. Steel, "Confinement losses in microstructured optical fibers," Opt. Lett. **26**, 1660-1662 (2001).
9. C.D. Poole and D.L. Favin, "Polarization-Mode Dispersion Measurements Based on Transmission Spectra Through a Polarizer," J. Lightwave Technol. **12**, 917-929 (1994).
10. M.J. Steel, T.P. White, C.M. de Sterke, R.C. McPhedran, and L.C. Botton, "Symmetry and degeneracy in microstructured optical fibers," Opt. Lett. **26**, 488-490 (2001).
11. L.N.G. Filon, "On the variation with the wave-length of the double refraction in strained glass," Proceedings of the Cambridge Philosophical Society **XI**, 478-492 (1902).
12. L.N.G. Filon, "On the variation with the wave-length of the double refraction in strained glass," Proceedings of the Cambridge Philosophical Society **XII**, 313-337 (1904).
13. Z. Zhu and T.G. Brown, "Stress-induced birefringence in microstructured optical fibers," Opt. Lett. **28**, 2306-2308 (2003).
14. N.A. Mortensen, M.D. Nielsen, J.R. Folkenberg, A. Petersson, and H.R. Simonsen, "Improved large-mode area endlessly single-mode photonic crystal fibers," Opt. Lett. **28**, 393-395 (2003).

1. Introduction

Since the invention of the so-called endlessly single-mode fiber [1], photonic crystal fibers (PCFs) have attracted much attention, because of the many novel fiber properties that may be realized. For a recent review see [2]. In particular, the ability to make large-mode area fibers

#3854 - $15.00 US Received 20 February 2004; revised 1 March 2004; accepted 2 March 2004

(LMA-fibers) which are single-mode at any wavelength and the large birefringence that may be achieved [3,4] is very interesting for fiber devices such as fiber lasers and fiber based gyroscopes.

LMA-fibers have been studied quite thoroughly [5], and it has been shown that the practical bandwidth of single-mode operation is limited at short wavelengths by micro- and macro bending losses, and at long wavelength by leakage losses. Different approaches to polarization maintaining fibers have also been investigated [3,4,6], all of which are based on form birefringence. Generally, the form birefringence is largest for wavelengths, λ, close to the pitch, Λ, of the cladding hole structure [4], but for larger values of Λ/λ the birefringence decreases rapidly such that LMA-fibers with a birefringence on the order of 10^{-4} cannot be realized using form birefringence.

It is well known from solid silica fibers, that birefringence may be introduced using stress-applying parts (SAP), for an overview of conventional polarization maintaining (PM) fibers see [7]. That is, a part of the fiber consists of a material with a different thermal expansion coefficient than that of silica which gives rise to a stress field in the fiber when it is cooled below the softening temperature of silica during fabrication. In this way the fiber is given a built-in stress field and, because of the elasto-optic effect, the glass becomes birefringent.

In the present work we report on the first combination of PCF LMA-fibers and SAPs, to make polarization maintaining large-mode area fibers (PM-LMA).

2. Description of fibers

In Fig. 1, a microscope image of the realized PM-LMA structure is shown. It consists of an undoped silica core region surrounded by four periods of air holes in a triangular lattice, which forms the cladding. Outside the cladding, two SAPs are placed opposite to each other. The SAPs are made of boron-doped silica, with properties similar to the ones used for PANDA fibers [7].

The core and cladding region of the fiber resembles the so-called endlessly single-mode fibers [1], where the pitch, Λ, and hole size, d, has been chosen to minimize leakage and macro bending losses in the visible to near infrared region. Three different values of the pitch are realized, all having a relative holes size, d/Λ, of approximately 0.48. In the following the three fibers will be referred to as PM-LMA-1 (Λ = 3.20 μm), PM-LMA-2 (Λ = 4.40 μm) and PM-LMA-3 (Λ = 5.94 μm). The fibers have all been fabricated from the same preform, by varying the outer diameter of the fibers.

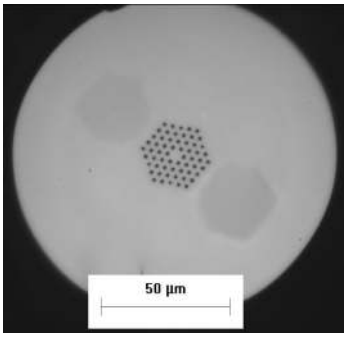

Fig. 1. Microscope image of PM-LMA fiber.

3. Optical properties

In Fig. 2, the spectral attenuation of the three fibers is shown, measured using the conventional cut-back method with a Tungsten-halogen white light source. For PM-LMA-1 an increased attenuation is observed at long wavelengths, which is ascribed to leakage losses [8]. The attenuation spectra indicate that the fiber is single-mode at all wavelengths, since no

#3854 - $15.00 US Received 20 February 2004; revised 1 March 2004; accepted 2 March 2004

spectral features are observed which may be ascribed to a higher-order mode cutoff. This was verified by inspecting the near fields of the fibers at 635 nm and 1550 nm, showing only the fundamental mode.

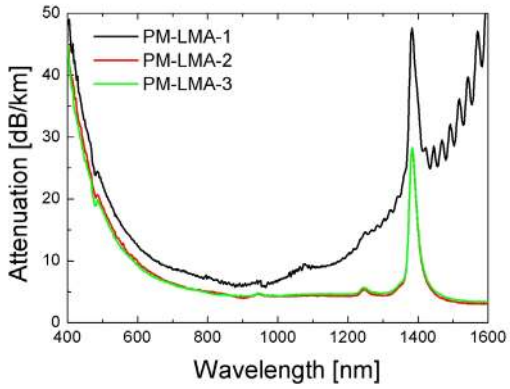

Fig. 2. Spectral attenuation for the three fibers.

The birefringence of the fibers was measured using the so-called crossed polarizer technique [9], illustrated in Fig. 3. Linearly polarized white light is launched into the fiber with the polarization oriented at 45 degrees with respect to the polarization axis of the fiber. On the fiber output, a second polarizer (analyzer) is oriented at 45 degrees with respect to the polarization axis of the fiber. The transmitted light is focused into a multi-mode fiber and the spectrum recorded with an optical spectrum analyzer. Using a Jones matrix analysis of the setup, it may be shown that the intensity transmission is given by:

$$T = \cos^2(\Delta\beta L) \tag{1}$$

Here $\Delta\beta = \beta_x - \beta_y$ is the difference between the propagation constants of the polarization axes of the fiber and L is the length of the fiber. The crossed polarizer setup yields a transmission with spectral oscillations, the period of which may be related to the birefringence. In Fig. 4, typical spectra are shown for PM-LMA-1 at long wavelengths and PM-LMA-3 at short wavelengths.

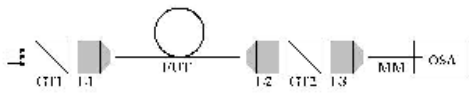

Fig. 3. Measurement set-up for group birefringence. GT1 : Input Glan-Thomson polarizer. L1 : Coupling lens into fiber under test (FUT). L2 : Collamating lens for fiber output. GT2 : Output Glan-Thomson polarizer (analyser). L3 : Focussing lens. MM : Multi-mode fiber for light collection and detection in optical spectrum analyser (OSA).

It is emphasized, that the analysis of the spectral oscillations yields the group birefringence, which may be shown by calculating the derivative of the phase in Eq. (1), $\varphi = \Delta\beta L$, with respect to the wavelength:

#3854 - $15.00 US Received 20 February 2004; revised 1 March 2004; accepted 2 March 2004

$$\frac{\partial \varphi}{\partial \lambda} = \frac{2\pi L}{\lambda^2}\left[\lambda \frac{\partial \Delta n_{ph}}{\partial \lambda} - \Delta n_{ph}\right] = \frac{2\pi L}{\lambda^2}\Delta n_g \qquad (2)$$

Here Δn_{ph} is the phase birefringence and Δn_g is the group birefringence. One oscillation period, $\Delta\lambda$, of the spectrum in Fig. 4 corresponds to $\Delta\varphi = 2\pi$, from which the group index on the right hand side of Eq. (2) may be calculated. The results are shown in Fig. 5, and have been averaged over intervals of 100 or 200 nm.

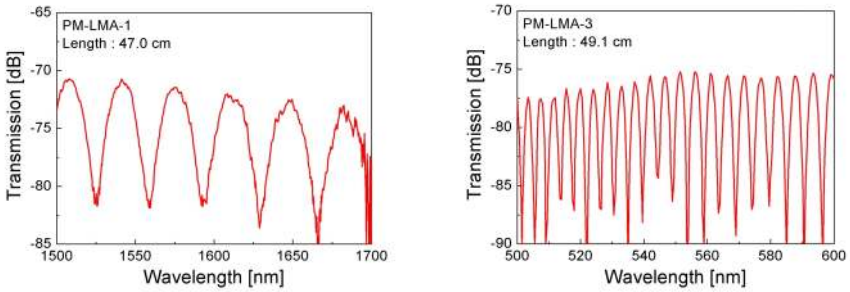

Fig. 4. Measured polarization osciallations, for the largest (left) and smallest (right) values of the relative wavelength, λ/Λ.

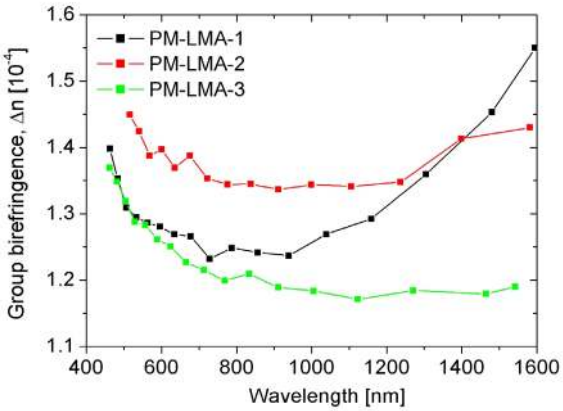

Fig. 5. Group birefringence vs. wavelength for the three fibers.

Finally, the polarization holding parameter (h-parameter) was also investigated using the setup shown in Fig. 3. For this experiment the first polarizer was aligned with one of the optical axis of the fiber, and at the output the transmitted intensity in the polarization axis was measured using the second polarizer. For PM-LMA-1 we obtained 13.3 dB extinction on a length of 390 m at 650 nm, corresponding to $h=1.2\cdot10^{-4}$ m^{-1}. This value may be influenced by many intrinsic or extrinsic factors, such as the fiber homogeneity, the wavelength, the bending radius and, probably most important, the magnitude of the birefringence itself. However, this investigation will not be discussed further here.

4. Discussion of results

The likely contributions to the birefringence in the present fiber may be divided into the categories known from solid-glass fibers, namely form birefringence and stress-induced birefringence. It has previously been shown that the six-fold symmetry of the cladding of large-mode area fiber does not allow inherent birefringence [10]. Furthermore, any asymmetry of the core region will only contribute negligibly to the birefringence measured, since the

#3854 - $15.00 US Received 20 February 2004; revised 1 March 2004; accepted 2 March 2004

magnitude of the relative wavelength, λ/Λ, is too large [4]. Hence, the birefringence is expected to originate only from the stress field, and since the mode field diameter is known to be almost constant for LMA fibers [5], we may expect that the birefringence does not depend on the wavelength as it does for step-index fibers at small V-parameters [7].

Indeed, the values plotted in Fig. 5 show that the birefringence is practically constant for the three fibers that have been studied here. The small birefringence variation observed is attributed to diameter variations of the SAPs used in the preform, which are typically 10% along the length. Indeed, the SAP diameter as function of position in the preform correlates very well with the observed birefringence variations. Because the wavelength dependence is very small, we may assume that the term $\lambda\, d/d\lambda(\Delta n)$ in Eq. (2) is negligible and the phase birefringence is equal to the group birefringence.

For all three fibers the birefringence is increasing for decreasing wavelengths in the 400 nm – 900 nm region of the spectrum. We attribute this effect to the dispersion of the elasto-optic coefficient, which was discovered for bulk glasses in the beginning of the 20th century [11,12], but to our knowledge never reported for optical fibers. The birefringence is increasing in PM-LMA-1 for $\lambda > 900$ nm and to a smaller extend in PM-LMA-2 for $\lambda > 1200$ nm. In PM-LMA-1 this coincides with the spectral region showing leakage losses, and may be explained by the gradual expansion of the mode into the cladding region. Since the stress field cannot exist in the air holes, the magnitude of the stress field in the silica regions between the 6 air holes must be larger than in the core region itself, explaining the observed increase. For PM-LMA-2 no leakage losses are seen, but the increase of birefringence could be explained by dispersion of the elasto-optic coefficient at long wavelengths.

The SAPs used for the present fibers were designed to yield a birefringence of $3\cdot10^{-4}$ if used in a solid-glass PANDA fiber with similar SAP sizes and spacing. The reason for the lower birefringence in the present fibers is attributed to screening of the strain field by the holes. For $d/\Lambda=1$ the core is mechanically detached from the SAPs and thus not strained, while for $d/\Lambda=0$ the fiber is solid and thus comparable to a conventional PANDA fiber. Hence as d/Λ increases above zero, the strain experienced by the core is expected to decrease if the rest of the structure is kept constant. Yet, the level of birefringence obtained here is promising for fiber designs where SAPs are placed outside a cladding with air holes, and the result is somewhat surprising in the light of recent work. E.g. in [13] it is shown that an externally applied stress field on a photonic crystal fiber, obtained by a lateral force on the fiber cladding, yields a significant reduction of the birefringence even for relative hole sizes, d/Λ, smaller than 0.5. For the fibers studied here, the screening of the stress field may be reduced further, either by decreasing the number of periods of air holes or by using fiber designs with smaller holes [14].

5. Conclusion

We have demonstrated, to our knowledge for the first time, a polarization maintaining large mode area endlessly single mode PCF. The birefringence is induced by SAPs positioned outside the cladding region of the PCF. The optical properties of the LMA-PCF lead to a close to wavelength independent birefringence in the order of $1.5\cdot10^{-4}$.

Acknowledgments

M.D. Nielsen acknowledges financial support by the Danish Academy of Technical Sciences.

#3854 - $15.00 US Received 20 February 2004; revised 1 March 2004; accepted 2 March 2004